NAVAL POSTGRADUATE SCHOOL
Monterey, California

THESIS

INTERACTIONS OF LARGE-SCALE TROPICAL MOTION SYSTEMS DURING THE 1996-1997 AUSTRALIAN MONSOON

by

Sylvia C. Taylor

September 1998

Thesis Advisor: Chih-Pei Chang
Second Reader: Patrick A. Harr

Approved for public release; distribution is unlimited.

REPORT DOCUMENTATION PAGE

Form Approved OMB No. 0704-0188

1. AGENCY USE ONLY *(Leave blank)*	2. REPORT DATE	3. REPORT TYPE AND DATES COVERED
	September 1998	Master's Thesis

4. TITLE AND SUBTITLE
INTERACTIONS OF LARGE-SCALE TROPICAL MOTION SYSTEMS DURING THE 1996-1997 AUSTRALIAN MONSOON

5. FUNDING NUMBERS

6. AUTHOR(S)
Taylor, Sylvia C.

7. PERFORMING ORGANIZATION NAME(S) AND ADDRESS(ES)
Naval Postgraduate School
Monterey, CA 93943-5000

8. PERFORMING ORGANIZATION REPORT NUMBER

9. SPONSORING / MONITORING AGENCY NAME(S) AND ADDRESS(ES)

10. SPONSORING / MONITORING AGENCY REPORT NUMBER

11. SUPPLEMENTARY NOTES
The views expressed in this thesis are those of the author and do not reflect the official policy or position of the Department of Defense or the U.S. Government.

12a. DISTRIBUTION / AVAILABILITY STATEMENT
Approved for public release; distribution is unlimited.

12b. DISTRIBUTION CODE

13. ABSTRACT *(maximum 200 words)*

During the northern winter monsoon, several large-scale tropical motion systems are active in the southern tropical region of the ITCZ and SPCZ, including the maritime continent, northern Australia and the West Pacific. Superimposed on the mean state are transient large-scale systems including the Madden-Julian Oscillation (MJO) propagating from the equatorial Indian Ocean, the northeasterly cold surges from the northern hemisphere, and the easterly waves from the central or western Pacific. This work studied the possible interactions among these large-scale systems and their roles in the development of tropical cyclones. GMS water vapor data and NCEP reanalysis data during December 1996 to March 1997 were used. Examination of daily maps revealed that most of the TC development requires the interaction of two or more large-scale transient systems. The most frequent occurrences involved the interaction of the MJO and cold surges, followed by the interaction of the MJO and easterly waves.

14. SUBJECT TERMS
Australian monsoon, northern winter monsoon, MJO, tropical cyclone, cold surge

15. NUMBER OF PAGES
118

16. PRICE CODE

17. SECURITY CLASSIFICATION OF REPORT	18. SECURITY CLASSIFICATION OF THIS PAGE	19. SECURITY CLASSIFI- CATION OF ABSTRACT	20. LIMITATION OF ABSTRACT
Unclassified	Unclassified	Unclassified	UL

Approved for public release; distribution is unlimited

INTERACTIONS OF LARGE-SCALE TROPICAL MOTION SYSTEMS DURING THE 1996-1997 AUSTRALIAN MONSOON

Sylvia C. Taylor
Captain, United States Air Force
B.S., Pennsylvannia State University, 1991

Submitted in partial fulfillment of the
requirements for the degree of

MASTER OF SCIENCE IN METEOROLOGY

from the

NAVAL POSTGRADUATE SCHOOL
September 1998

Author: Sylvia C. Taylor
Sylvia C. Taylor

Approved by:
Chih-Pei Chang, Thesis Advisor

Patrick A. Harr, Second Reader

Carlyle Wash, Chairman
Department of Meteorology

ABSTRACT

During the northern winter monsoon, several large-scale tropical motion systems are active in the southern tropical region of the ITCZ and SPCZ, including the maritime continent, northern Australia and the West Pacific. Superimposed on the mean state are transient large-scale systems including the Madden-Julian Oscillation (MJO) propagating from the equatorial Indian Ocean, the northeasterly cold surges from the northern hemisphere, and the easterly waves from the central or western Pacific. This work studied the possible interactions among these large-scale systems and their roles in the development of tropical cyclones. GMS water vapor data and NCEP reanalysis data during December 1996 to March 1997 were used. Examination of daily maps revealed that most of the TC development requires the interaction of two or more large-scale transient systems. The most frequent occurrences involved the interaction of the MJO and cold surges, followed by the interaction of the MJO and easterly waves.

TABLE OF CONTENTS

ACKNOWLEDGMENT

I would like to thank Professor Chang for his expertisse and enthusiasm throughout this entire project. Without his guidance and patience this would not have been possible. In addition, I would like to thank in part the Office of Naval Research and the National Science Foundation for their support. I would like to thank his staff, especially Bao-Fong Jeng and Hway-Jen Chen for their responsive support of providing data in a format that I could use. I am appreciative of the help I received from Professor Harr in coding and writing. Other staff personnel that assisted me in coding and data issues were Bob Creasey and Mary Jordan, thank you.

I would like to thank my husband, Steve, for providing me the love and patience needed to finish this project while he was finishing his thesis also. May our child remember some of those long nights and realize that hard work and perserverance always pays off in the end.

I. INTRODUCTION

The Inter-tropical Convergence Zone (ITCZ) and the South Pacific Convergence Zone (SPCZ) contain the most expansive cloud bands on earth. Studies of these two tropical zones are motivated by their important roles in the earth's climate and in the development of tropical cyclones. This paper will study the motion systems in the vicinity of these zones during the northern winter monsoon (Australia summer monsoon), which occurs from December 1996 to March 1997.

The large-scale convection center moves from south/southeast Asia during the northern summer monsoon to the maritime continent and northern Australia equatorial region during the northern winter monsoon, which increases convection and produces favorable conditions for tropical cyclone development. The ITCZ and SPCZ convection is effected by other large-scale tropical convection systems as well, such as the Madden-Julian oscillation (Madden and Julian 1971), the northeasterly cold surges, and tropical synoptic-scale waves. Both the ITCZ and the SPCZ are characterized by strong low-level cyclonic vorticity. When the ITCZ and SPCZ are active, convection is enhanced and may be favorable for tropical cyclone development.

In the Indian and West Pacific Oceans, studies by Liebmann et al. (1994) showed that more favorable conditions

exist for the occurrence of tropical depressions and storm development during the active or convective phase of the Madden-Julian oscillation (MJO). The storm development appears to be related to the large-scale low-level cyclonic vorticity and convergence that occurs westward and poleward of the MJO convection (Liebmann et al. 1994). The MJO is a global scale disturbance within the tropics whose period varies between 20-60 days, with the most frequent occurrence around 45 days. The oscillation signal can be seen in the convection and wind fields in the Eastern Hemisphere, but only in the wind fields in the Western Hemisphere. The convection follows the semi-annual migration of the ITCZ across the equator.

Several studies (Rui and Wang 1990; Wang and Rui 1990; Weickmann and Khalso 1990) showed that during the onset of the MJO, convection remains almost stationary over the eastern Indian Ocean. The convection then propagates eastward and weakens when moving over the maritime continent (Indonesia and Malaysia) and northern Australia. The convection continues to propagate eastward and intensifies above the warm water of the western Pacific Ocean. The eastward movement slows as the convection moves towards the dateline where it weakens before moving toward the eastern Pacific Ocean. This study shows that the primary convective

signal slows down and propagates to the southeast into the SPCZ.

There are two main signatures of the MJO; the "super cloud cluster"(SCC) and the westerly wind burst (WWB). Nakazawa (1988) studied the structure of the SCC with 3 hourly geostationary OLR data and found that the SCC and associated westward-moving cloud clusters were confined within 15 degrees of the equator. Zangvil (1975) showed these eastward moving clouds or SCCs in a time-longitude cross section to be more evident on the summer side of the equator. The SCC is defined as a large area of organized convection whose dimension can extend 1000 km from west to east and have duration of 2 and 10 days border. There exists smaller cloud clusters whose lifetime ranges between 2 and 10 days and propagate to the west within the SCC. The propagation speed of the SCC usually ranges between 5 and 15 m/s. The propagation is due to new cells of cloud clusters forming on the eastern border and dissipating cloud cells on the western border (Ferreira et al. 1996). Consequently, the SCC of the MJO forces the circulation pattern, which has been described as being Rossby gyres and near equatorial wind bursts to the west of the convection and a Kelvin wave signature to the east of the convection. The circulation pattern propagates with the MJO convection eastward from the Indian Ocean to the western Pacific where the Kelvin wave

breaks free of the dying convection and propagates faster into the Western Hemisphere (Ferreira et al. 1996).

Leibmann et al. (1994) showed that large-scale, slowly varying anomalies such as the MJO can produce favorable conditions for clustering of tropical cyclones. With the arrival of the MJO, cyclones tend to form around the low-level vorticity that is poleward and westward of the MJO convection. As mentioned previously, the signal of the MJO is strong between 5-15 degrees latitude of the summer hemisphere, which coincidentally is where tropical cyclone development is most prevalent. Liebmann et al. (1994) concluded that the MJO does influence the development of tropical cyclones but not in a unique fashion. They observed more tropical cyclone development in the convective phase than the dry phase of the MJO because there were more tropical depressions to begin with. But, the percentage of depressions that developed into tropical cyclones is the same between the convective and dry phases of the MJO.

Another large-scale convection system that affects the tropics during the northern winter is the northeasterly cold surge. From 20N to the equator, the northeast monsoon winds covers a broad tropical area from Southeast Asia to the Central Pacific. During cold surge events, the northeasterly flow freshens. There can be dramatic effects on synoptic- and planetary-scale convective patterns. The first effect is a general increase of deep convection over

the maritime continent during the winter monsoon as the cold surges seem to spawn near-equatorial cloud systems. Localized episodes of heavy rainfall and flooding often occurs during strong cold surge events. Secondly, the cold surge has an influence on the associated convection and circulation pattern of the Southern Hemisphere (Australian) summer monsoon and its onset (Johnson and Houze 1987). Thirdly, the northeasterly cold surge has a possible influence on Southern Hemisphere tropical storms. The winter monsoon pattern varies from early to late winter; northeasterly flow across the South China Sea is strongest and deepest in early winter and becomes shallower and weaker toward the end. The peak convection of the Australian summer monsoon occurs in late January and February when the near equatorial trough lies between 10 and 15 degrees south (Johnson and Houze, 1987).

Another disturbance that will be studied is the tropical synoptic waves often called "easterly waves". This wave is more easily detected as a low-level cyclonic disturbance moving from east to west. The system can bring either convection into the region, or have only cyclonic low-level winds without significant convection. In this study, we will show that sometimes they can interact with pre-existing convection in the area to produce heavy convection, flooding and tropical storm development.

The purpose of this work is to study the possible interactions among the transient large-scales systems, such as the MJO, northeasterly cold surges and easterly waves, and their roles in development of tropical cyclones. The period of the study is from 1 December 1996 to 31 March 1997, using the Geostationary Meteorology Satellite (GMS) water vapor IR data and National Center for Environmental Predication (NCEP) reanalysis fields.

II. DATA

Data used for this paper were the radiance observations from the water vapor channel of Geostationary Meteorological Satellite infrared (GMS IR) data taken at 0.5 x 0.5 degree resolution and the National Center for Environmental Prediction (NCEP) reanalysis 1000 hPa wind field at 2.5 x 2.5 degree resolution. The GMS data were used to identify convection patterns and the NCEP data were used to define low-level circulations. For both data sets, only daily averages are used. The period of this study was between December 1996 and March 1997 and was chosen because the NASA Scatterometer (NSCAT) data fields could be used to supplement the GMS and NCEP data in order to verify tropical wave and tropical cyclone positions.

The area used of study is 30N to 30S, 90E to 160W (Figure 1). Some convection and tropical cyclone development are concentrated in the equatorial region, so only GMS water vapor data from 20N to 20S were used. Two area-averaged indices were defined; a convective index (CI) that was derived from the GMS data, and a cold surge index that was computed from the 1000 hPa wind.

The CI was calculated by first converting the radiance values to their equivalent blackbody temperature (TBB). If the TBB was less than or equal to 255K then the CI was set

to 0 and those values above it were set to respectively from 1 to 70. For example;

TBB<=255 CI=0
TBB>255 CI=255-TBB 1<=CI<=70

The cold surge index was calculated from the meridional (v) component of winds at 7.5N, 105E-115E, which is the southern part of the South China Sea. Next, the cold surge index (v) was used to define the cold surge events, and were composited according to the time relevance to the surge event. The beginning of a "surge" is defined as day 0 which is the day of weakest northerly winds. An event was identified if the northerly acceleration can be sustained for at least three days and/or reach approximately -4.5 m/s. There were 7 surge events during the four-month period. The composites were done daily from four days prior to the beginning of the surge to five days after the beginning of the surge.

All tropical depression and cyclone positions were extracted from the Joint Typhoon Warning Center (JTWC) archives (JTWC 1997) with additional collaboration using the monthly Darwin Tropical Diagnostic statements published by the Bureau of Meteorology Northern Territory Region (BM/NTR) (BM/NTR 1997). Since the purpose was to study the development of tropical cyclones (TC), positions of tropical depression, when the sustained winds reached 30 knots, were

identified as "pre-formation" occurrences. The events that lead to these occurrences will be the focus of this study.

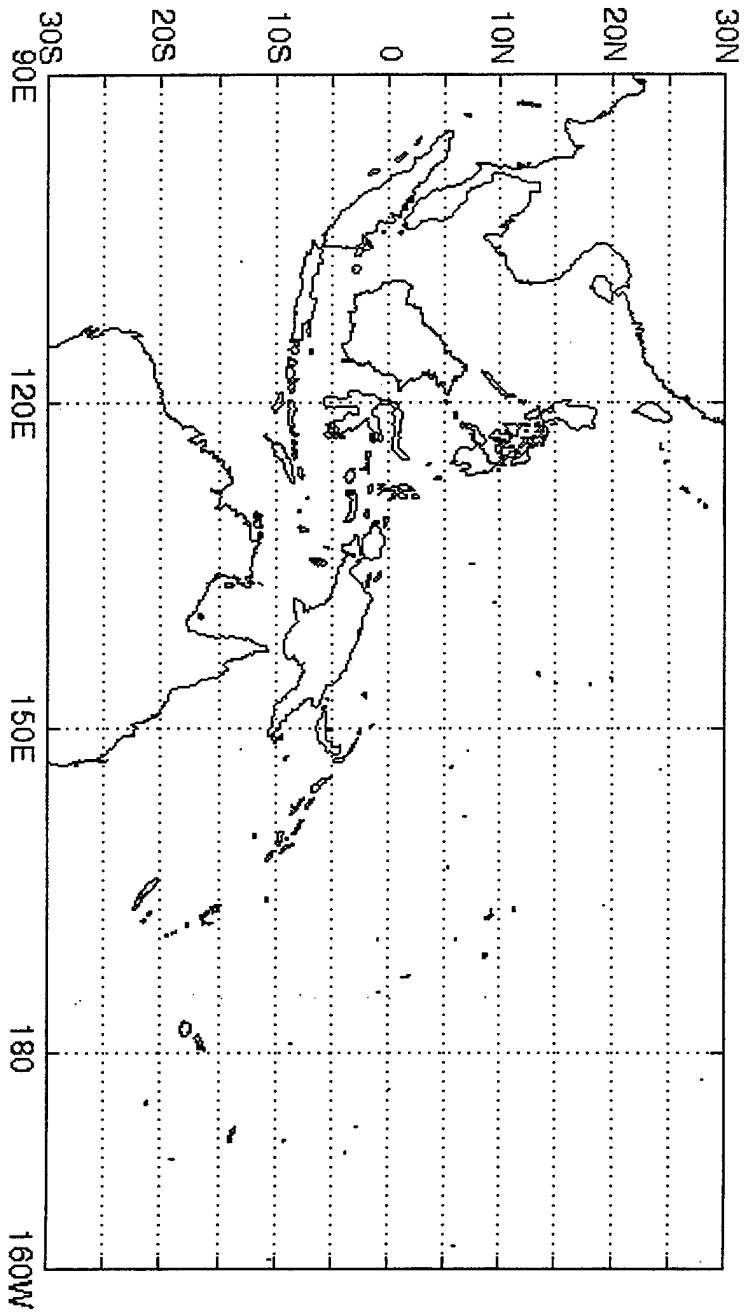

Figure 1. The region of interest for this study.

III. MEAN FLOW

Before looking at any of the analysis, the mean flow of the region will first be discussed. The 1000 hPa synoptic flow will be examined in conjunction with the convection patterns using the convective index from the GMS data. The December 1996 to March 1997 season will be discussed over the area in Figure 1. The general characteristic of the winter monsoon circulation systems and cloud patterns have shown that the most extensive, vigorous clouds are found to the north of the Southern Hemisphere monsoon trough axis, from Sumatra across Indonesia to the southwest Pacific (Johnson and Houze 1987). The general circulation and convection pattern will be examined initially by using monthly average charts and a seasonal average chart.

A. CIRCULATION PATTERN

The 1000 hPa monthly average synoptic flows are depicted for December 1996, January 1997, February 1997, and March 1997 in Figure 2. Figure 3 shows the seasonal average that covers all four months. Both the monthly and seasonal means show that northeasterly trades prevail over most of the region between the equator and 20N. A strong north to south cross-equatorial flow is seen across the South China Sea region in December through February with a slightly weaker crossing in March. In addition, there is also strong

cross-equatorial flow to the east of the Philippines. Both of these cross-equatorial flows enhance the cyclonic vorticity to the south and southeast of New Guinea in the SPCZ region. In March 1997, there is stronger cross-equatorial flow between 125E and 150E, which sets up a cyclonic vortex between 5S to 15S, and 150E to 180. To the west of this vortex, another closed circulation appears around 15S, 150E to 160E. This circulation appears to be strongly incluenced by the southern midlatitudes.

As these Northern Hemisphere northeasterlies cross the equator, the flow turns westerly into the Australian summer monsoon trough located between 10S and 20S from 90E into Northern Australia. As the flow crosses the equator and turns westerly, this sets the patterns needed for the ITCZ and SPCZ circulations. Convergence zones are set in the Australian monsoon region, between 90E to approximately 140E, and cyclonic circulation occurs in the SPCZ to the southeast of New Guinea into the southwest Pacific Ocean. Two specific circulation patterns stand out in the Southern Hemisphere, the strong cyclonic circulation in the SPCZ region and the cyclone/anticyclone pair to the west of Australia between 10S and 30S. There is strong cyclonic turning to the south and southeast of New Guinea, which depicts the SPCZ region. The strongest circulation appears to be in January and March where there is strong cross-equatorial flow and enhanced flow from the Southern

Hemisphere midlatitude systems, which is apparent from the band of 5 m/s winds to the south. The second Southern Hemisphere circulation that stands out is the cyclone/anticyclone pair to the west of Australia. This circulation is evident in each monthly average and will later be seen on the daily charts as well. In January and February the anticyclone appears to be stronger than the cyclonic circulation. The cyclone appears to maintain a constant intensity from December through February and then weakens in March to become a simple trough or open wave. These patterns will be related to the northeasterly cold surge in the next chapter.

B. CONVECTION PATTERN

The convection pattern will also be discussed using monthly average CI (Figure 4) and the seasonal average (Figure 5). As seen on the monthly and seasonal charts the strongest convection occurs to the south of the equator or in the summer hemisphere monsoon region. The seasonal CI chart blends all the convection so it appears to be one large band. In fact, from month to month the variation is quite large. In December, January, and February the strongest convection is in the west while in March the strongest convection is in the Central Pacific. This shift in strong convection has also been documented in other studies (Sui and Lau 1992). When convection flares east of

Sumatra then there is usually reduced convection in the central Pacific. The ITCZ and SPCZ cloud areas can clearly be seen in these Figures. The ITCZ is oriented zonally to the north of the equator and the SPCZ is oriented from New Guinea to the southeast. The important aspect to this season is that the strongest convection is in the summer hemisphere, or in the Australian Monsoon region. In the daily charts, which will be shown in Chapter VI, there is convection to the north of the equator but this is due to late season tropical cyclone development.

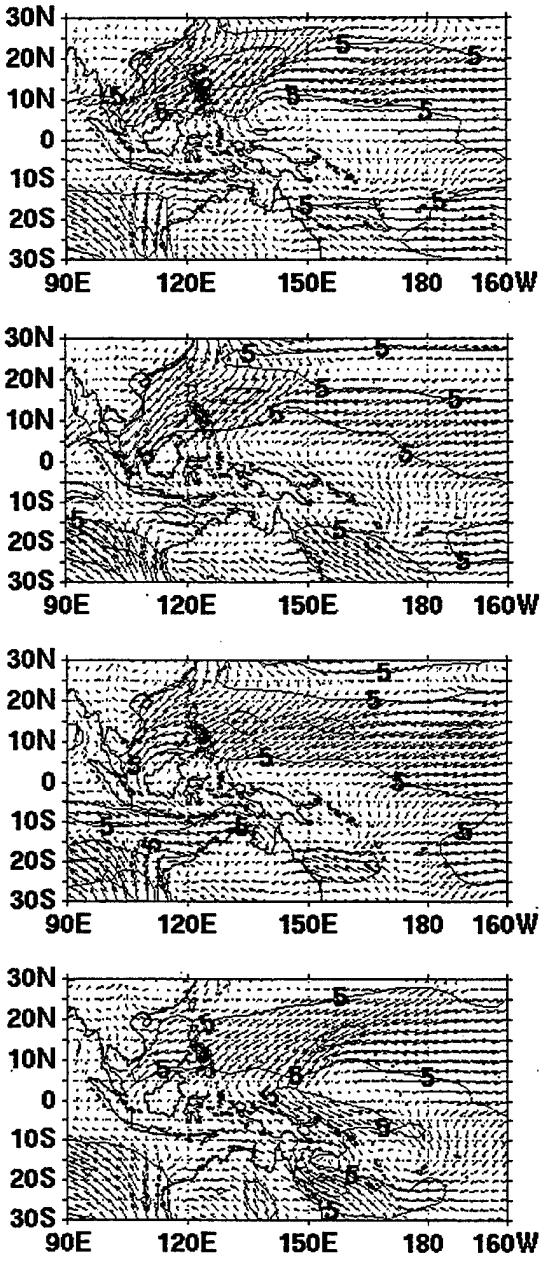

Figure 2. The monthly average winds for 1000 hPa from December 1996 (top), January 1997 (second from top), February 1997 (third from top), and March 1997 (bottom).

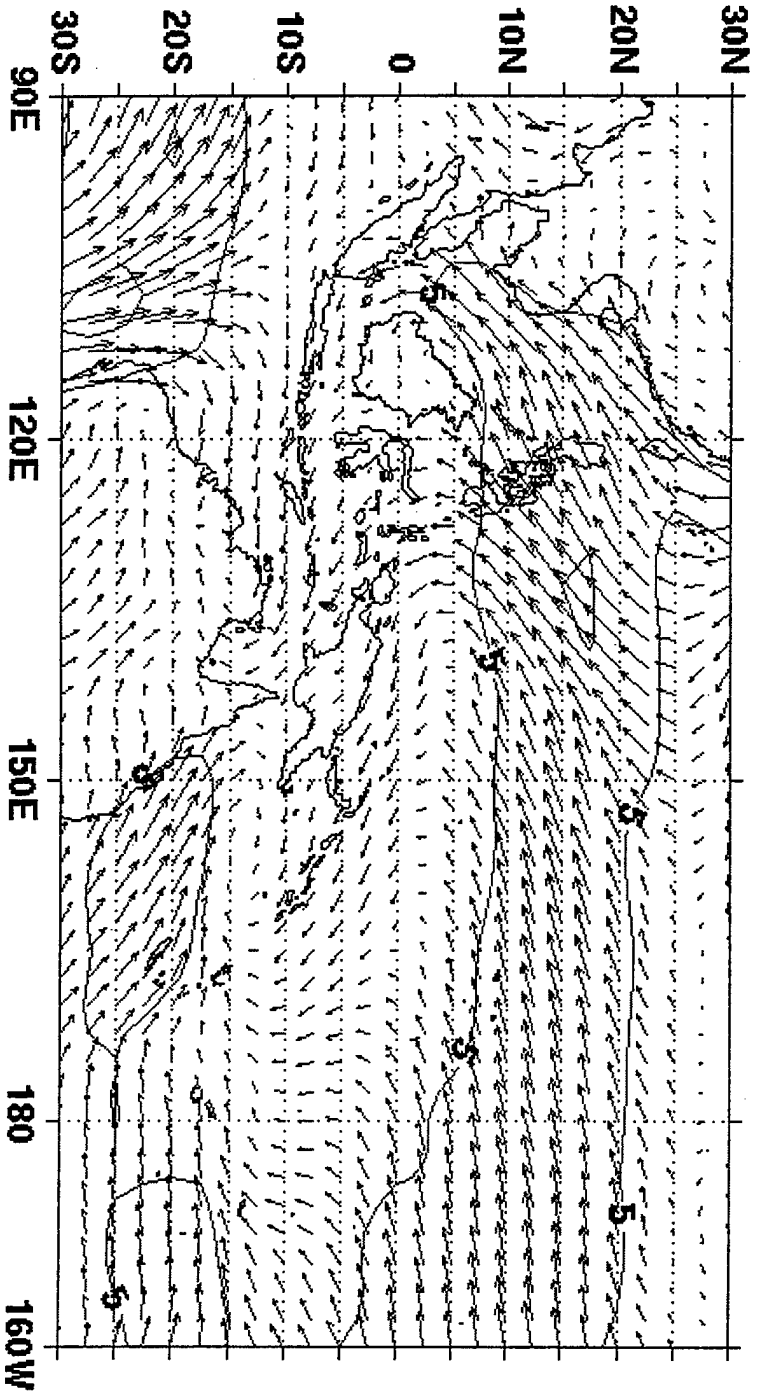

Figure 3. The seasonal average of 1000 hPa winds for December 1996 to March 1997.

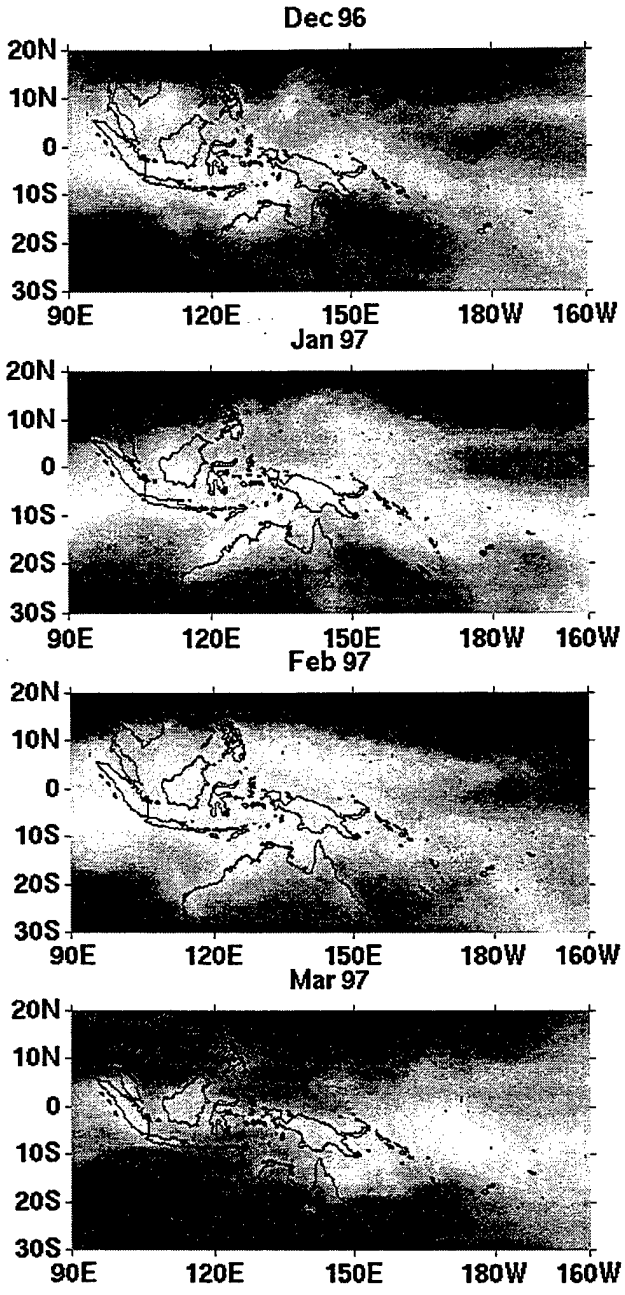

Figure 4. The monthly average clouds using the convective index (CI). Months are configured the same as Figure 2.

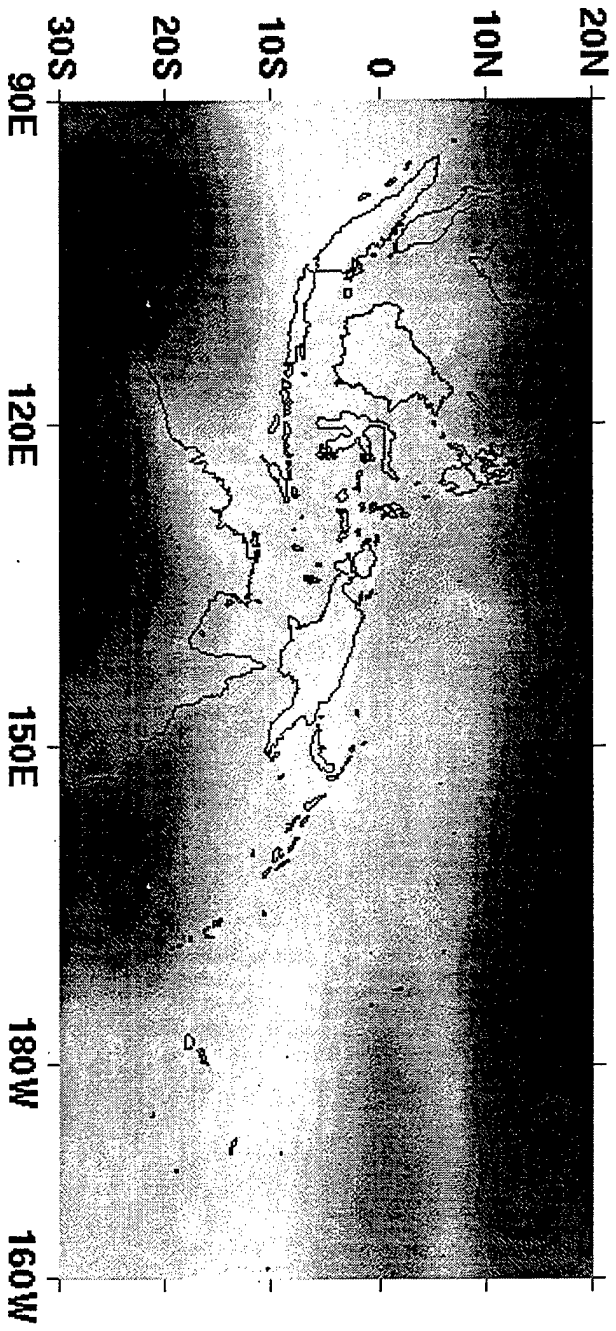

Figure 5. The seasonal average convection using the CI.

IV. SOUTH CHINA SEA/WEST PACIFIC COLD SURGES

Initially, the effect of the northeasterly cold surge on the circulation patterns of the regions is examined. The northeasterly cold surge is characterized by cold continental air from the east that is funneled equatorward. The sharp drop in temperature in East Asia is accompanied by a "surge" of northeasterly wind into East China and the South China Sea (Boyle and Chen 1987). The average zonal (u) and meridional (v) wind components over the South China Sea from 7.5N, 105E to 115E are used to define a surge event. The time series of the average wind components (Figure 6) indicates that the zonal and meridional wind components are positively correlated. When the easterlies are weak (smaller negative values), the northerlies are also weak (smaller negative values). A surge index was defined using the v component of winds. Day 0 of the surge is defined when the northerly winds were weakest (less negative). Composite diagrams of total winds were taken from 4 days prior to the surge to 5 days after the surge. There were 7 surge events during this season (Table 1). By comparing the composites (Figures 7-16) it will be seen that as the northeasterlies increase (decrease) over the South China Sea the intensity of a cyclonic circulation in the Southern Hemisphere also increases (decreases). In addition there are clearly two branches to the surge that occur

almost simultaneously. The first is the increase of wind speeds over the South China Sea and the second is the increase to the east of the Phillipines.

Four days prior to the beginning of the surge, it is evident from Figure 6 that as the beginning of the surge (Day 0) is approached the northeasterlies weaken. At day -4 (Figure 7), the northeasterly winds cover almost the entire area from approximately 5N to 20N then proceeding toward day 0 (Figures 8-11) the northeasterlies weaken as they retreat northward and also do not extend as far to the east.

The Southern Hemisphere response appears directly correlated with the South China Sea surge. As the surge weakens (Figures 8-11) and there is less cross-equatorial flow, there is less cyclonic response along northwestern Australia and in the SPCZ region. Beginning in the west, the anticyclone, cyclone couplet between 10S and 30S to the west of Australia weaken as time progresses from 4 days prior to the beginning of the surge to the beginning of the surge (day 0) (Figures 7-11). At day -4, the anticyclone covers an area from 7.5S to 30S and 90E to 107.5E. Proceeding to Day 0, the zonal extent shrinks but the anticylonic does not reach as far north. The cyclone adjacent to the anticyclone begins as a closed circulation on shore at day -4 then moves offshore and weakens. By day 0, the circulation is much weaker and moves onshore again.

As seen in the time series (Figure 6) after the beginning of the surge, day 0, as northerlies increase and it is assumed that the Southern Hemisphere response will also increase. Proceeding in time from day 0 (Figures 11-16), the band of northeasterlies broadens in both latitude and longitude and also strengthens. The cross-equatorial flow becomes much stronger in the South China Sea and the Philippine Sea as time progresses to day 5. The Southern Hemisphere response acts in the same manner; as time progresses and the northeasterly surge strengthens the cyclone/anticyclone off of Northwest Australia and the circulation in the SPCZ both increases. Starting in the west, the cyclone begins to strengthen and have a much more compact circulation. The anticyclone broadens in latitude and longitude and the intensity also increases. In the SPCZ region, the cross-equatorial flow contributes to increasing the low-level circulation. The other factor that contributes to increases in circulation is the 5 m/s winds from the southeast, which broaden in longitude and helps increase the cyclonic vorticity.

As the northeasterly cold surges strengthen and the Southern Hemisphere responses also increase, the areas become favorable for tropical cyclone development. Increased low-level vorticity northwest of Australia and in the SPCZ produces an environment that is conducive for tropical cyclone development (Gray 1979).

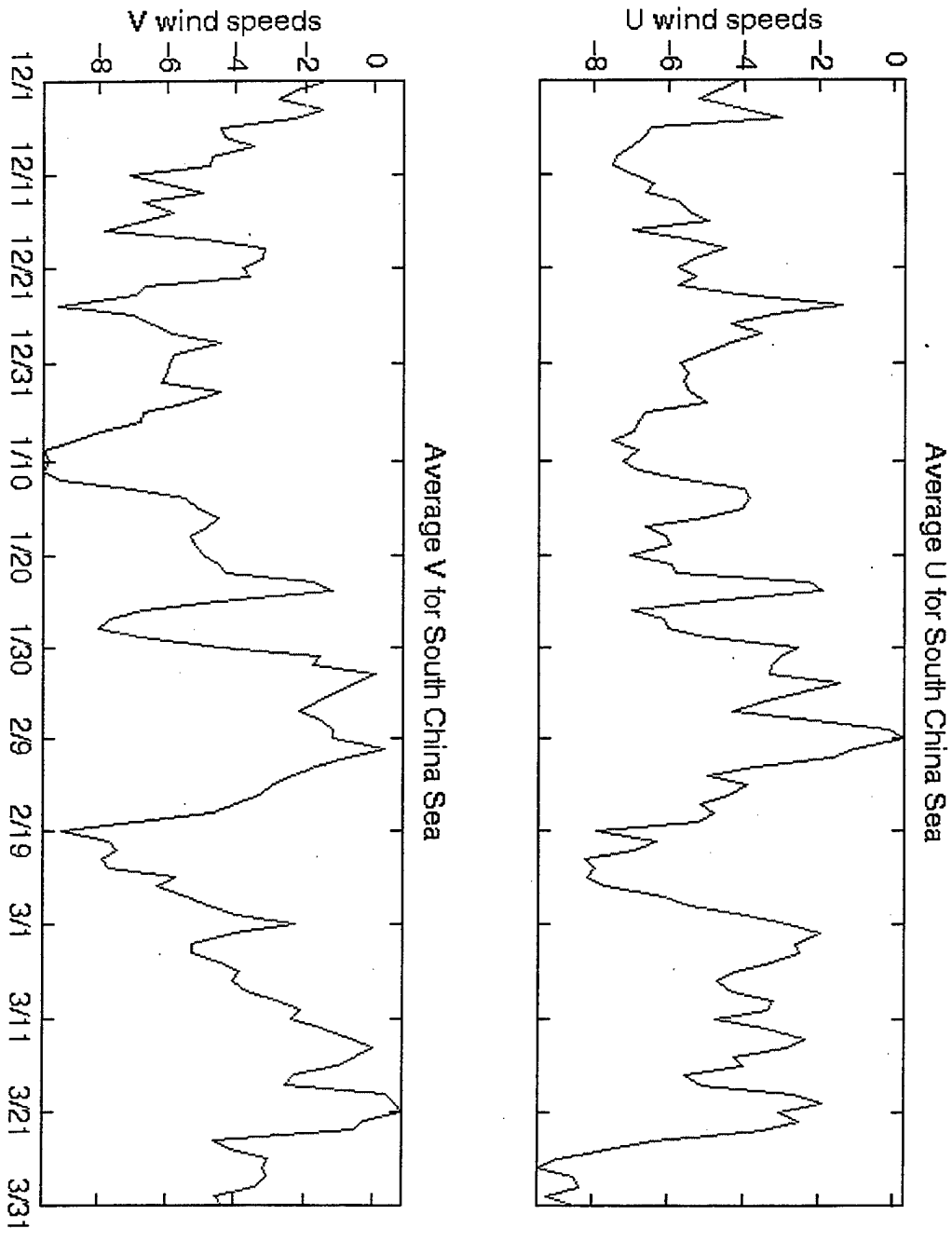

Figure 6. Times series of the u and v wind components averaged over 7.5N, 105E-115E. Northerly and easterly winds are indicated by more negative values.

South China Sea

Day	Category	Day	Category	Day	Category	Day	Category
1 Dec 96	0	1 Jan 97	-2	1 Feb 97		1 Mar 97	0
2 Dec 96	1	2 Jan 97	-1	2 Feb 97		2 Mar 97	1
3 Dec 96	2	3 Jan 97	0	3 Feb 97		3 Mar 97	2
4 Dec 96	3	4 Jan 97	1	4 Feb 97		4 Mar 97	3
5 Dec 96	4	5 Jan 97	2	5 Feb 97	-5	5 Mar 97	
6 Dec 96	5	6 Jan 97	3	6 Feb 97	-4	6 Mar 97	
7 Dec 96	6	7 Jan 97	4	7 Feb 97	-3	7 Mar 97	
8 Dec 96		8 Jan 97	5	8 Feb 97	-2	8 Mar 97	
9 Dec 96		9 Jan 97	6	9 Feb 97	-1	9 Mar 97	
10 Dec 96		10 Jan 97		10 Feb 97	0	10 Mar 97	
11 Dec 96		11 Jan 97		11 Feb 97	1	11 Mar 97	
12 Dec 96		12 Jan 97		12 Feb 97	2	12 Mar 97	
13 Dec 96		13 Jan 97		13 Feb 97	3	13 Mar 97	
14 Dec 96	-5	14 Jan 97		14 Feb 97	4	14 Mar 97	
15 Dec 96	-4	15 Jan 97		15 Feb 97	5	15 Mar 97	-5
16 Dec 96	-3	16 Jan 97		16 Feb 97	6	16 Mar 97	-4
17 Dec 96	-2	17 Jan 97		17 Feb 97		17 Mar 97	-3
18 Dec 96	-1	18 Jan 97		18 Feb 97		18 Mar 97	-2
19 Dec 96	0	19 Jan 97	-5	19 Feb 97		19 Mar 97	-1
20 Dec 96	1	20 Jan 97	-4	20 Feb 97		20 Mar 97	0
21 Dec 96	2	21 Jan 97	-3	21 Feb 97		21 Mar 97	1
22 Dec 96	3	22 Jan 97	-2	22 Feb 97		22 Mar 97	2
23 Dec 96	4	23 Jan 97	-1	23 Feb 97		23 Mar 97	3
24 Dec 96	5	24 Jan 97	0	24 Feb 97	-5	24 Mar 97	4
25 Dec 96	6	25 Jan 97	1	25 Feb 97	-4	25 Mar 97	5
26 Dec 96		26 Jan 97	2	26 Feb 97	-3	26 Mar 97	
27 Dec 96		27 Jan 97	3	27 Feb 97	-2	27 Mar 97	
28 Dec 96		28 Jan 97	4	28 Feb 97	-1	28 Mar 97	
29 Dec 96	-5	29 Jan 97				29 Mar 97	
30 Dec 96	-4	30 Jan 97				30 Mar 97	
31 Dec 96	-3	31 Jan 97				31 Mar 97	

Table 1. Northerly surge events based on the v wind component index. Seven events were found and day 0 is the day of weakest northerly winds defined as the beginning of the surge. Composites were taken from day -4 to day 5.

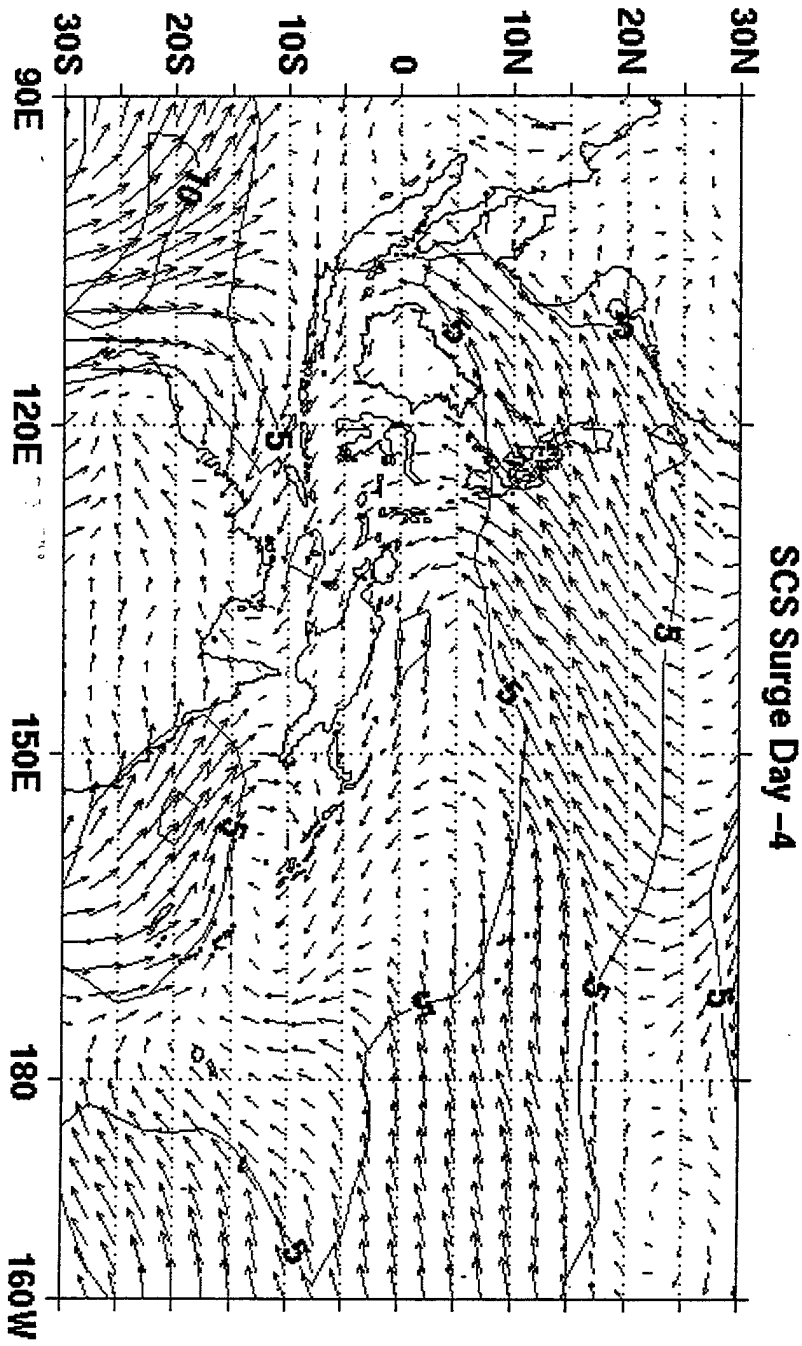

Figure 7. Four days prior to the beginning of the South China Sea Surge.

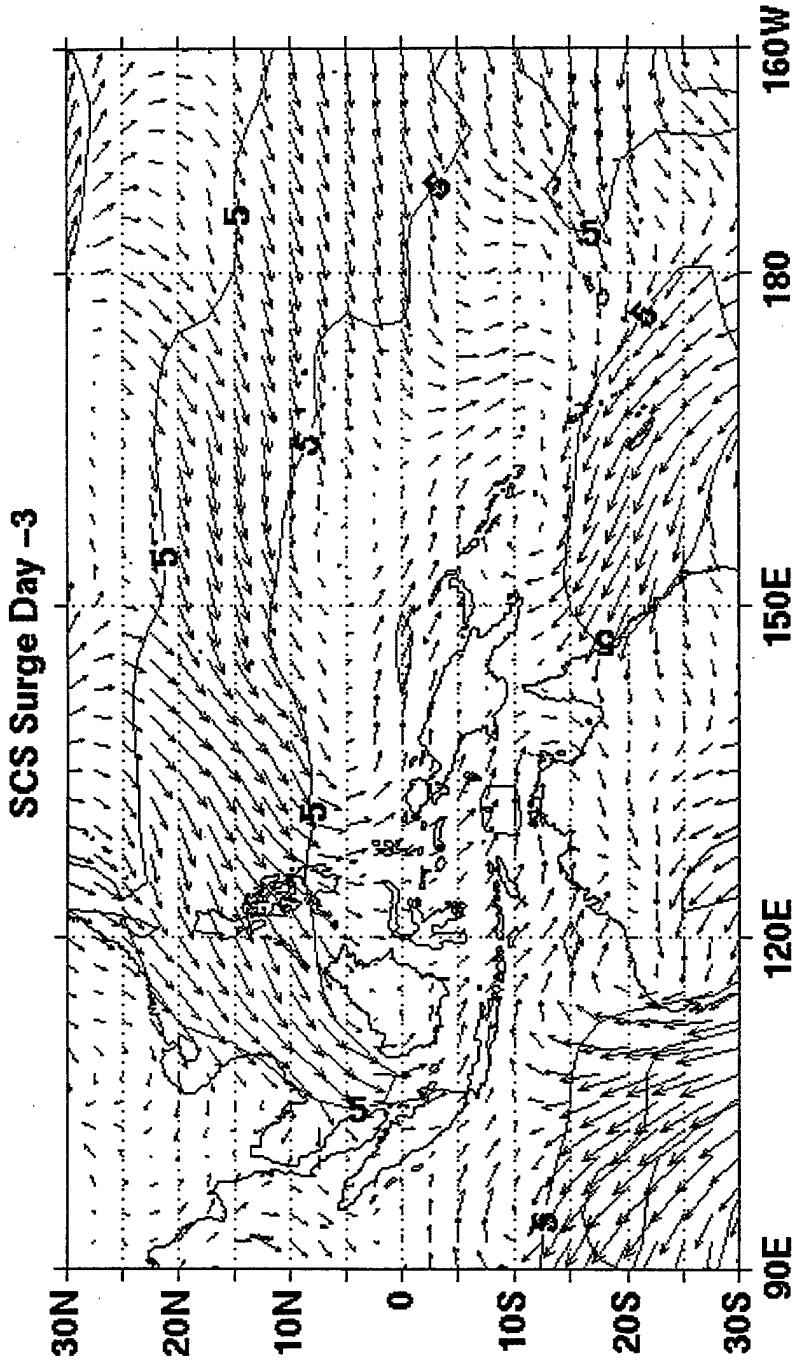

Figure 8. Three days prior to the beginning of the South China Sea Surge.

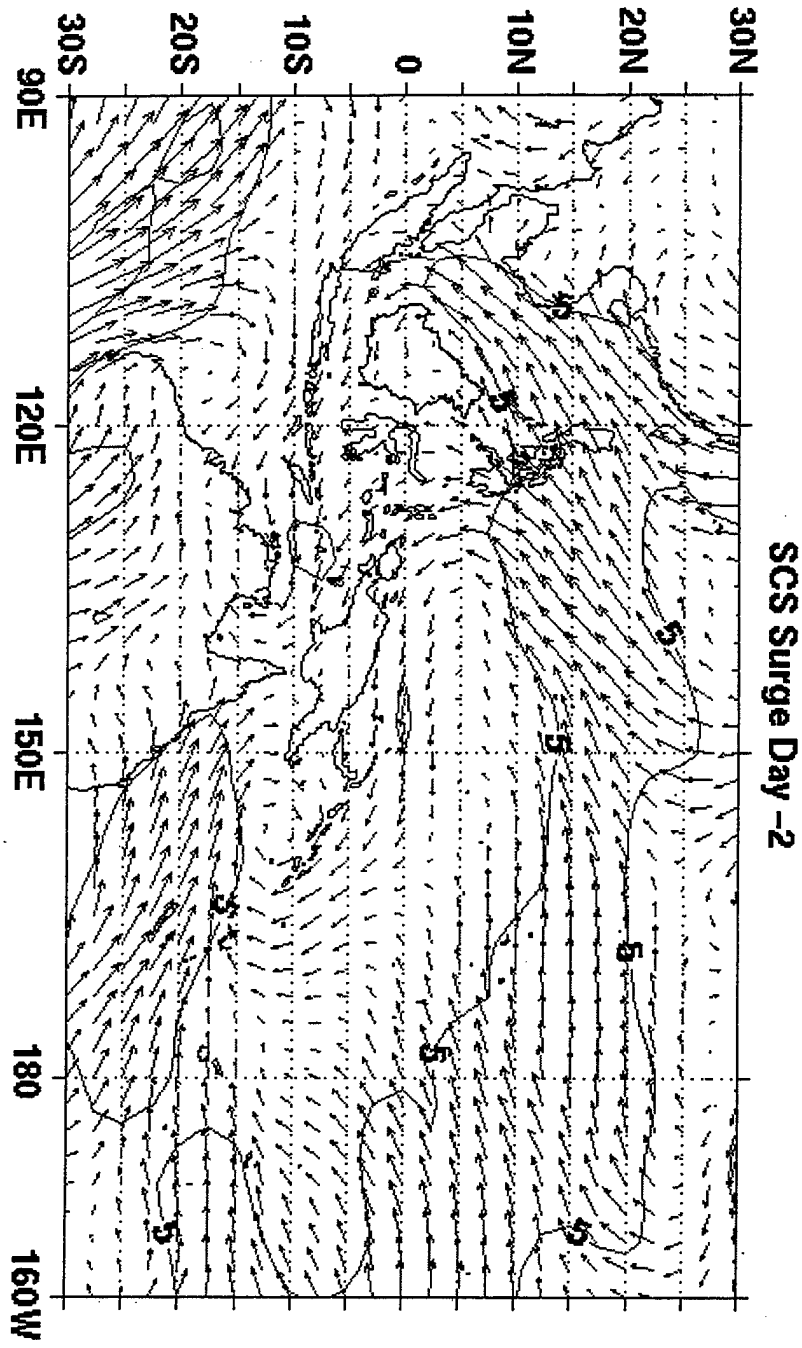

Figure 9. Two days prior to the beginning of the South China Sea Surge.

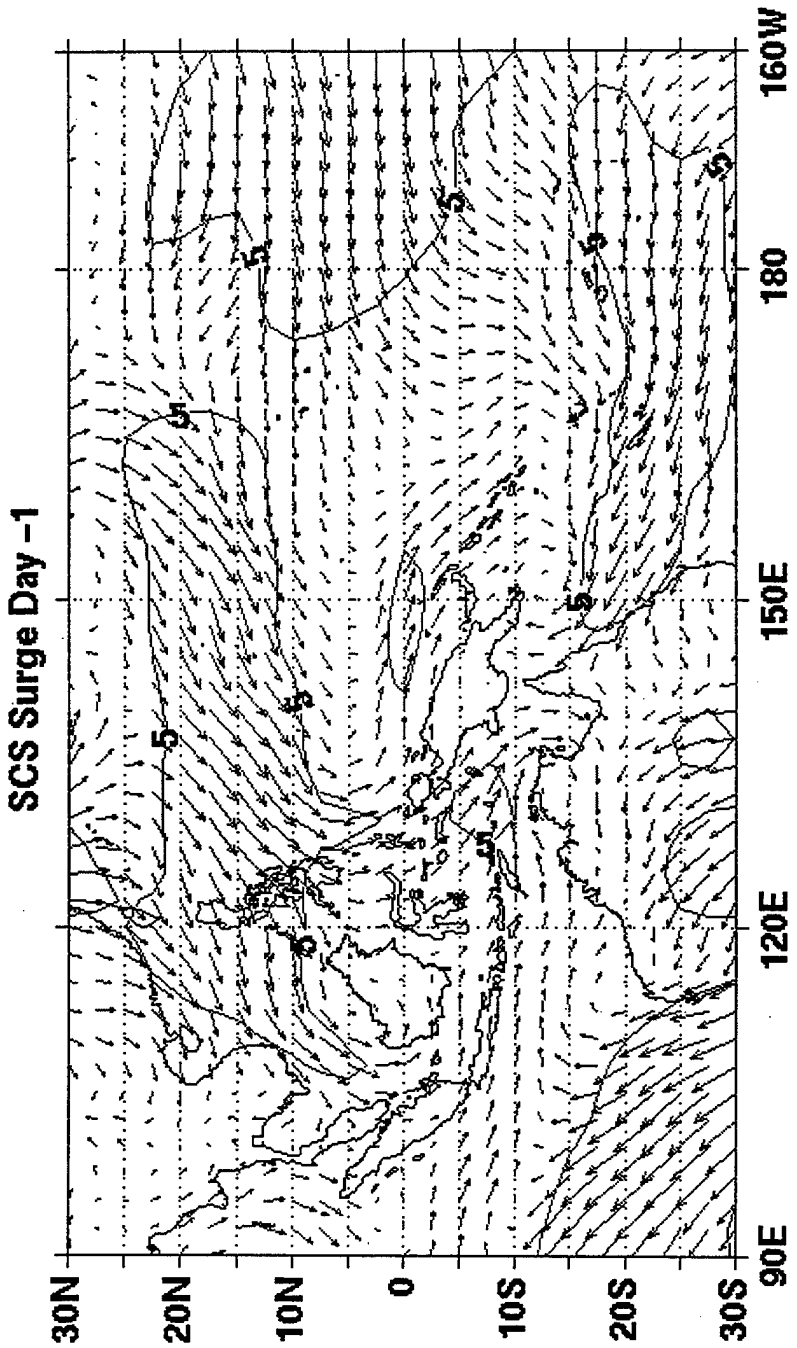

Figure 10. One day prior to the beginning of the South China Sea Surge.

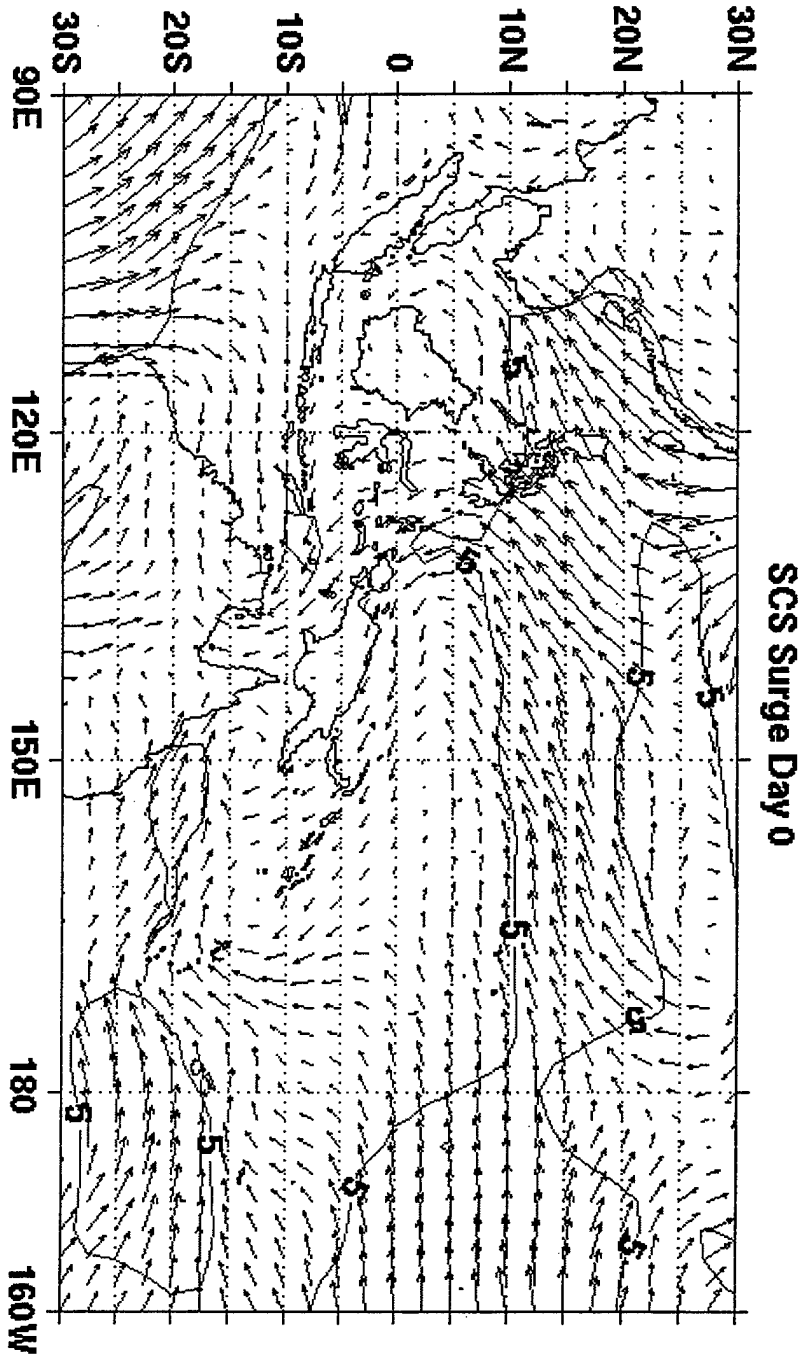

Figure 11. The beginning of the South China Sea surge, Day 0, which is the day of the weakest northerly winds.

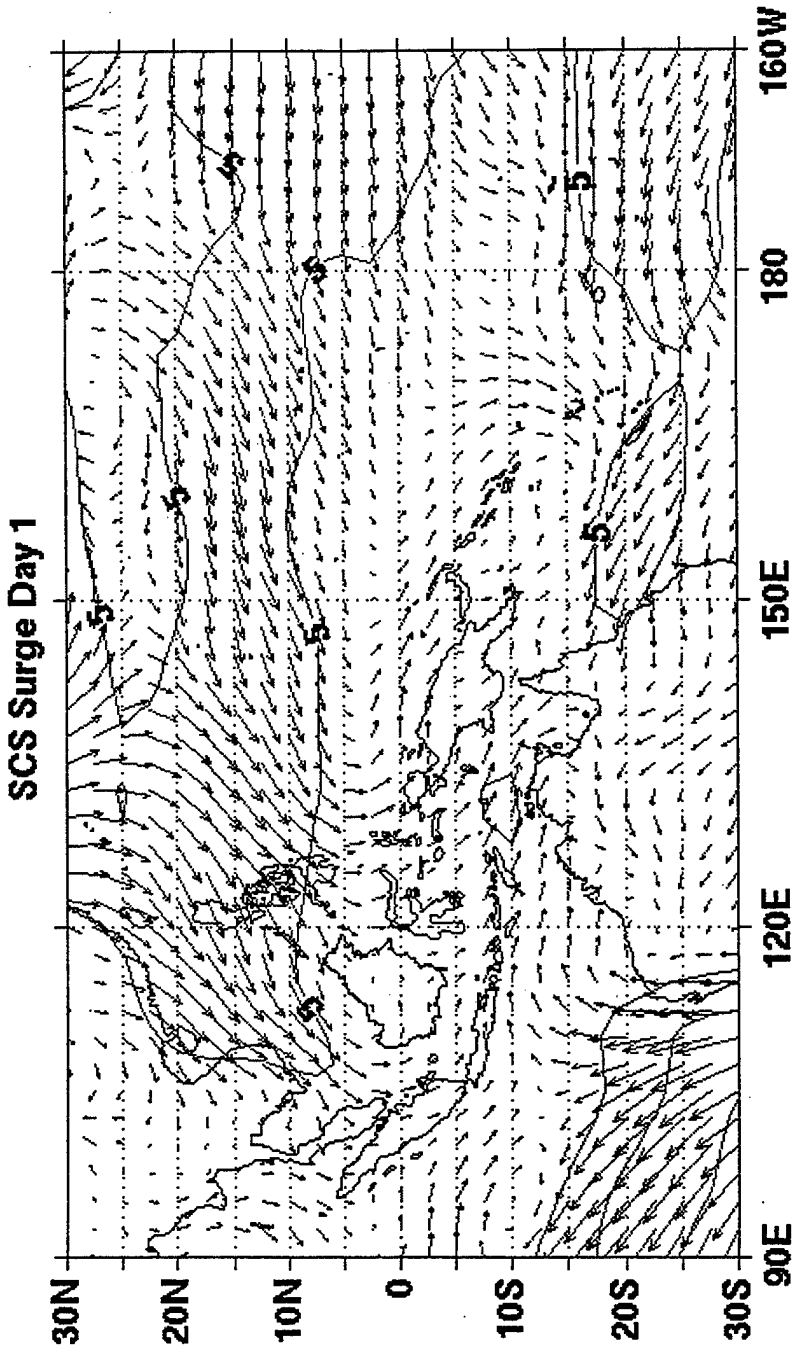

Figure 12. One day after the beginning of the South China Sea Surge.

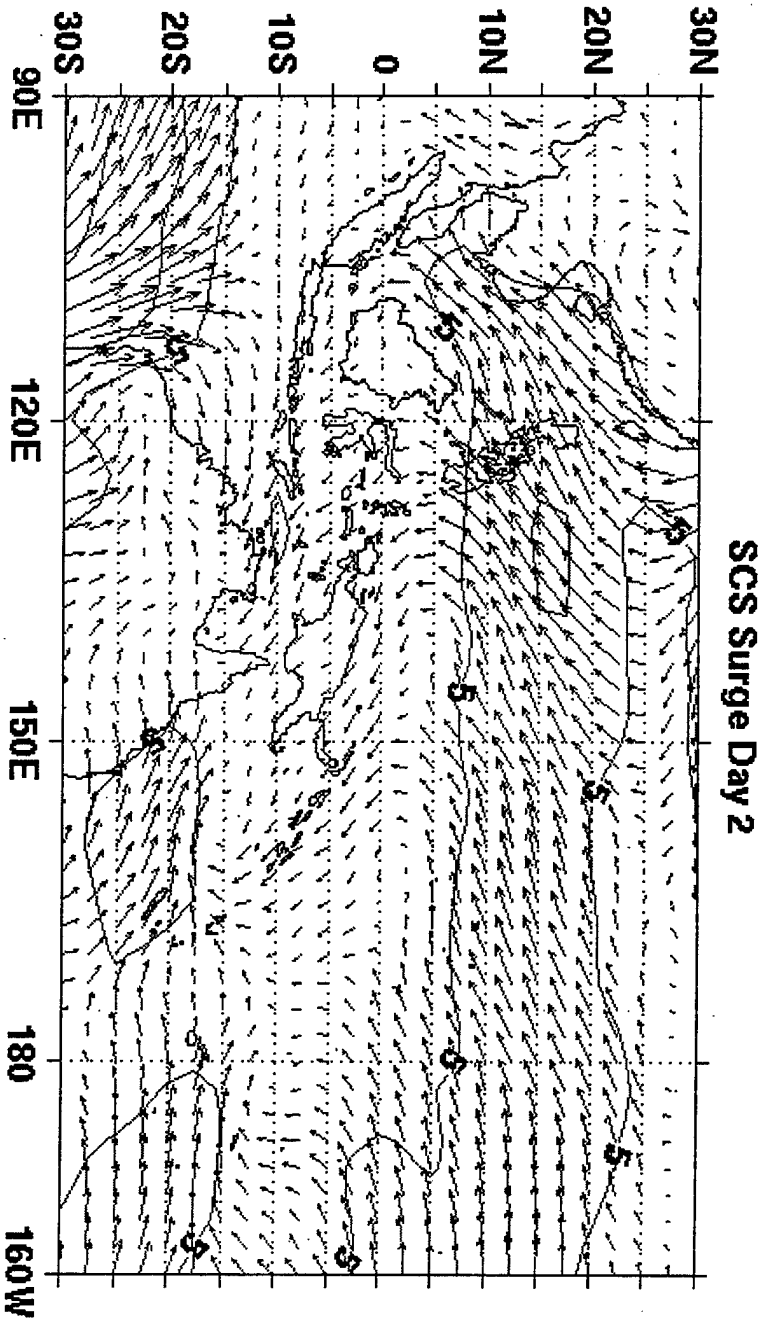

Figure 13. Two days after the beginning of the South China Sea Surge.

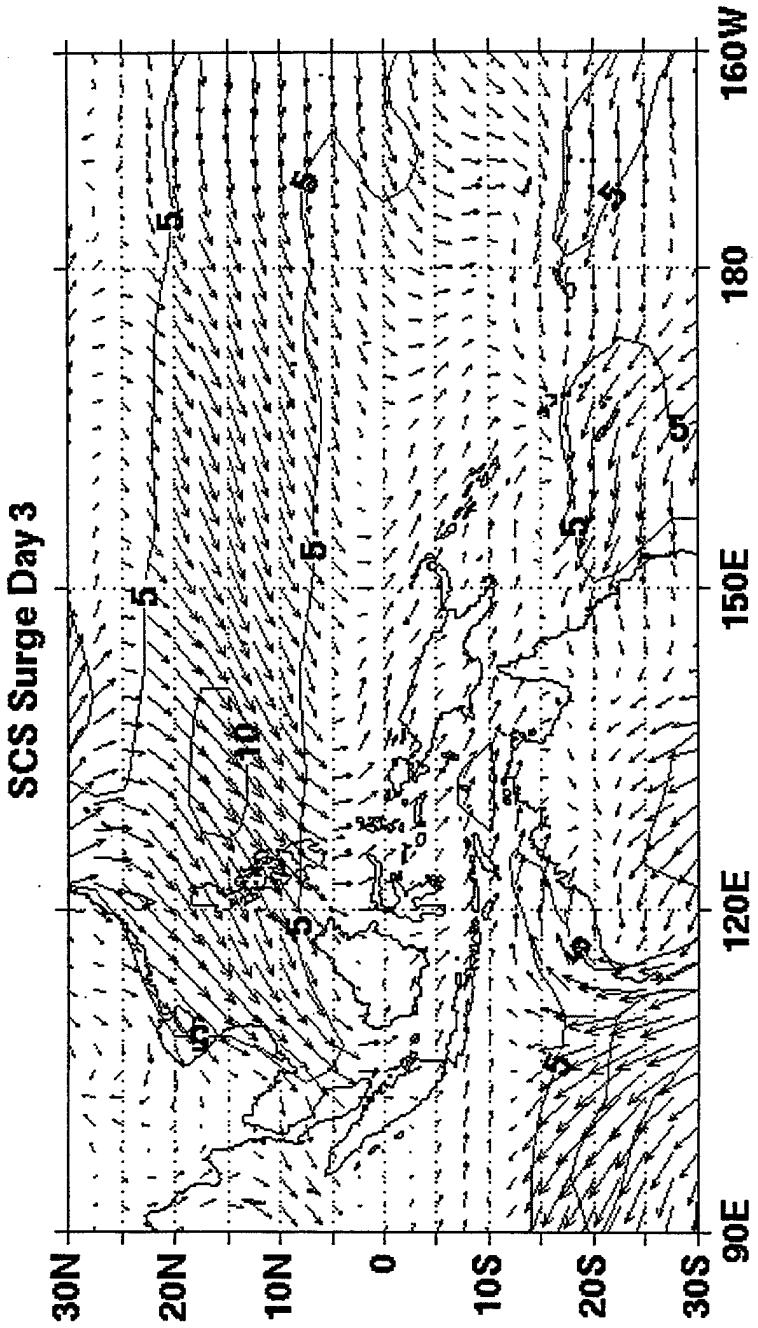

Figure 14. Three days after the beginning of the South China Sea Surge.

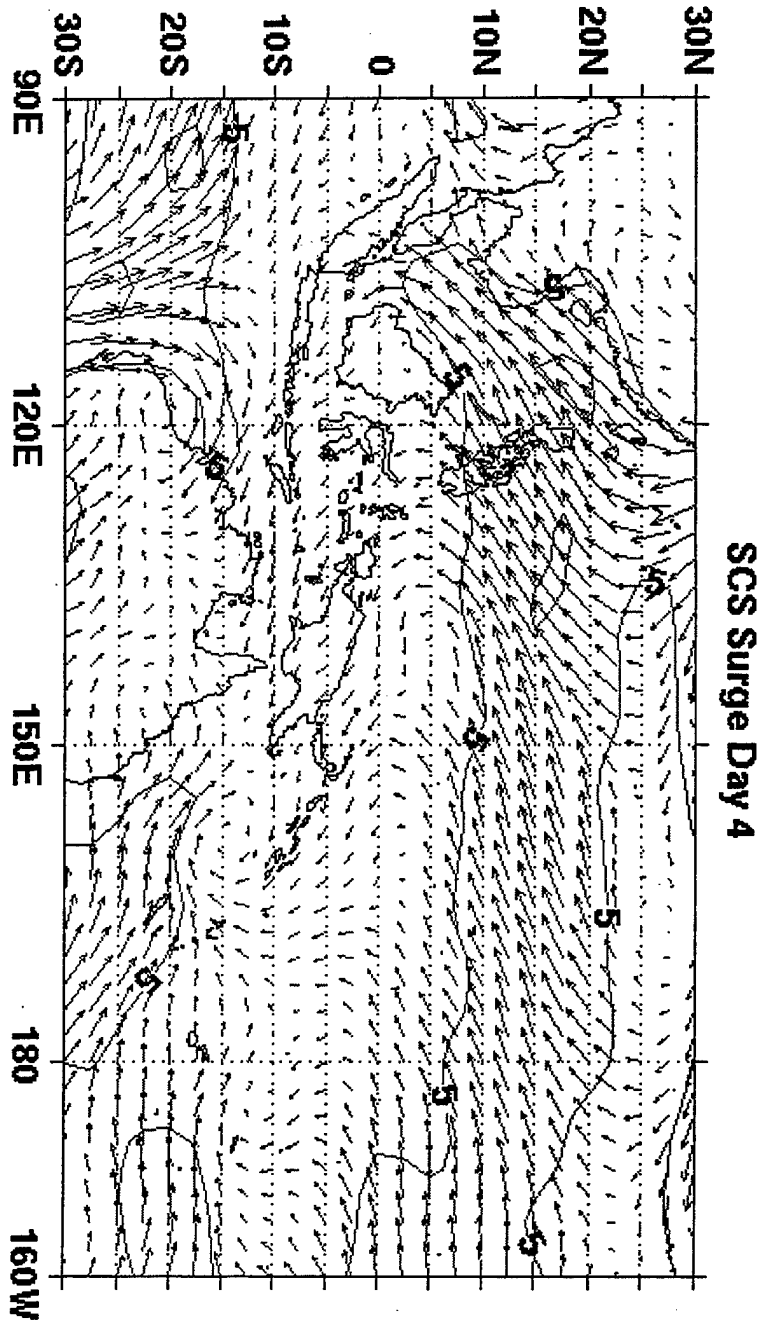

Figure 15. Four days after the beginning of the South China Sea Surge.

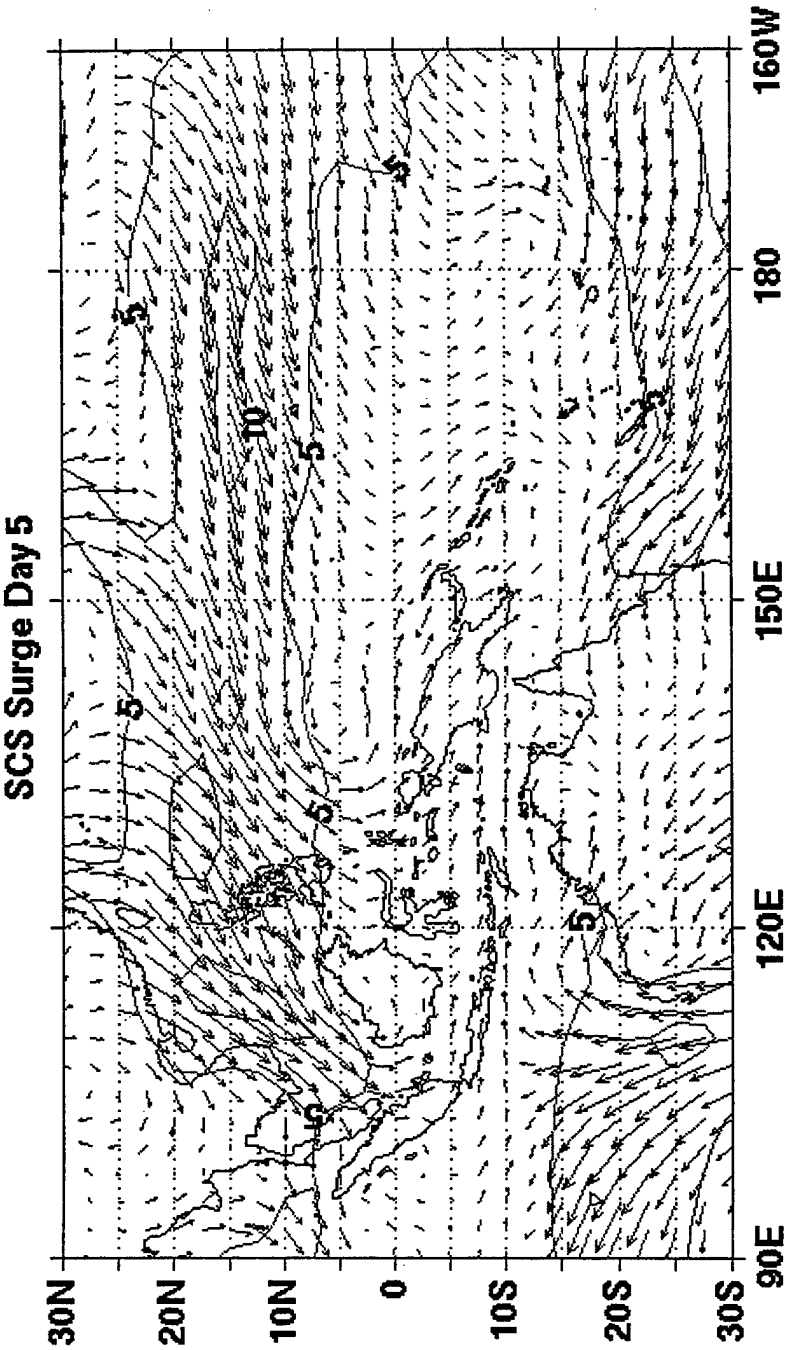

Figure 16. Five days after to the beginning of the South China Sea Surge.

V. TIME SECTION OF THE CONVECTIVE INDEX (CI)

To show the time evolution of the tropical cloud clusters, time-longitude cross sections of the CI for three different latitudinal bands are plotted. Figures 17, 18 and 19 show the CI averaged between the equator and 10N, between 5S and 5N, and between 15S and the equator, respectively. From these diagrams it will be easier to trace both standing and propagating cloud patterns. For example, the MJO would appear as eastward propagating waves with a period of around 30-60 days, where the cloudy areas are the wet phase and the relatively clear area are the dry phase. As a reminder, most of the convection will occur in the summer hemisphere, so in this case the 15S-equator strip (Figure 19, which covers the Australian monsoon trough axis, is expected to contain more convection.

Figure 17 shows the CI averaged between the equator and 10N, or the activity that is in the winter hemisphere. The chart shows that the majority of the convective activity occurs west of the dateline. It appears that the most active convection occurs during most of December over the eastern Indian Ocean and over northern Sumatra and northwestern Maylasia to the east of Borneo (90E to 120E). A weaker signal of convection occurs over the same area during February. This chart show both westward and eastward propagating cloud patterns. Several westward-propagating

cloud clusters may be associated with tropical easterly waves. The more prominent clusters are in mid to late December and there is a stronger one in mid to late January that starts near 170E. There are two eastward-propagating patterns that start from the western boundary in early December and around 9 February. The former appear to propagate to 120E and the latter to a few degrees beyond 120E. As will be seen later, these two patterns are part of the wet phase of two MJO episodes whose main convective activity was located south of the equator.

Figure 18 depicts the CI averaged between 5S to 5N. This average takes into account both the winter and summer hemisphere convection. The convection here is significantly stronger with more extensive horizontal coverage than from the equator to 10N, but again diminishes east of the dateline. The strongest convective signals are the two eastward-propagating cloud patterns associated with the wet phase of two MJO episodes that extend from the Indian Ocean to the central Pacific Ocean in December and early February to early March. Westward propagating patterns are also prominent in January and early February, a period between the two MJO wet phases, resulting in active convection in the equatorial Indian Ocean and the Sumatra-Borneo region that are not associated with the passing of an MJO (BM/NTR 1997).

Figure 19 shows the convection averaged between the equator and 15S. This is more representative of the summer hemisphere convection activity since the Australian monsoon trough axis is located within or slightly to the south of this latitude band. This chart actually shows many more features than the previous two. The convection does not decrease east of the dateline, but actually appears to propagate into the SPCZ. Two eastward-propagating cloud clusters, one in December and the other in early February, can be traced across the entire region starting from the Indian Ocean, crossing the dateline and continuing into the SPCZ. These are clear signals of the wet phases of two MJO episodes. Compared to the previous two figures, the MJO cloud clusters are centered in the southern equatorial belt and show persistent convection as they propagate through the region. Since the signals disappear beyond the dateline in the equatorial section (Figure 18), it appear that the MJO's cloud clusters turn southeastward and move into the SPCZ. In the meantime, signals of westward-propagating waves can still be seen clearly in Figure 19. The westward-propagating waves west of the dateline in early December and east of the dateline between mid January and mid February appear outside of the MJO cloud clusters. Thus they do not seem to be the westward-propagating shorter waves spawned from the super cloud clusters of the MJO as reported by several previous investigators (e.g., Nakazawa 1988).

Rather, they seem to be easterly waves that originated from the central or eastern Pacific independent of MJO. Based on Figure 19, it can be determined that it took about 35 days for the MJO super cloud clusters to propagate from the eastern Indian Ocean on the western boundary of the chart to the eastern Pacific Ocean on the eastern boundary.

Liebmann et al. (1994) reported that the active convection areas of MJO's are favorable areas of tropical cyclogenesis. They showed that this is simply due to the fact that there are more tropical depressions in these areas compared to the inactive (dry phase) areas. On the other hand, the percentage of cyclone development from the depressions is about the same between the active and inactive areas. To study the roles of the MJO in tropical cyclone formation, the location of tropical depression centers in the equatorial region, whose maximum winds first reached 30 knots, are plotted in the northern equatorial (equator to 10N) and southern equatorial (15S to equator) CI time sections and shown in Figures 20 and 21 respectively. At 30 knots the depression is relatively intense but it is still below the JTWC definition of a tropical cyclone and it will be referred to as a pre-formation center.

In the northern equatorial belt (Figure 20), three depressions that eventually developed into tropical cyclone Fern, Greg and Hannah, are shown. The first two locations are near the vicinity of an MJO active area, while the third

is not. In the southern equatorial belt (Figure 21), the two MJO wet phases can be delineated by tracing the two super cloud clusters eastward through the entire domain, so straight lines are plotted to mark the active areas. It can be seen that seven depression centers can be identified in the first MJO wet phase and five can be identified in the second MJO wet phase. Centers in the first MJO wet phase lead to the development of tropical cyclones Nicholas, Ophelia, Phil, Fergus, Drena, Rachel and Evan. Centers in the second MJO wet phase lead to the development of tropical cyclones 27S, Ita, Gavin, Justin and Hina. In between the two MJO wet phases, only three pre-formation centers were found: one of which leading to the development of tropical cyclones Pancho and Helinda is in the eastern Indian Ocean near the western boundary of our domain. The other two centers, leading to the development of tropical cyclones Cillian and Harold, are in the vicinity of the ITCZ and SPCZ where influences of cold surges or easterly waves from the eastern and central Pacific are more likely to reach. The development of each of these centers will be studied individually by examining the daily 1000 hPa wind analysis and the CI maps in the next chapter.

The time sections of CI can help in answering the question of whether the northeasterly cold surge events may in some way be triggered by the passage of an MJO active phase in the tropics. Figure 22 contains each of the 7 cold

surge events from day 0 to day 5 (indicated by the black box). It is clear that other than the fifth surge occurring around middle February, the surges in the South China Sea are clearly not "induced" by the passage of an MJO active phase. On the contrary, there is some evidence that surges in the equatorial South China Sea tend to start during the inactive phase.

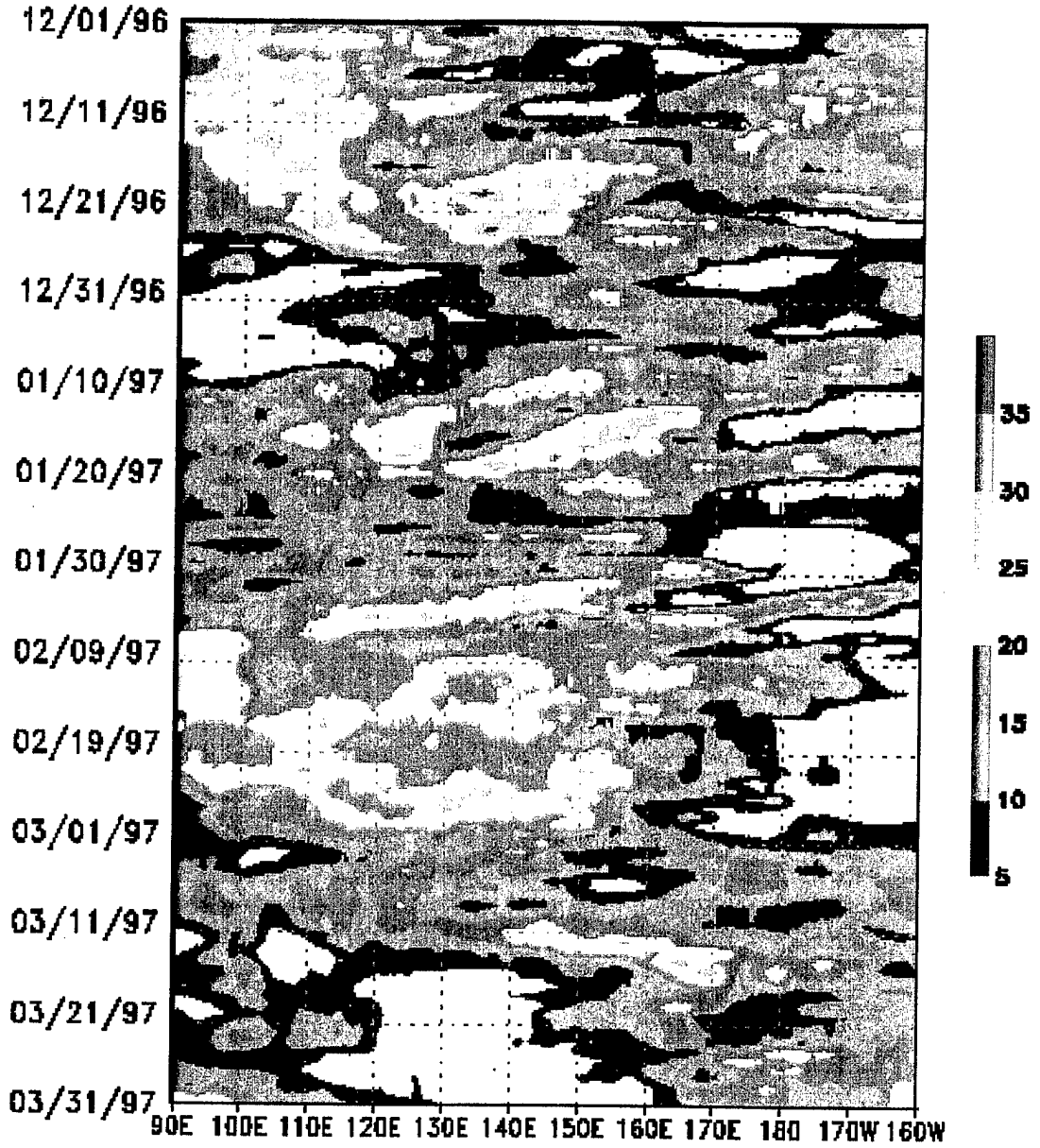

Figure 17. The time longitude cross section of the CI averaged over the equator to 10N.

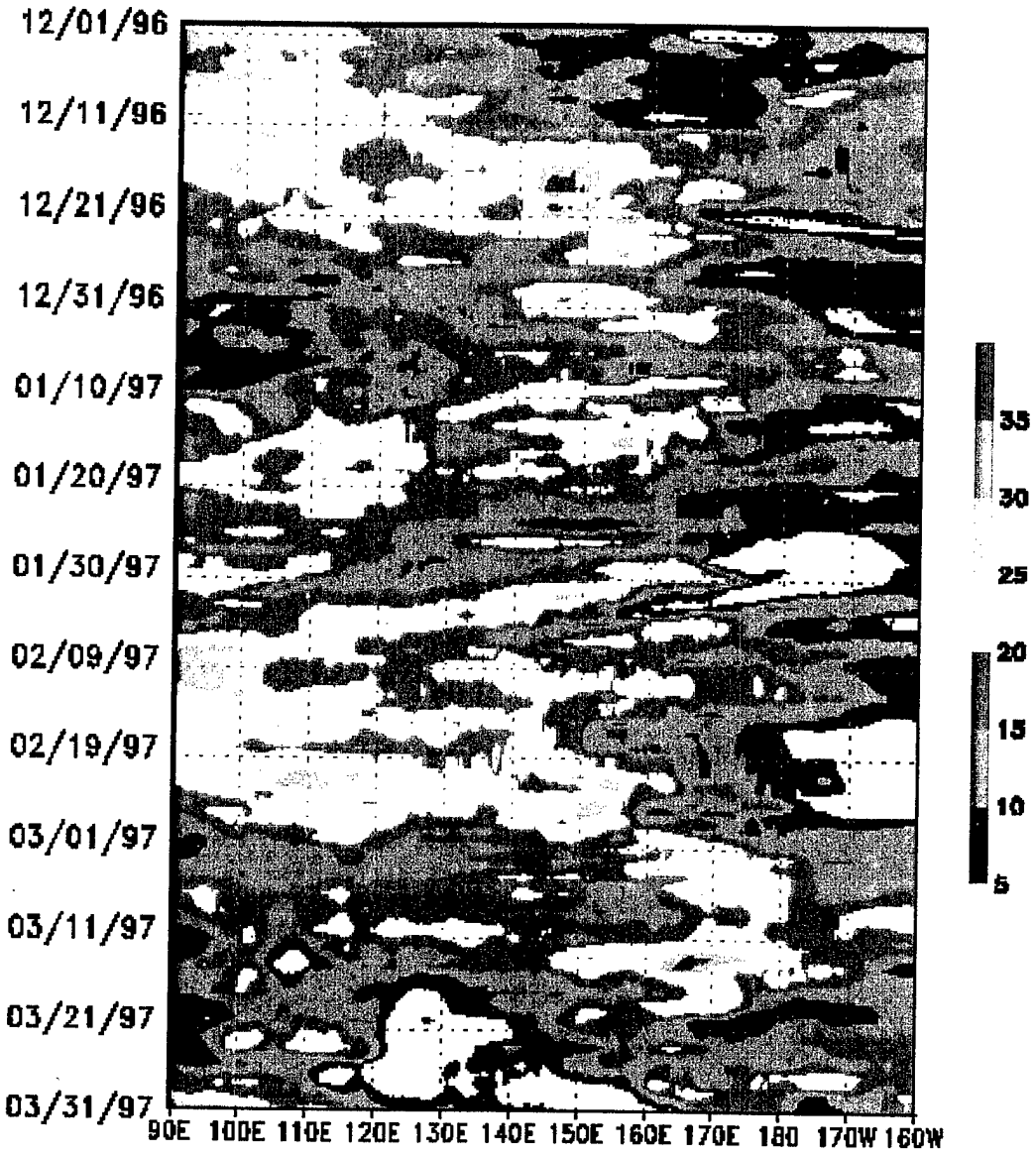

Figure 18. The time longitude cross section of CI averaged over 5S to 5N.

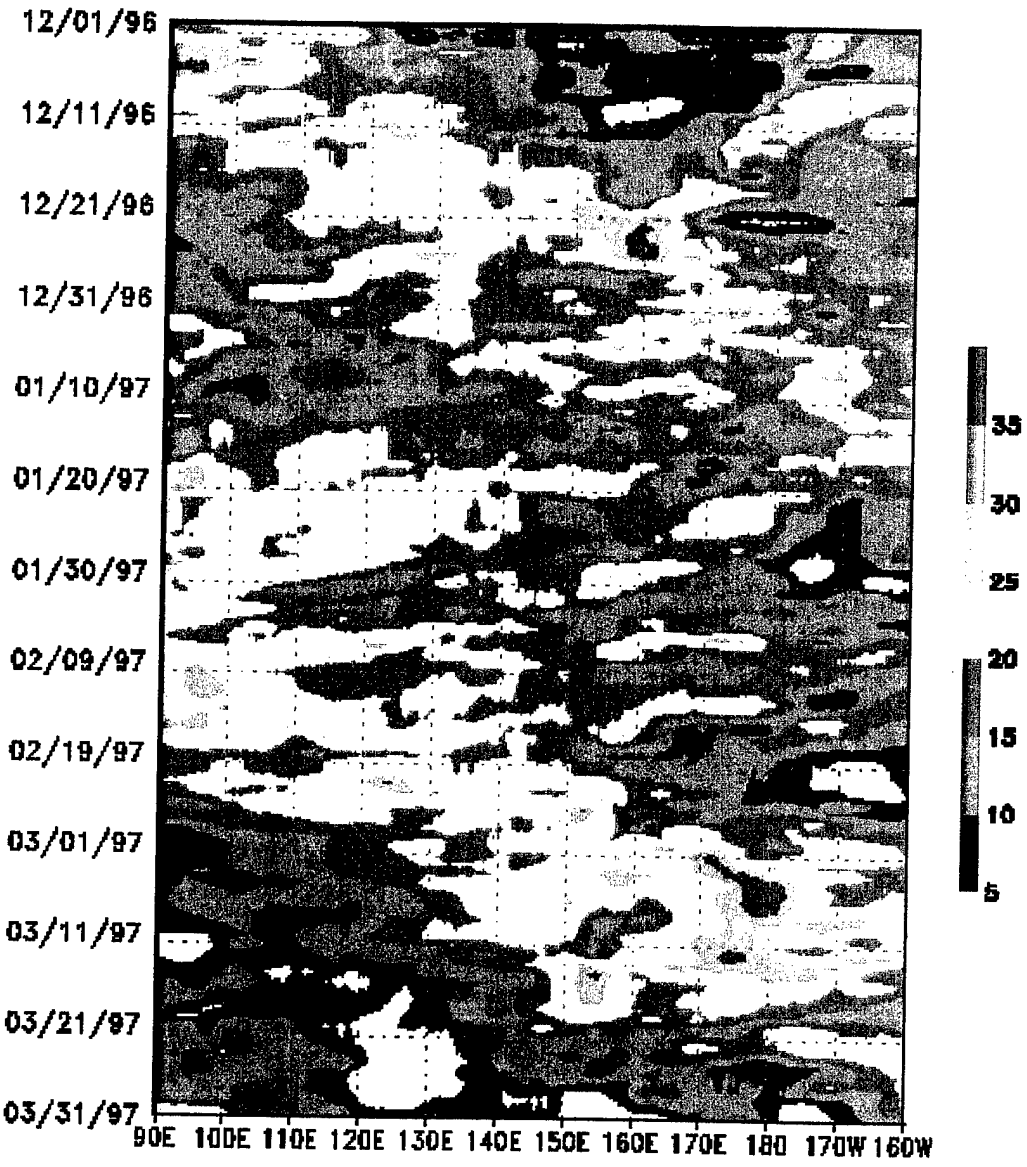

Figure 19. The time longitude cross section of CI averaged from the equator to 15S.

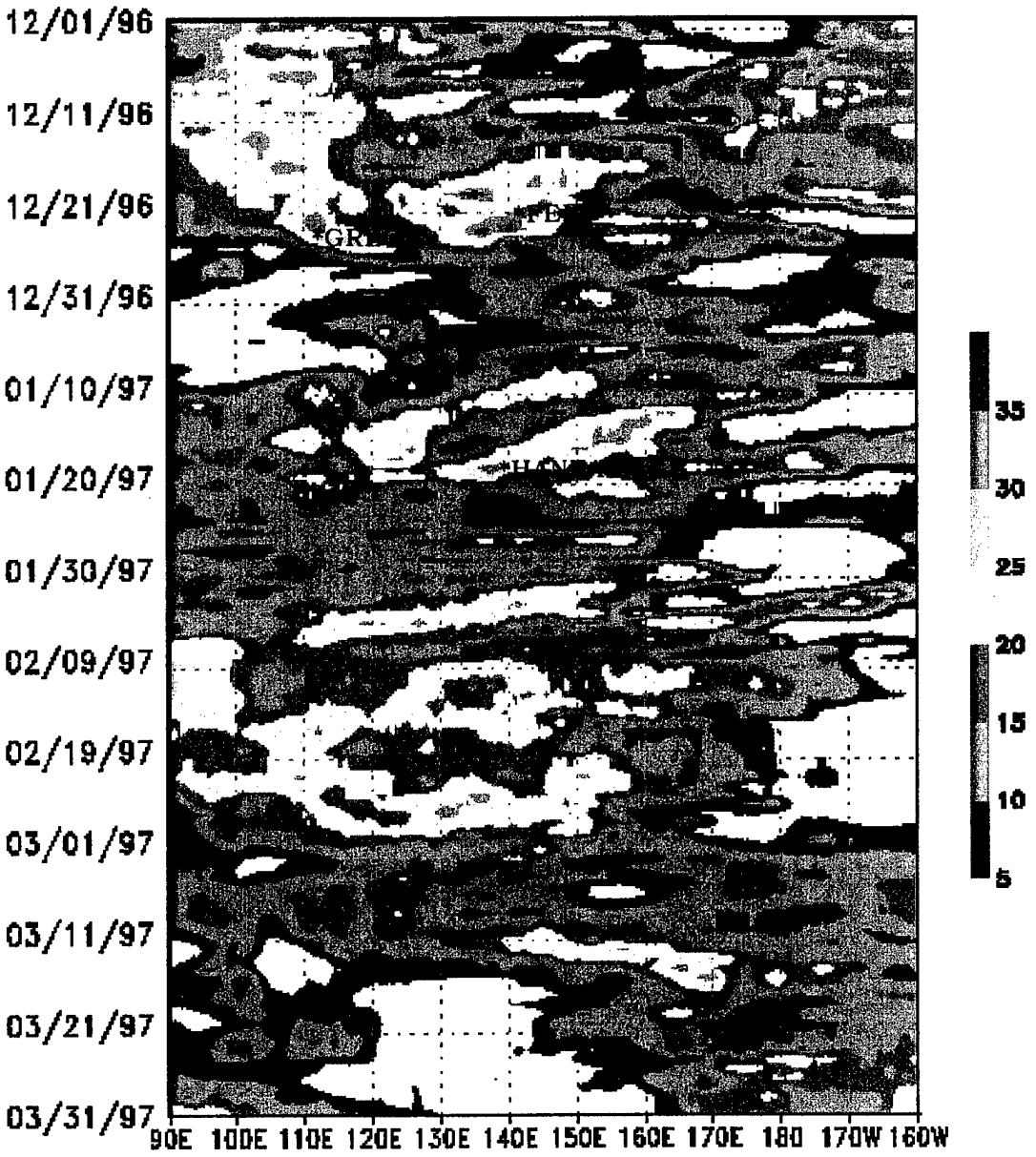

Figure 20. The same as Figure 17 with pre-formation centers plotted by day and longitude.

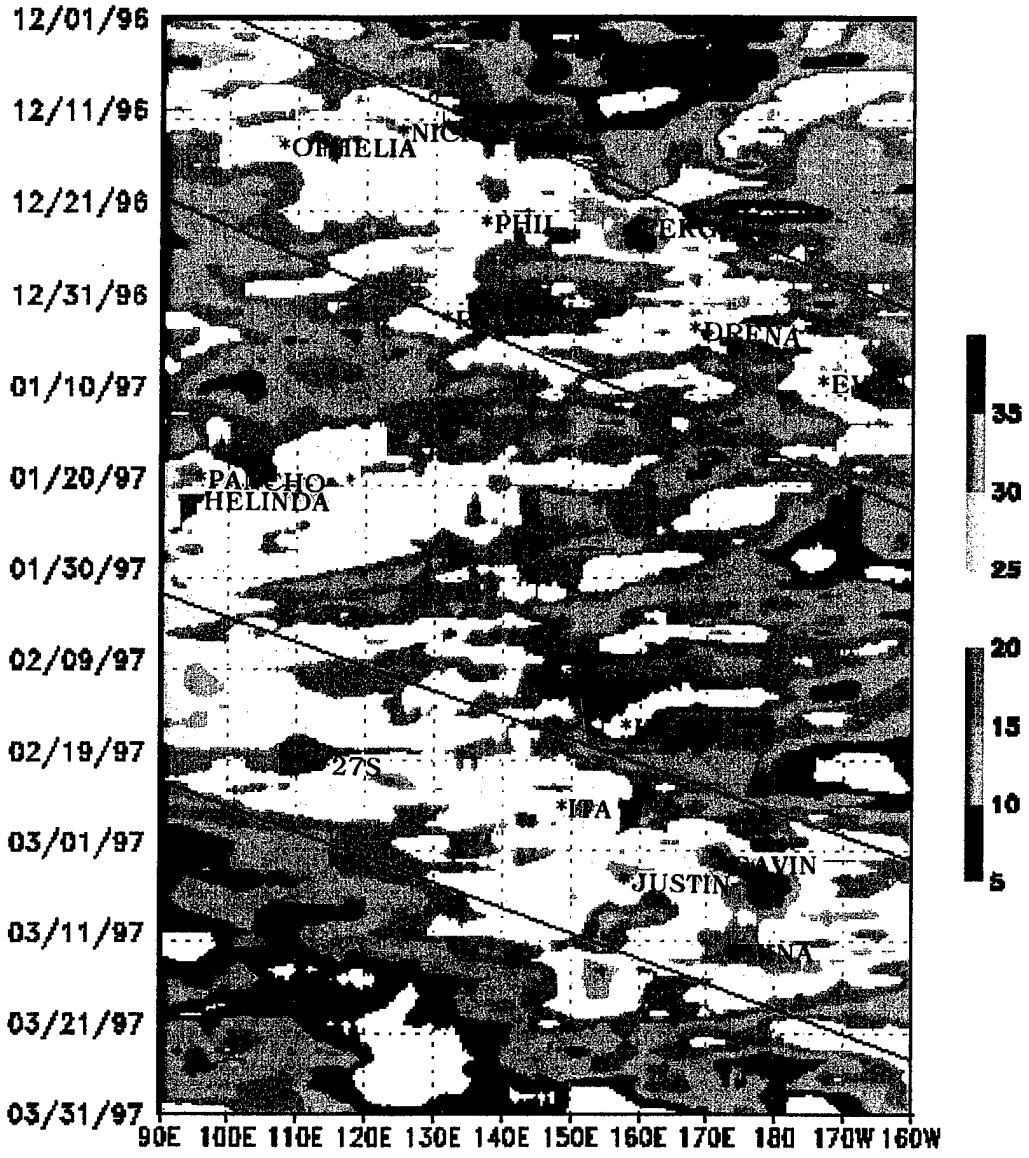

Figure 21. The same as Figure 19 with the MJO boundaries (black lines) and pre-formation centers plotted by day and longitude.

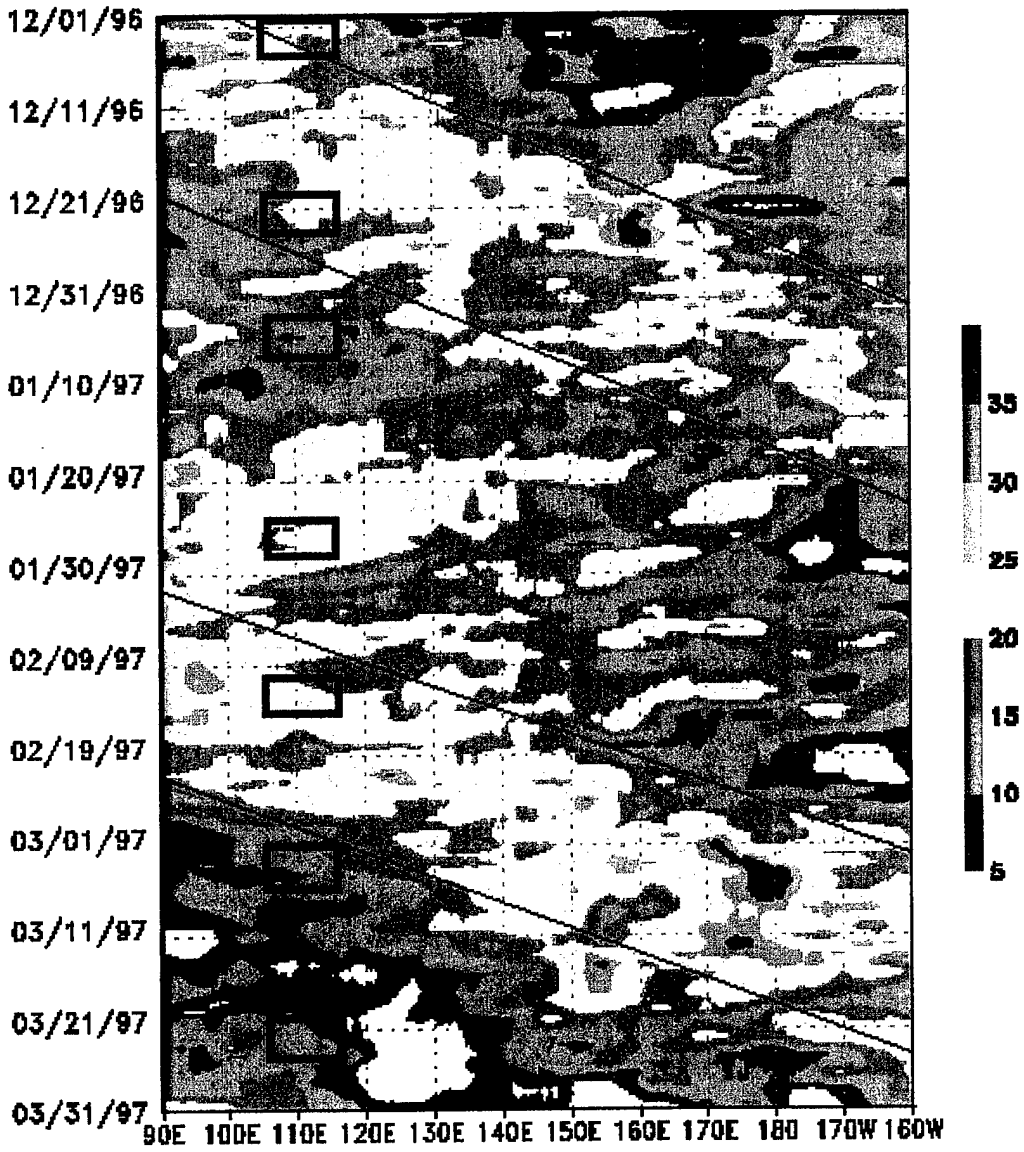

Figure 22. The CI averaged between the equator and 15S with the South China Sea cold surge events from day 0 to day 5 plotted in the black boxes and the MJO outlined by black lines.

VI. TROPICAL STORM DEVELOPMENT

Now that the South China Sea cold surges and the MJO have been identified for this period, attention is turned to how these and tropical waves may interact, and whether they may be associated with the development of tropical cyclones. This will be done by examining the daily charts of both the 1000 hPa winds and the CI. This chapter is divided into two parts; the first discusses all pre-formation centers in the northern tropics (equator to 20N), followed by a discussion of all pre-formation centers in the southern tropics (equator to 30S). When the NCEP wind circulation and the cloud pattern represented by the CI seem to indicate two different center locations, the NSCAT level-2 data will be used to verify the locations. In the examination of the daily charts, special emphasis is placed on finding possible relationships between tropical storm development and the transient systems including easterly waves, cold surge events and the passage of the MJO active phase.

A. NORTHERN HEMISPHERE TROPICAL STORM DEVELOPMENTS

There were 3 pre-formation centers that occurred in December and January in the Northern Hemisphere, each of them developed into a tropical storm. The development sequence of all three are shown in Figure 23 which is

comprised of the daily maps from 1 December to January 25 for the Northern tropics.

During the first half of December there was a general trend of increasing northeasterlies in the equatorial South China Sea. Daily charts indicate that the freshening of northeasterlies occurred across the entire area between 10N and 20N in the diagram, from the South China Sea to the central Pacific. Every few days the strength of the winds can be seen to diminish but rapidly increases again until around 16 December when the first cold surge event as defined by the surge index ended (Figure 6).

The first distinguishable easterly wave in the central Pacific appeared in the 1000 hPa wind field on 8 December. The cyclonic turning is seen from 6N,163W to 0,167W and is labeled *A* in Figure 23. Wave *A* continued to move rapidly westward along the equator through 11 December, maintaining its north-northeast to south-southwest orientation. Convection was observed to the northeast of the wave trough in a region of speed convergence. On 12 December, *A* became a closed circulation center at 3N,172.5E and continued to move westward and strengthened. The strengthening appeared to be helped by the increasing northeasterly winds to its north. The center was relatively free of convection between 14-15 December, after which the convection occurred to the south. The circulation continued increasing with increased

convection as it entered into a region that was the northern edge of the MJO active phase shown in Figure 20. By 21 December the maximum sustained winds of *A* reached 30 knots and it was identified as a pre-formation center for Tropical storm Fern. Therefore, the development of Fern appeared to be associated with an interaction of Wave *A* and the MJO.

Starting on 19 December, daily charts indicated a freshening of the northeasterlies which occurred from the South China Sea to the central Pacific. In addition, increased convection occurred to the south which was when the MJO active phase crossed the region. As early as 15 December, a closed circulation feature was seen at 2N, 111E, which appeared to be strengthened by the northeasterlies to the north. On 24 December, the sustained winds reached 30 knots and a pre-formation center for tropical storm Greg was identified. Since the deepest convection was not located near the low-level circulation center, the circulation pattern was cross-examined with NSCAT data and the patterns agreed. Since the development of this pre-formation center seems associated with the strengthening of the northeasterlies, it may therefore be related to the cold surges. In Figure 23.1 the timing of the center is compared with the cold surge index. The Figure shows that this pre-formation center occurred on day +5 of the second surge event.

The next distinguishable wave, *B*, started 22 December around 10N, 170W to 5N, 168W. The wave propagated west and on 24 December, convection occurred to the west of the trough for two days and then by 27 December the wave evolved into tropical storm Fern's circulation. As December drew to a close, there was minimum convection until around 9 January. According to the Australian bulletins, this convection was due to a high frequency disturbance (BM/NTR 1997). There was a freshening of northeasterlies which started on 3 January. As time progressed the northeasterlies broadened in longitude and by 8 January covered from the South China Sea to 160W between 7.5N to 20N. Around 13 January, the northeasterlies began to weaken across the entire region.

Another disturbance, *C*, was distinguishable on 5 January. This appeared as a zonally oriented cyclonic zone at 3N, 160E-170E. There was minimum convection with this system as it slowly moved westward. Convection did not generate until 10 January when the circulation became closed at 1N, 148E. Wave *C* then weakened into a trough for 2 days and became a closed circulation for two days, and finally weakened and disappeared by 16 January.

The next distinguishable disturbance, *D*, was located through cyclonic turning and convection on 11 January around 8N, 178E to 2.5N, 178W. This disturbance, oriented

northwest to southeast, moved south and became a closed circulation on 14 January at 3N, 157E. This closed circulation moved westward for a few days, gained strength and reached sustained winds of 30 knots on 19 January. It became the pre-formation center for tropical storm Hannah. The NCEP 1000 hPa winds did not pick up the closed circulation until 20 January, but the NSCAT data showed a closed circulation on 19 January (Figure 23.2).

There are no other tropical storms during this season in the Northern Hemisphere, so analysis of the daily charts will end here. A brief synopsis of all three pre-formation center is provided in Table 2 organized by names. This table shows the possible association between the formation of each northern tropical storm in this season and the other large-scale transient motions.

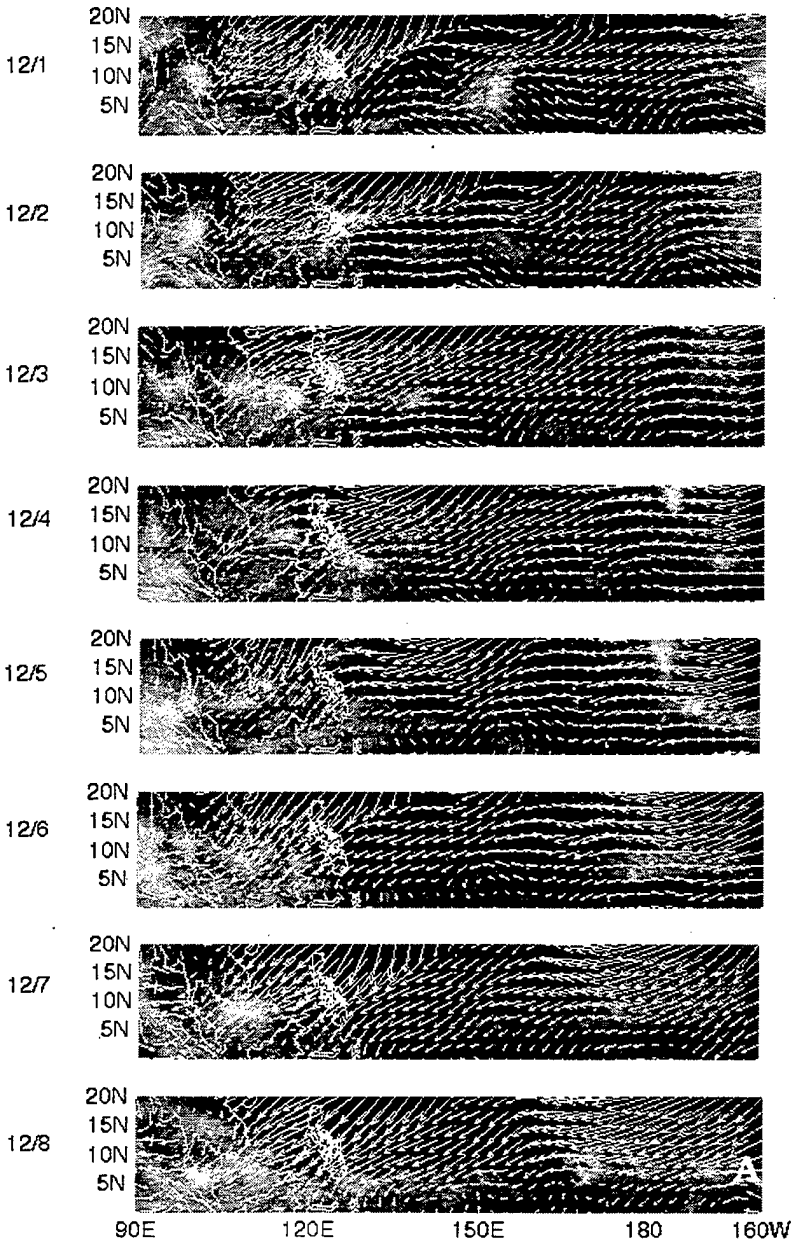

Figure 23 . Daily plots of 1000 hPa and CI of the Northern Hemisphere.

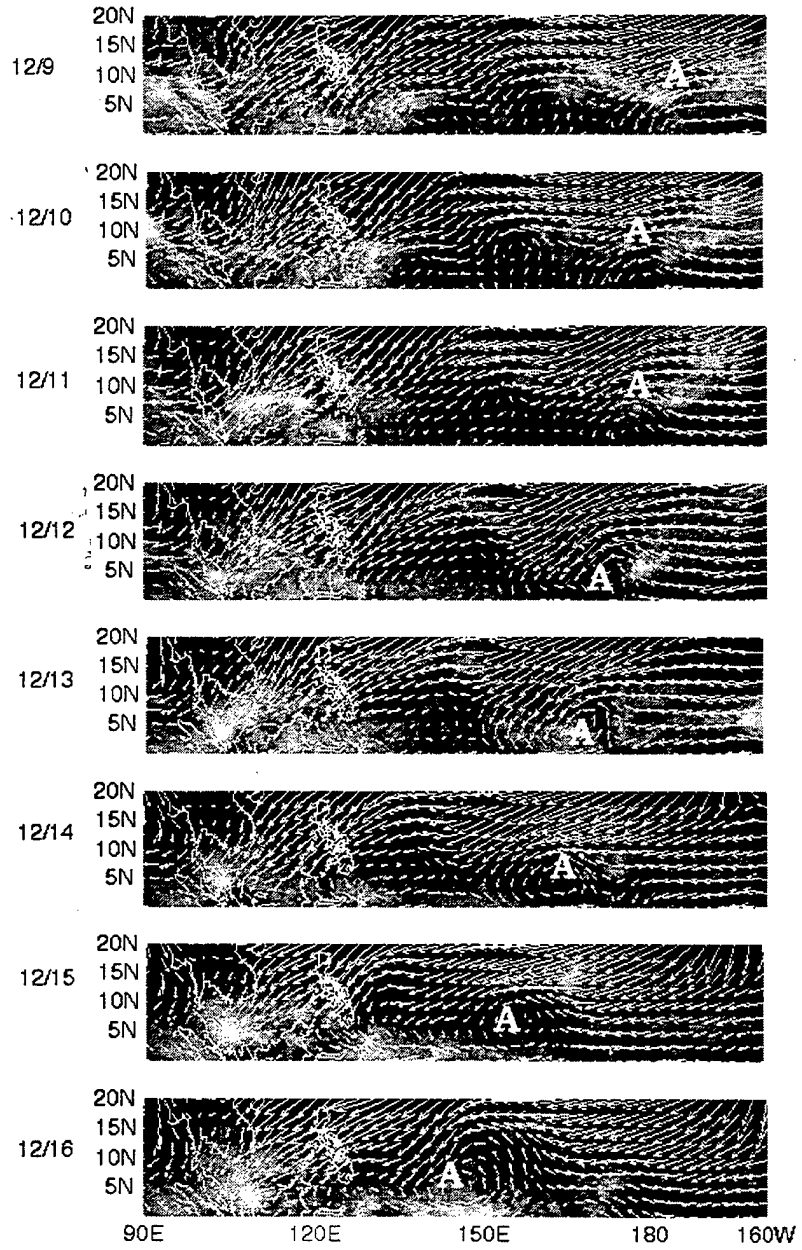

Figure 23 continued.

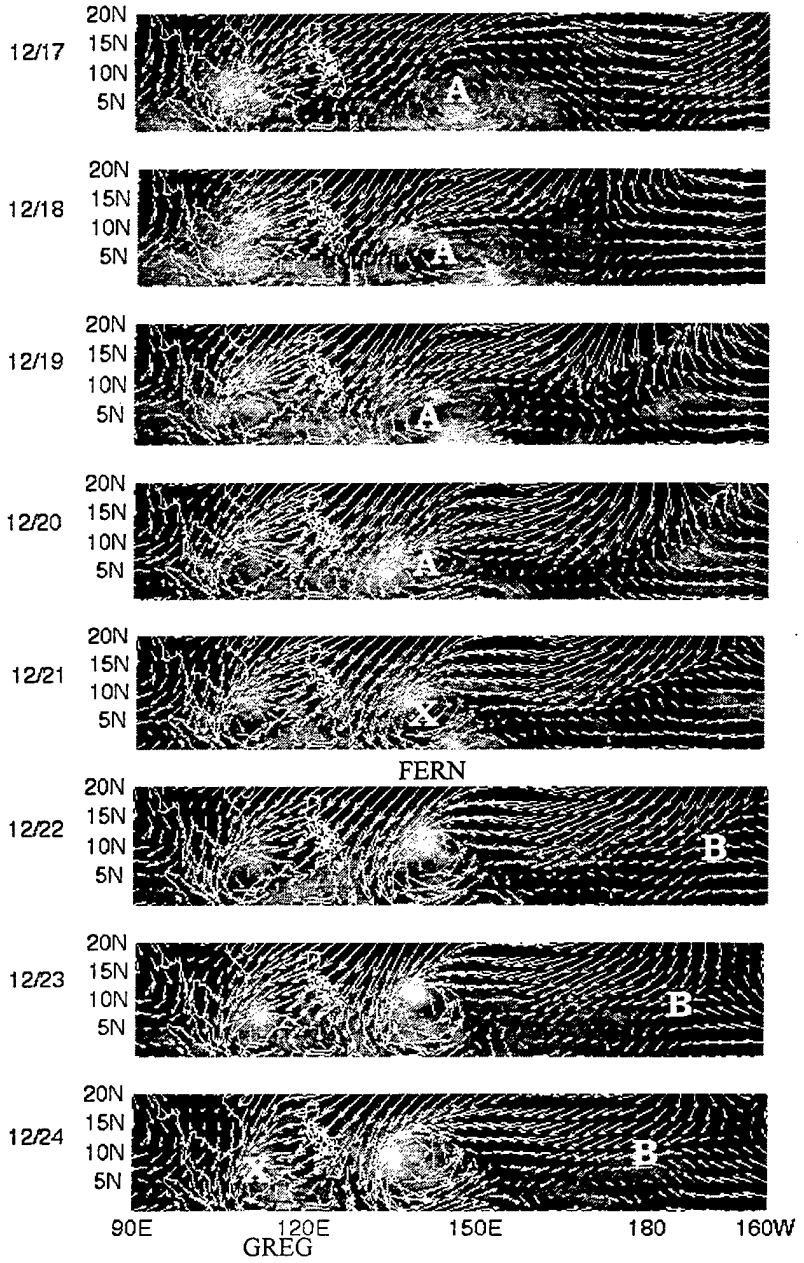

Figure 23 continued.

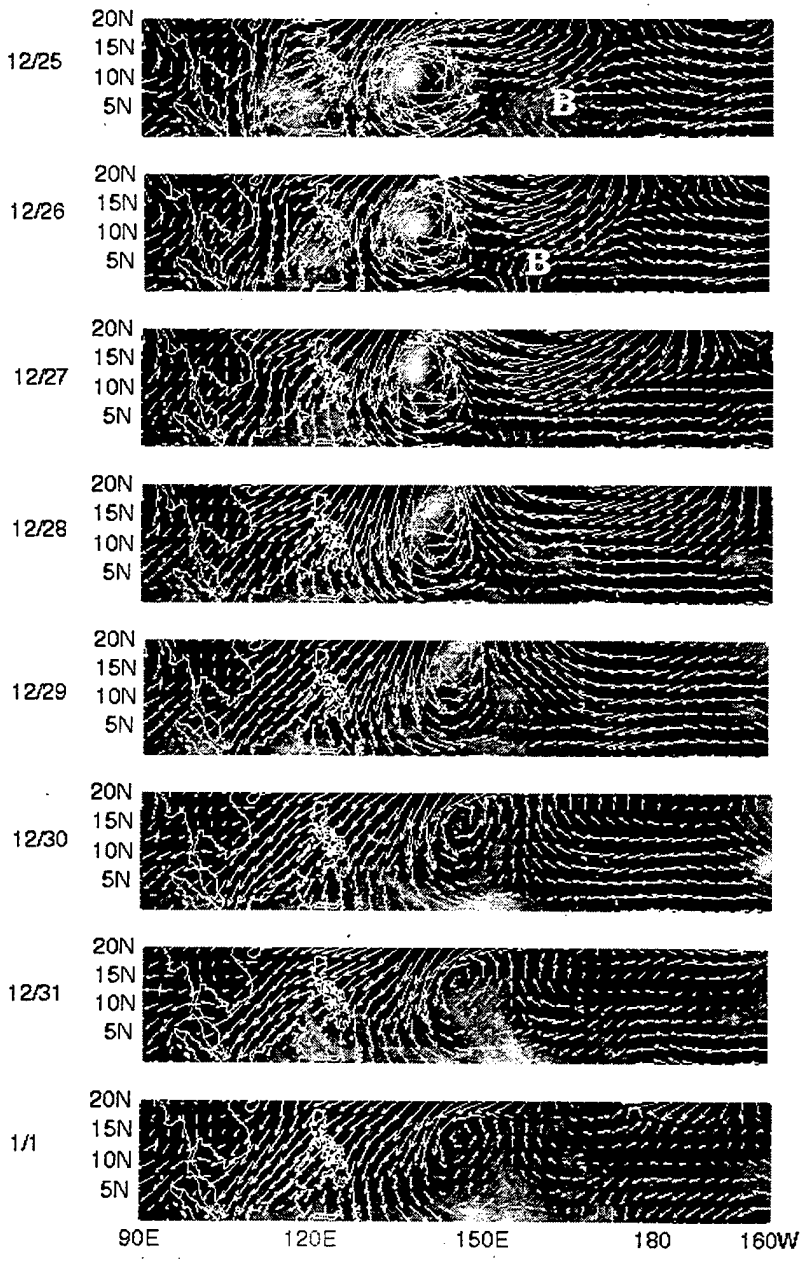

Figure 23 continued.

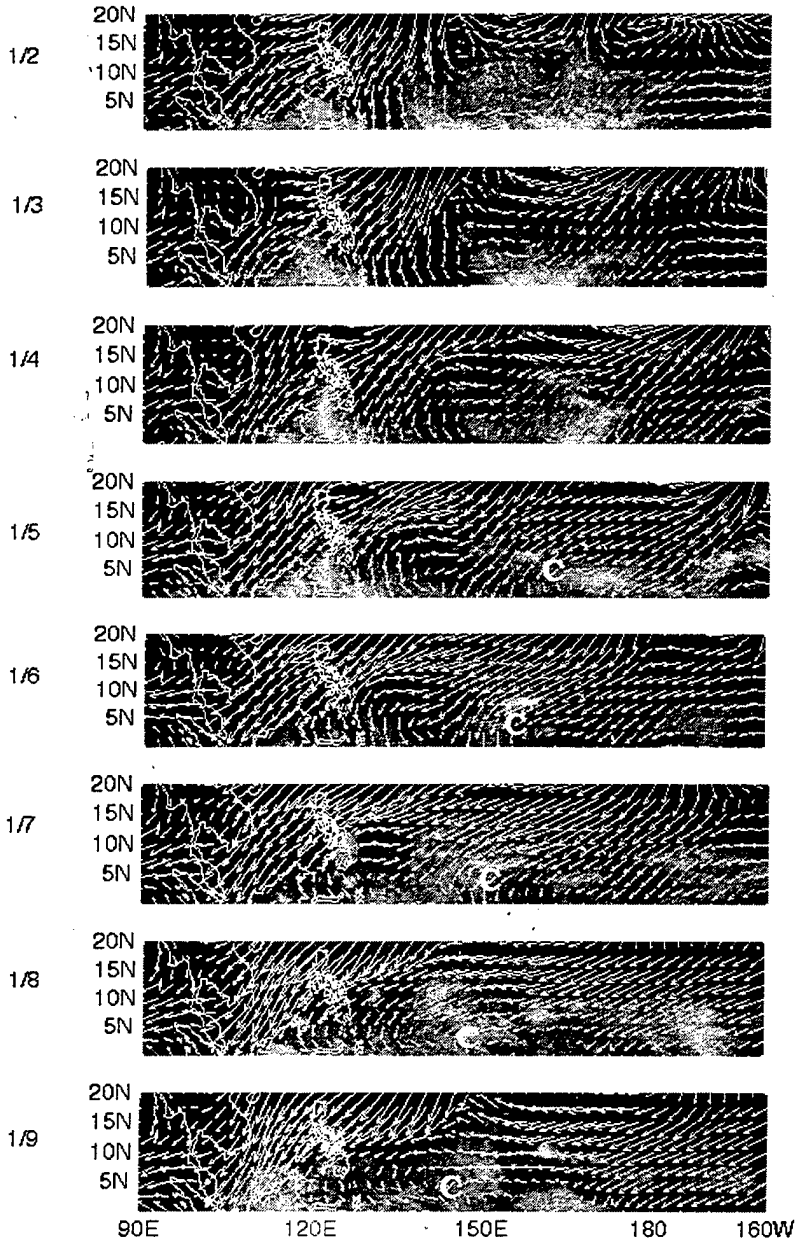

Figure 23 continued.

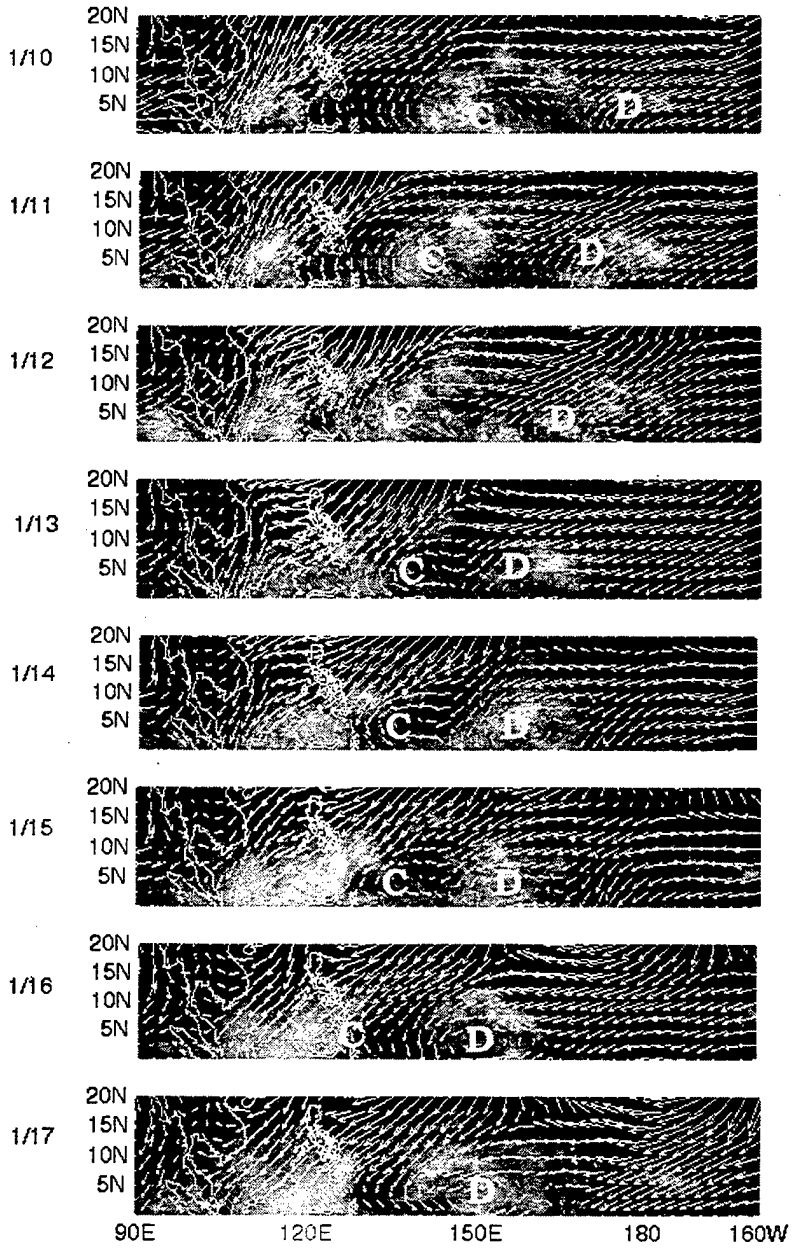

Figure 23 continued.

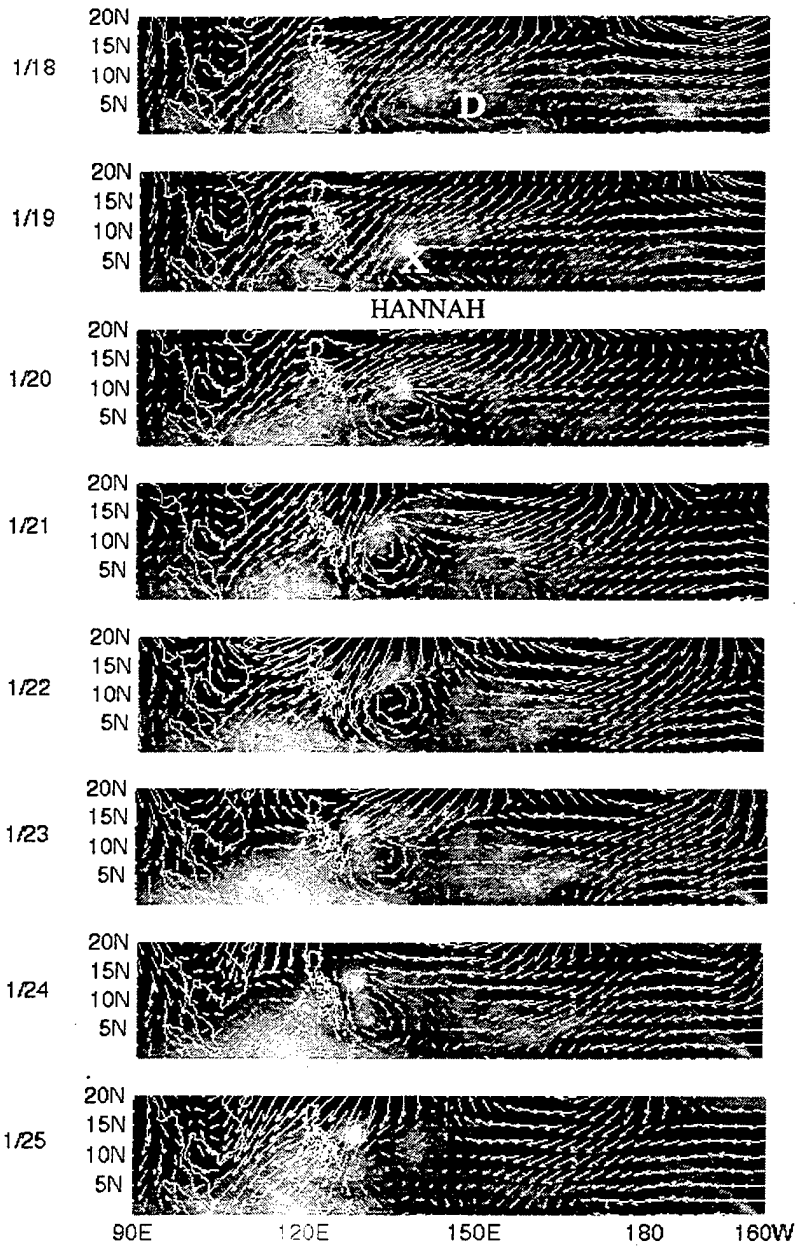

Figure 23 continued.

			Association			
Storm	Date	Location	MJO	Surge	Wave	Other
Fern	12/21/96	8.0N 141.8E	X		X	
Greg	12/24/96	7.3N 112.4E	X	X		
Hannah	1/19/97	6.0N 139.7E		X		

Table 2. A synopsis of the Northern Hemisphere tropical storms; the start of 30-knot winds and the facts associated with their development.

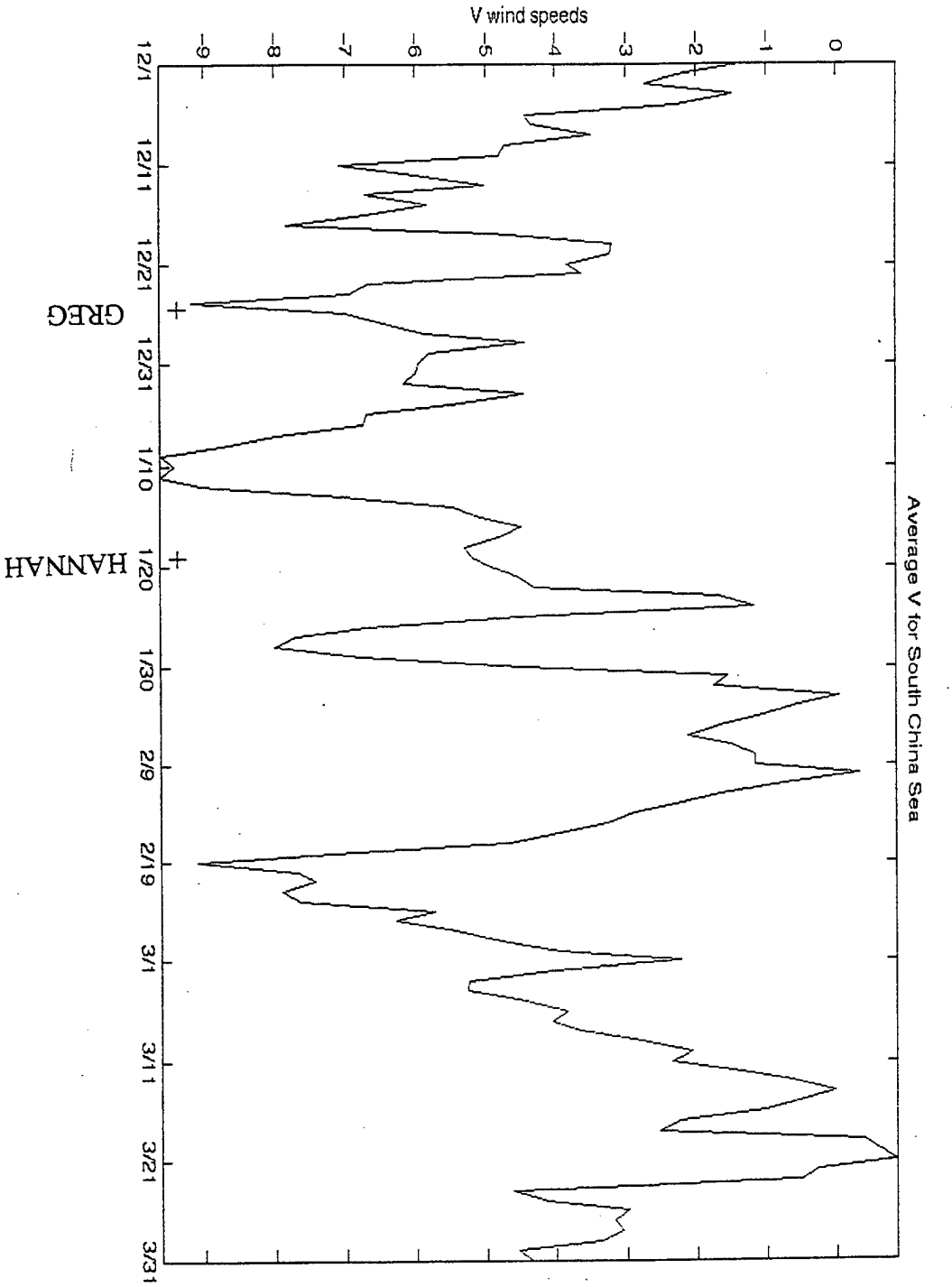

Figure 24. The Northern pre-formatin centers plotted on the cold surge index time series.

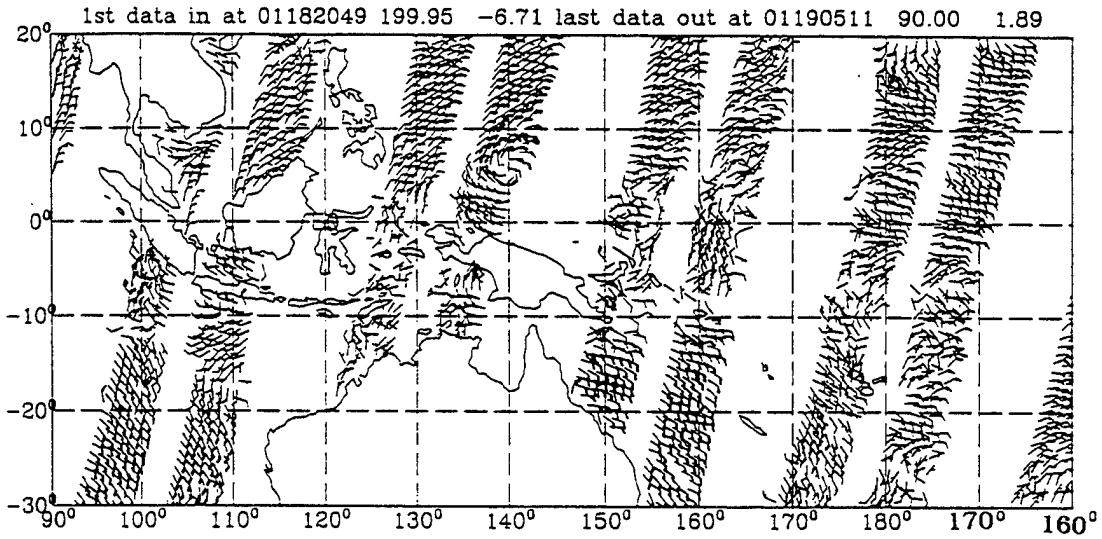

Figure 25. The wind field using NSCAT level 2 data to identify the pre-formation center that became Tropical Storm Hannah. Hannah is located at 6.0N, 139.7E.

B. SOUTHERN HEMISPHERE TROPICAL STORM DEVELOPMENTS

The daily charts for the Southern Hemisphere (Figure 26) will be used chronologically to discuss the activities of the easterly waves, cold surges and MJO's and their possible relationship with the pre-formation centers. The charts extend from the equator to 20S.

The first disturbance, easterly wave, *A*, was seen in the wind and CI pattern on 1 December extending from 8S, 180 to 15S, 170W. The trough moved slowly to the southwest and strengthened into a closed circulation center on 2 December at 10S, 178W. Convection remained to the east of the trough axis. The circulation weakened on 5 December and by 7 December, the wave disappeared against anticyclonic turning from the south. On 6 December, the second disturbance, *B*, propagated into the domain. The disturbance began around 10S, 160W and became a closed circulation 24 h later. The wave, associated with strong convection to the northeast of the wave trough, continued to strengthen and moved southwestward until 9 December where the propagation turned westward and the closed circulation became an open trough. Between 10-16 December, the convection stayed intense while the circulation pattern alternated between an open wave and a closed circulation. The convection to the east began to weaken on 15 December. *B* continued to move westward until

it became stationary on 19 December for a few days. It eventually was merged by another wave from the east, *C*, which will be discussed later.

While wave *B* was propagating westward, two pre-formation centers were located to its west. Both centers developed in the monsoon trough to the northwest of Australia. The first pre-formation center later developed into tropical storm Nicholas, which began as a tropical low in the northern Gulf of Carpentaria in the developing monsoon trough (Darwin Tropical Diagnostic Statement 1996). This storm formed in an area of increased convection which was part of the super cloud cluster during the active phase of the MJO depicted in Figure 21. In addition, as discussed in Chapter 6A, there was a sustained cold surge in the South China Sea during the first half of December. In Chapter IV, the composites of 1000 hPa winds indicated that during surges the Southern Hemisphere tropics tends to contain a strengthening of the cyclone/anticyclone pair to the west of Australia that gives rise to a favorable condition for cyclone development in the vicinity of the formation of Nicholas. Thus, both MJO and cold surges may be related to the formation of Nicholas.

The second pre-formation center to the west of *B* developed one day later, 10S, 108E on 14 December, also in the area of MJO convection. It became tropical storm Ophelia

almost immediately (BM/NTR 1997). The timing corresponds to day 5 of the first South China Sea cold surge (Table 1). The location of this pre-formation center is near the northern fringe of the cyclonic area northwest of Australia shown in the day 5 cold surge composite (Figure 16 and Table 1). Thus, it is possible that it may still be related to favorable conditions following the development of the South China Sea cold surge.

The next pre-formation center reached sustained winds of 30 knots on 23 December which led to the development of tropical storm Phil. It occurred in the middle of the active convection area of MJO at 11.9S, 138.2E. This also corresponds to day 4 of the second cold surge event in the South China Sea (Figure 16 and Table 1).

Wave *C* developed around 16 December with an axis extending from 0, 178W to 8S, 175W. It moved rapidly west-southwestward generating a great deal of convection on 19 December northeast of its axis. Its circulation caught up with wave *B* on 20 December and continued to intensify. By 23 December the circulation also reached pre-formation status and eventually became tropical Storm Fergus. Thus day 4 of the second South China Sea cold surge can also be related to this center. The location of the development was in the MJO active phase as depicted by Figure 21.

The development of the pre-formation center for Fergus followed by two days that of the Northern Hemisphere storm Fern. After Fergus formed, the 1000 hPa flow for the equatorial region began to resemble a slanted double vortex configuration. The evolution of the flow from 23 to 28 December is shown in Figure 26.1. Several previous investigators (e.g., Keen 1992; Ferreira et al. 1996) have pointed out the importance of cross-equatorial influence or MJO equatorial westerly wind burst that resulted in the development of a pair of tropical cyclones that straddle the equator. The pair may appear as a double vortex that is either north-south aligned (centered on the same longitude) or slanted (centered on different longitudes but the northerly cross-equatorial flow appeared to connect the two circulations). However, in the present case the development of the southern storm appeared to be influenced by several factors: wave *C*, the MJO, and the surge, plus the slanted double vortex configuration did not become mature until several days (27 or 28 December) after the formation of the southern storm. Thus, although a double vortex was observed, the tropical cyclone formation itself was not simply due to a "double-vortex mechanism" as proposed by the previous studies.

Another wave, *D*, transversed into the region on 20 December and oriented from 10S, 178W to 8S, 162W. Wave *D*

was simply a low-level feature and did not have any significant convection associated with it. This disturbance moved west and by 25 December merged with tropical storm Fergus' circulation and became part of it.

The next easterly wave to cross into the region occurred on 27 December. Wave *E*'s trough axis was located with the cloud feature from 2.5S, 162.5W to 12.5S, 162.5W, and it propagated quickly to the southwest and moved into an area of convection coming from the south. On 30 December, the wave merged completely into the super cloud cluster of the MJO (Figure 21) and the circulation became closed on 31 December. The system continued to intensify and on 2 January, the circulation reached pre-formation status and eventually became tropical Storm Drena. Another pre-formation center also formed on 2 January to the west of Drena at 11.3S, 131.9E which later became tropical storm Rachel. The formation of Rachel in the monsoon trough appeared to be largely a result of the passage of the active phase of the MJO, without any contribution from easterly waves or cold surges.

Wave *F* began on December 30 with ample convection and with its trough axis located at 10S, 162.5W to 15S, 160W. This axis was determined by both the cloud signature in SI and a cyclonic curvature in the NCEP wind field. The cloud feature stayed to the northeast of the cyclonic trough axis

as the disturbance continued to move southwest for more than 10 days. At the same time wave *F* was moving in, there was an increase in the cross-equatorial flow starting around 3 January. In addition, the cyclonic activity to the west and east of Australia strengthened until approximately 9 January, when it strengthened to 30 knots and became the pre-formation center for Evan. The timing corresponds to day 6 of the first South China Sea cold surge (Table 1) and the MJO was also reaching the vicinity of the disturbance (Figure 21). Thus, it appears that the formation of Evan was related to the development of the South China Sea cold surge, the MJO active phase and wave *F*.

The next storm included in Figure 26 developed in the open Indian Ocean away from most of the other formation areas. According to Darwin Tropical Diagnostic Statement (BM/NTR 1997), it developed from a "high frequency disturbance" in January. Pancho/Helinda had a convoluted track for two weeks and did not interact with the MJO, easterly wave or a South China Sea cold surge. During the remainder of January the entire region was under the inactive phase of MJO and there were also no discernable easterly waves, although a cold surge started around 24 January (Table 1).

The next discernible wave (*G*) moved in from central Pacific on 4 February, and its trough axis was oriented from

0, 180 to 12.5S, 175W. This wave moved to the west-southwest and became a closed circulation on 6 February and then began to weaken. The trough joined with a tropical low in the SPCZ and seemed to contribute to the spin up of a pre-formation center later named tropical storm Gillian. During the early part of February the active phase of MJO was still in the Indian Ocean and had not reached the west Pacific (Figure 21). Therefore, the development of the pre-formation center for Gillian was attributable to the wave disturbance only.

Wave *H* was seen in the convection field first on 7 February. This wave moved rapidly to the south and west toward the SPCZ. An increase in the cross-equatorial flow from a northeasterly cold surge began on 10 February and appeared to increase the cyclonic circulation of the SPCZ. As has been seen in previous disturbances, wave *H* was also associated with convection to the east of its trough axis. On 16 February its circulation enhanced and became a pre-formation center that developed into tropical storm Harold. It also appeared that the increased cross-equatorial flow around 140E-150E contributed to the spin up of the tropical storm. It is interesting to note that 16 February corresponds to day 6 of the fifth cold surge identified in Table 1.

The next wave, *I*, was first identified on 12 February when its convection can be seen on the eastern border of our area of interest. The low-level circulation became stronger on 14 February and moved southward out of our region by 18 February without becoming a pre-formation center.

The fifth cold surge that started on February 10 was followed by more than one pre-formation center. In addition to the pre-formation center for tropical storm Harold in the SPCZ region, the strengthening of the cyclonic circulation to the west and northwest of Australia appeared to have also affected the development of tropical storm 27S. The strengthening was interrupted temporarily between 12 and 13 February but resumed afterwards. The cyclonic circulation to the west of Australia reached maximum intensity around 19 February, which was the last day of the surge event with the South China Sea surge index reaching -9 m/s (Figure 6). During the same time, the active phase of the MJO was also moving into the region from the Indian Ocean (Figure 21). The conditions became conducive for a pre-formation center to develop and tropical storm 27S formed on 16 February. It reached a sustained maximum wind of 45 knots for four days, but it never became a named typhoon.

The third pre-formation center that may have been affected by the fifth surge event identified in Figure 6 was at 15.9S, 148.2E which led to the development of tropical

storm Ita. This storm reached sustained winds of 30 knots on 23 February. At this time, the fifth surge has already passed its maximum and the northerly winds in the South China Sea had retreated somewhat, but the surge index wind was still very strong, at about -7.8 m/s (Figure 6). Therefore both surge and MJO may have played a role in the development of this center.

Toward the beginning of March the MJO moved beyond the immediate vicinity of the maritime continent into the open western Pacific (Figure 21). Around 1 March there also appeared to be an increased cross-equatorial flow and an increase of wind into the SPCZ, which were apparently related to the sixth cold surge defined in Table 1. A pre-formation center at 9.1S, 172.0E, later named tropical storm Gavin, appeared to spin up as the result of the enhanced conditions produced by the cold surge and the active phase of the MJO on 3 March in the central Pacific.

Further to the southwest, another pre-formation center at 17.2S, 156.1E developed in the SPCZ. This storm was later named Justin and also appeared to be associated with both the increased convection from the MJO and the increased cyclonic circulation in the SPCZ area being forced by the sixth event shown in the South China Sea cold surge index. The last pre-formation center of this season occurred on 12 March at 12.7S, 175.9E during the active phase of the MJO (Figure 21). It became tropical storm Hina 24 h later.

This pre-formation center developed in the wake of Tropical Cyclone Gavin, which had moved southward of 20S on 8 March but appeared to leave a remnant of cyclonic circulation in the form of a wind trough that extended northward from its center. Several studies (Frank 1982, Briegel and Frank 1997) have discussed that in the wake regions of tropical storms that from in the monsoon trough, the conditions are favorable for subsequent topical cyclogenesis.

A double-vortex configuration can be seen on the 1000 hPa wind field of 17-18 March. The development of this configuration may be traced back to the evolutions of three tropical storms: Gavin, Justin and Hina, from 7-18 March (Figure 26.2). On 7 March Gavin was centered approximately at 17S, 177E and Justin was centered at 17S, 153E. The two storms appeared to produce a partial Fujiwara-like effect such that Gavin was steered southward out of the map on 12 March, apparently with the help of the strong northwesterly cross-equatorial flow associated with the surge in the western Pacific. Meanwhile, there was little effect on Justin whose center stayed nearly stationary. On 12 March the pre-formation center for Hina developed near 12.7S, 175.9E and formed a new "Fujiwara-like" pair with Justin. Hina was again steered by the northwesterlies associated with Justin and the cross-equatorial flow, in this case southeastward along the SPCZ. In the same time, a cyclonic circulation developed north of the equator starting from 15

March so that by 17 March a double vortex pattern appeared. The southern vortex was Hina, but the northern vortex was weaker and did not develop into any tropical storm. This was the second double vortex that occurred in this season, and it did not seem to be a mechanism for tropical cyclone development.

The timing of the pre-formation centers that have been associated with the cold surge events is plotted on the time coordinate of the South China Sea surge index and shown in Figure 27. Here it is seen that five of the seven surge events are related to the development of one or more pre-formation centers. Only the fourth and the seventh surge events are not associated with pre-formation development. The fourth surge, during the last 10 days of January, occurred when the entire domain was under an inactive phase of MJO (Figure 22). The seventh surge occurred at the end of the season and also during an inactive phase of MJO. A synopsis of the analysis for all the pre-formation cases is summarized in Table 3, where the possible association of each case with the three types of transient motions, MJO, cold surge and easterly wave, are identified. There were 15 storms that formed in the Southern Hemisphere during this season and 12 of them appeared to be associated with the active phase of the MJO. Out of these 12 formations, only two, Rachel and Hina, formed without apparent influences from other transient systems. In two other cases, Fergus

and Evan, all three types of transient motions appeared to contribute to the pre-formation centers. Among the remaining MJO-related formation centers, seven were related to cold surges (Nicholas, Ophelia, Phil, 27S, Ita, Gavin and Justin) and one(Drena) was related to an easterly wave. Of the three non-MJO related formations, two of them (Gillian and Harold) were identified with easterly waves, with the latter also related to a cold surge event. Only the formation of Pancho/Helinda, in the open Indian Ocean away from the vicinity of the maritime continent and Australia, was not related to any of the three types of transient motion in Table 3.

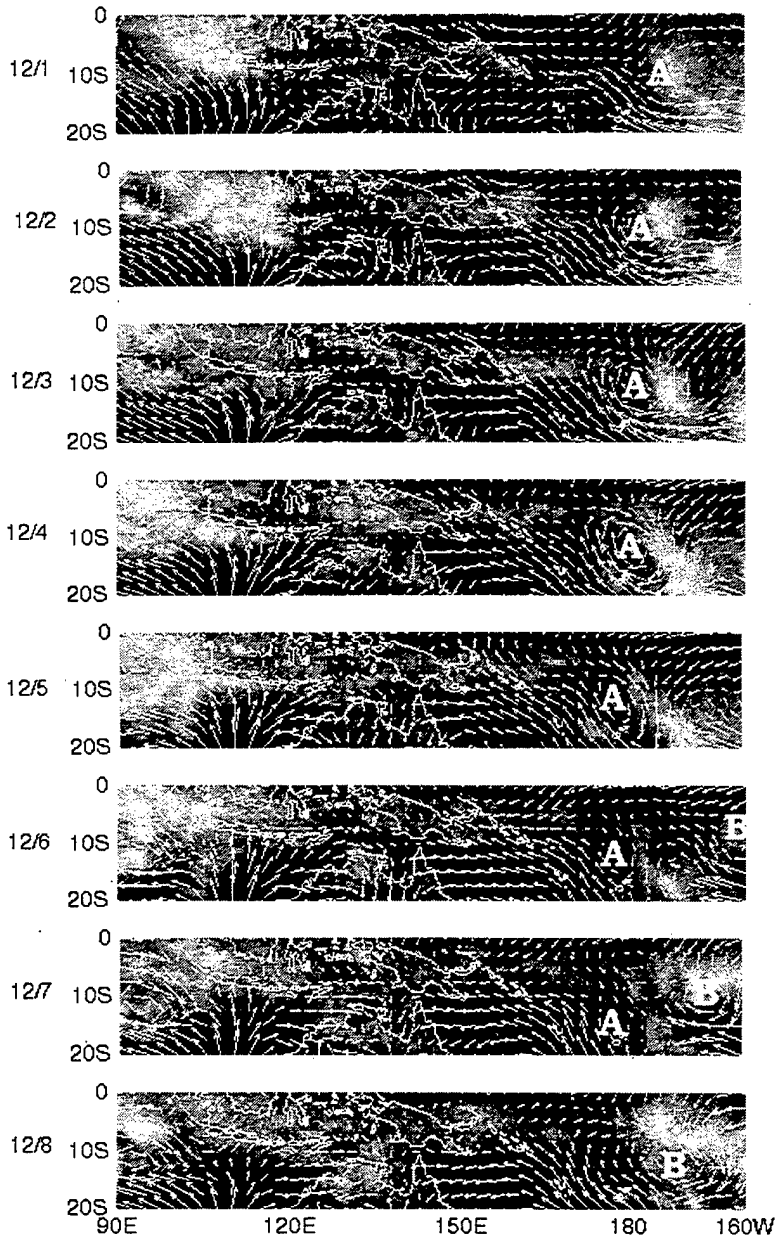

Figure 26. The daily 1000 hPa winds and CI charts for the Southern Hemisphere.

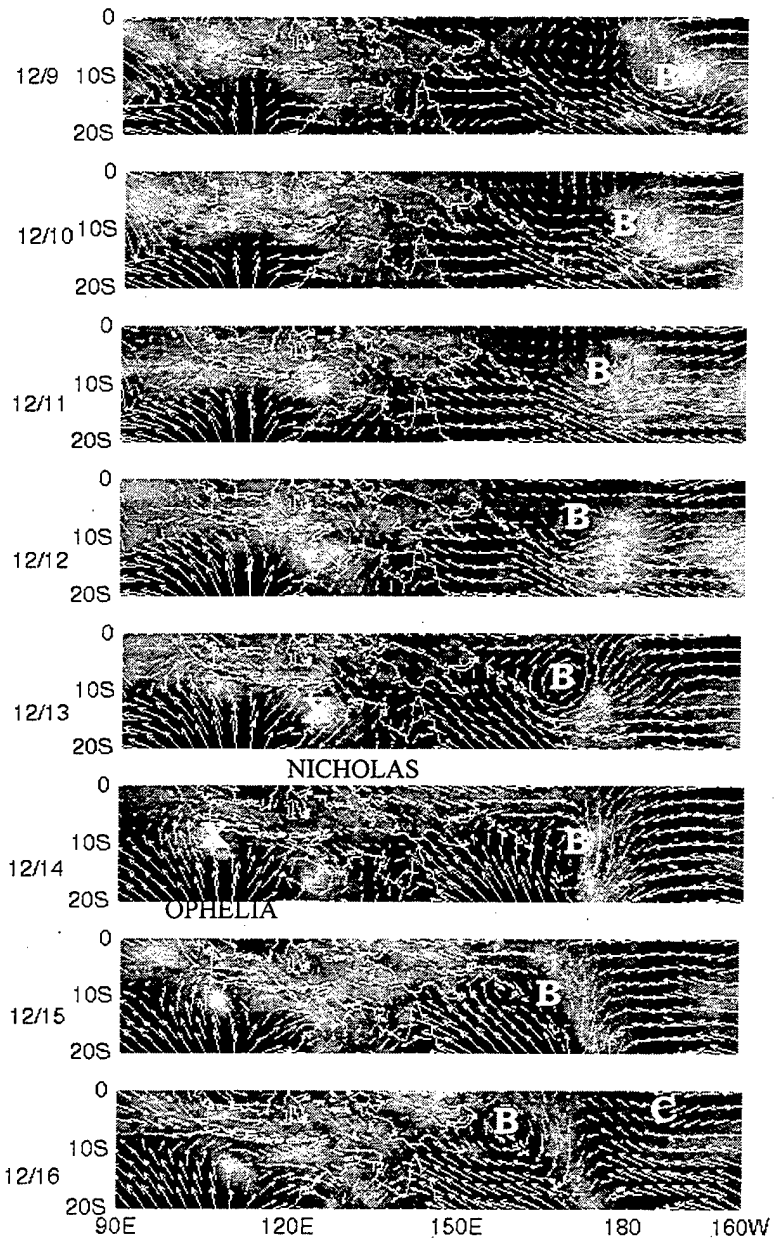

Figure 26 continued.

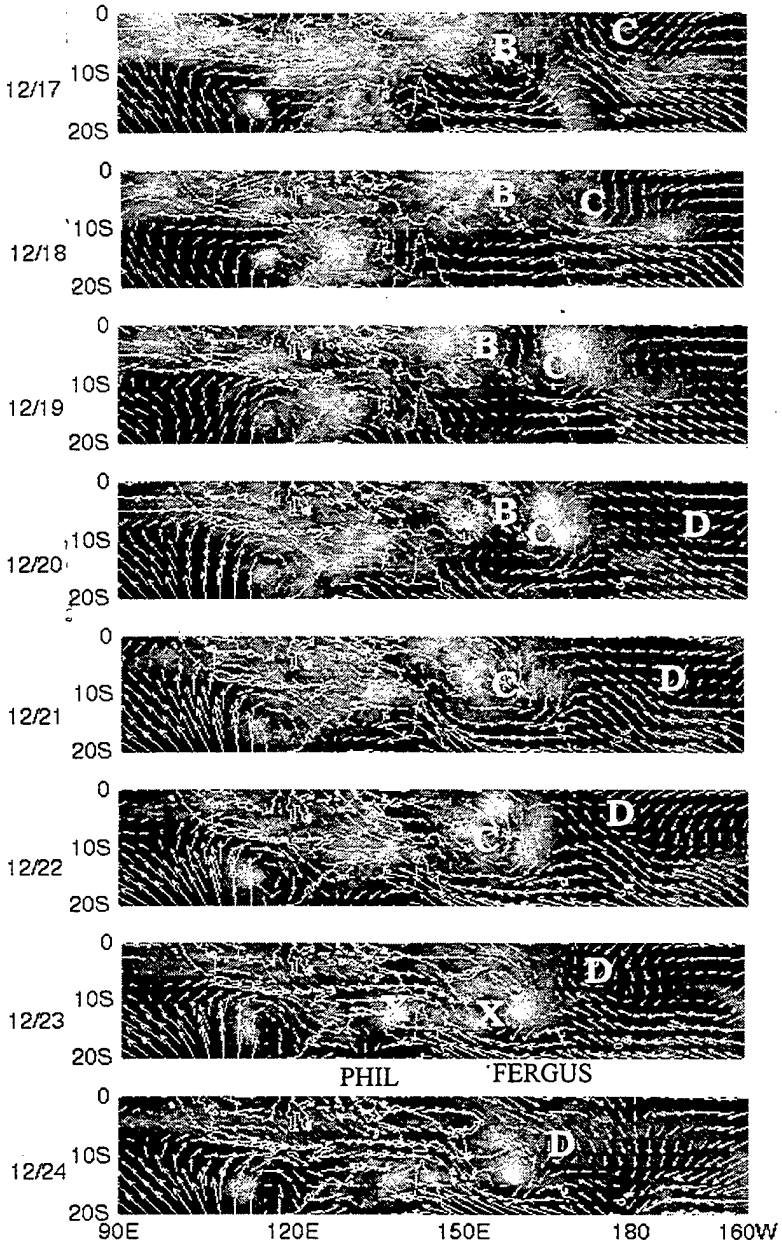

Figure 26 continued.

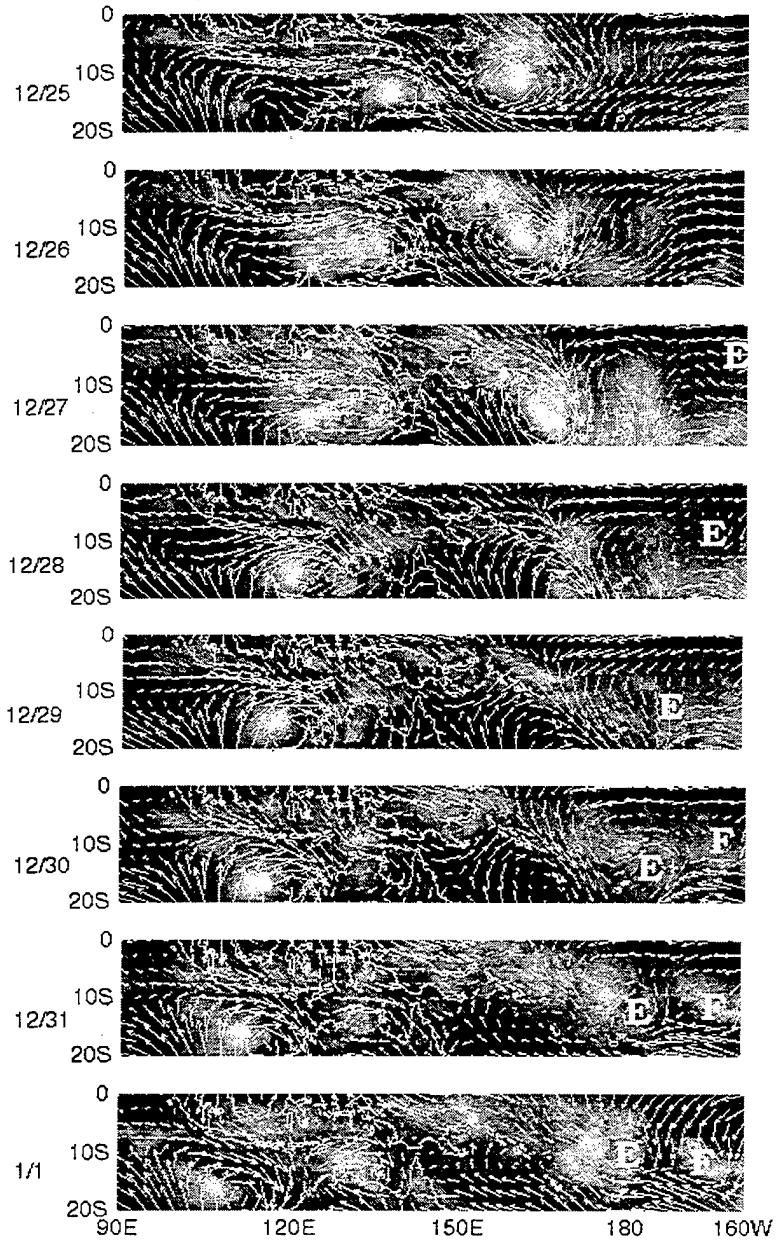

Figure 26 continued.

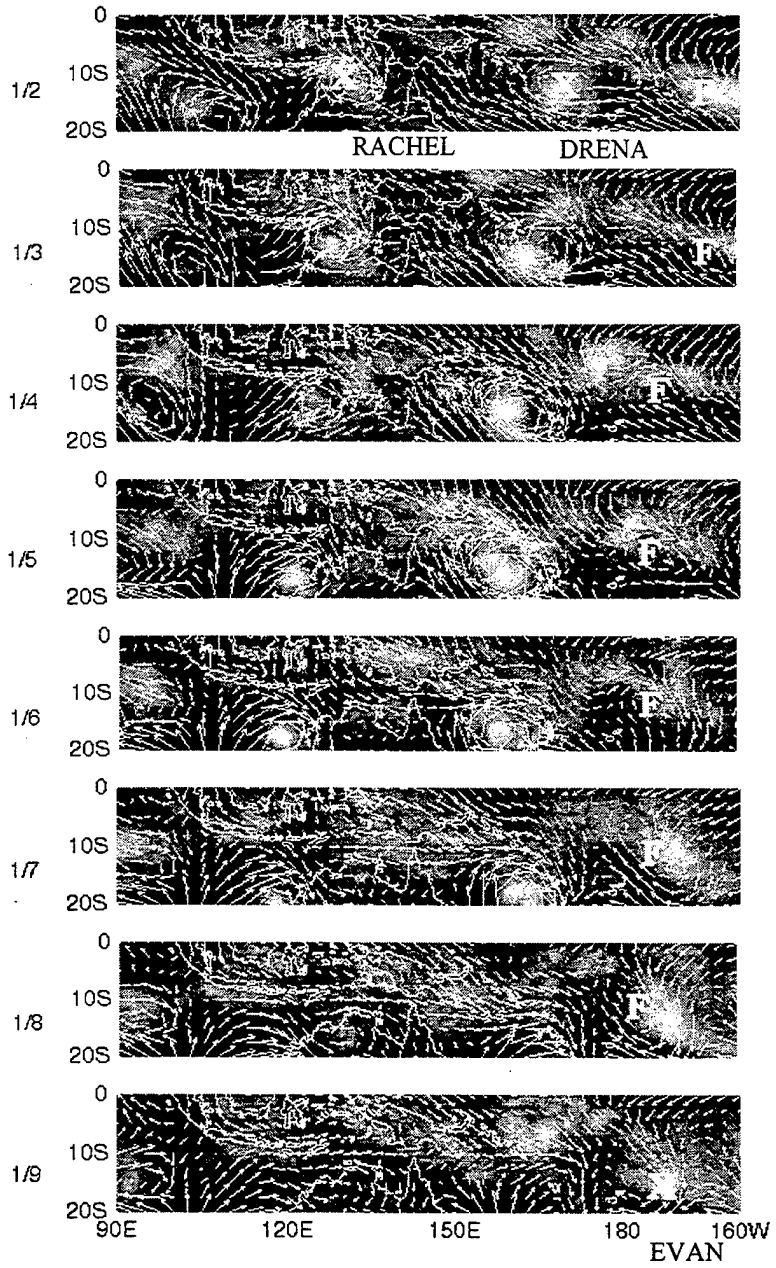

Figure 26. continued.

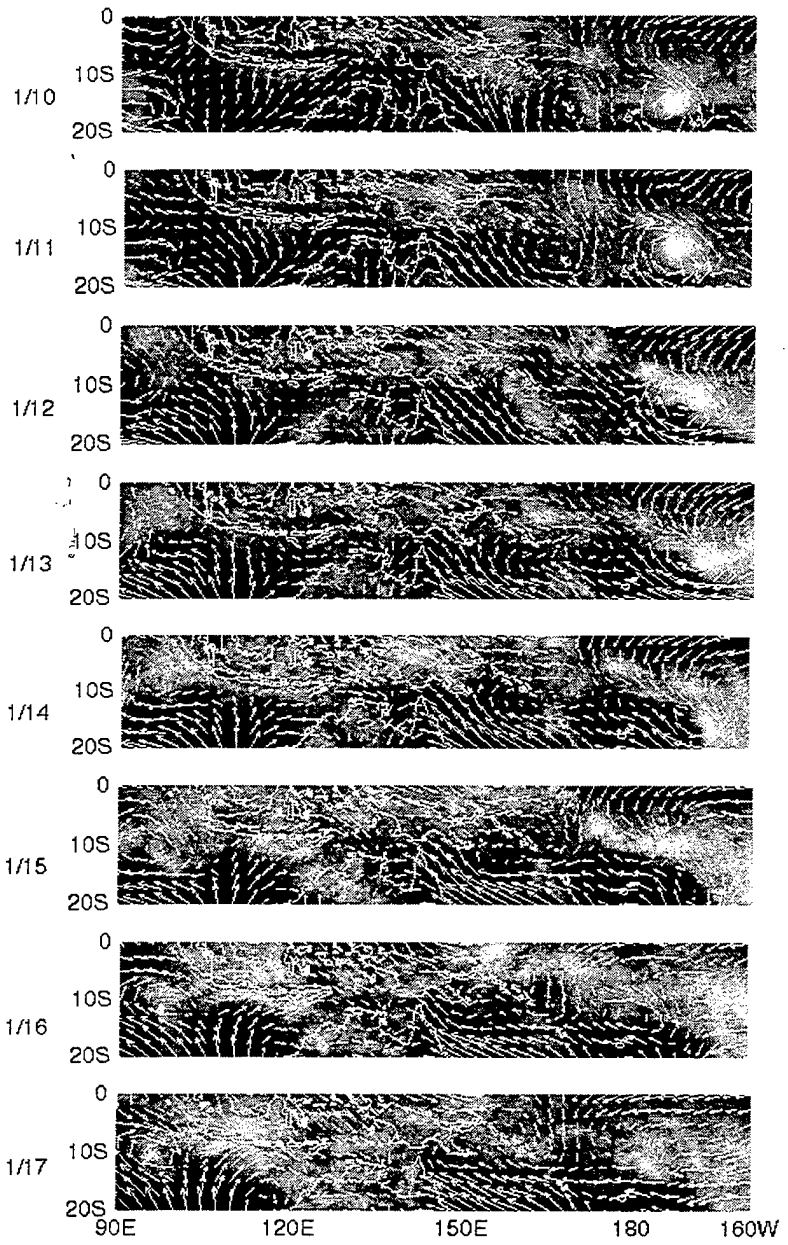

Figure 26 continued.

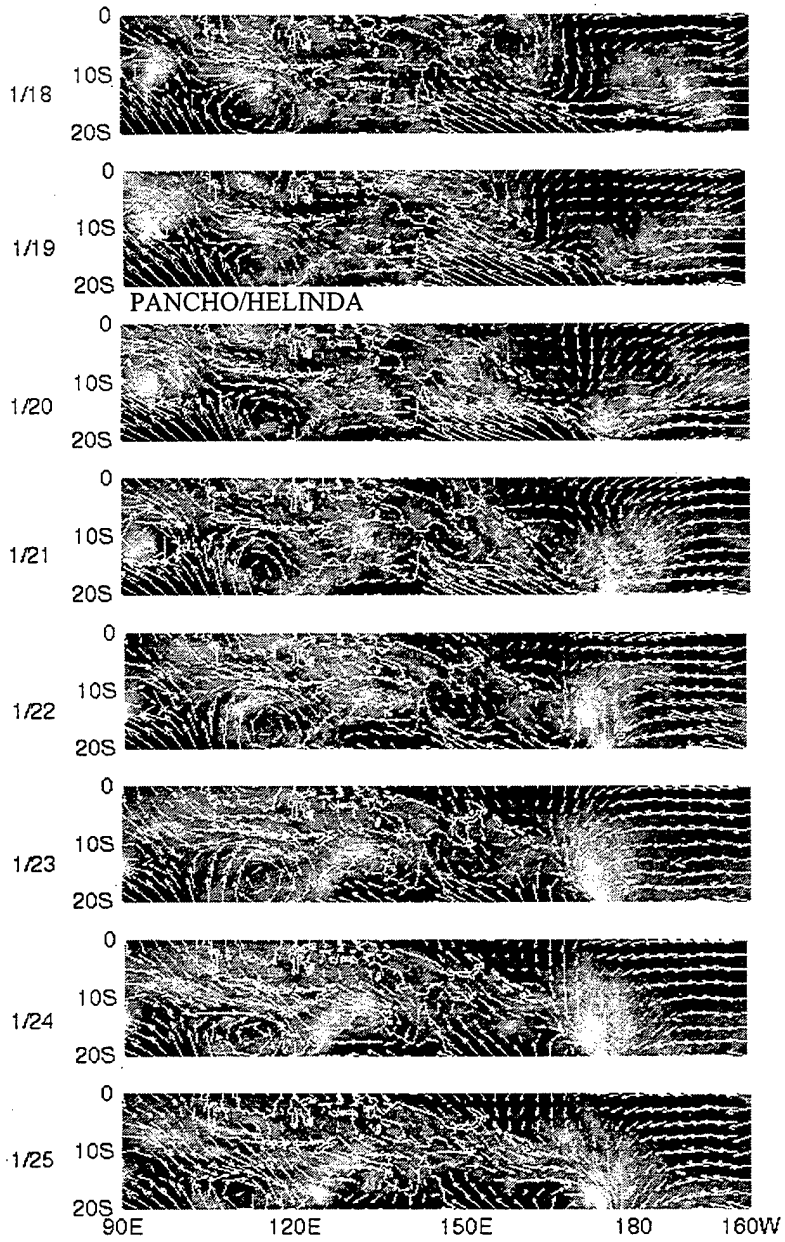

Figure 26 continued.

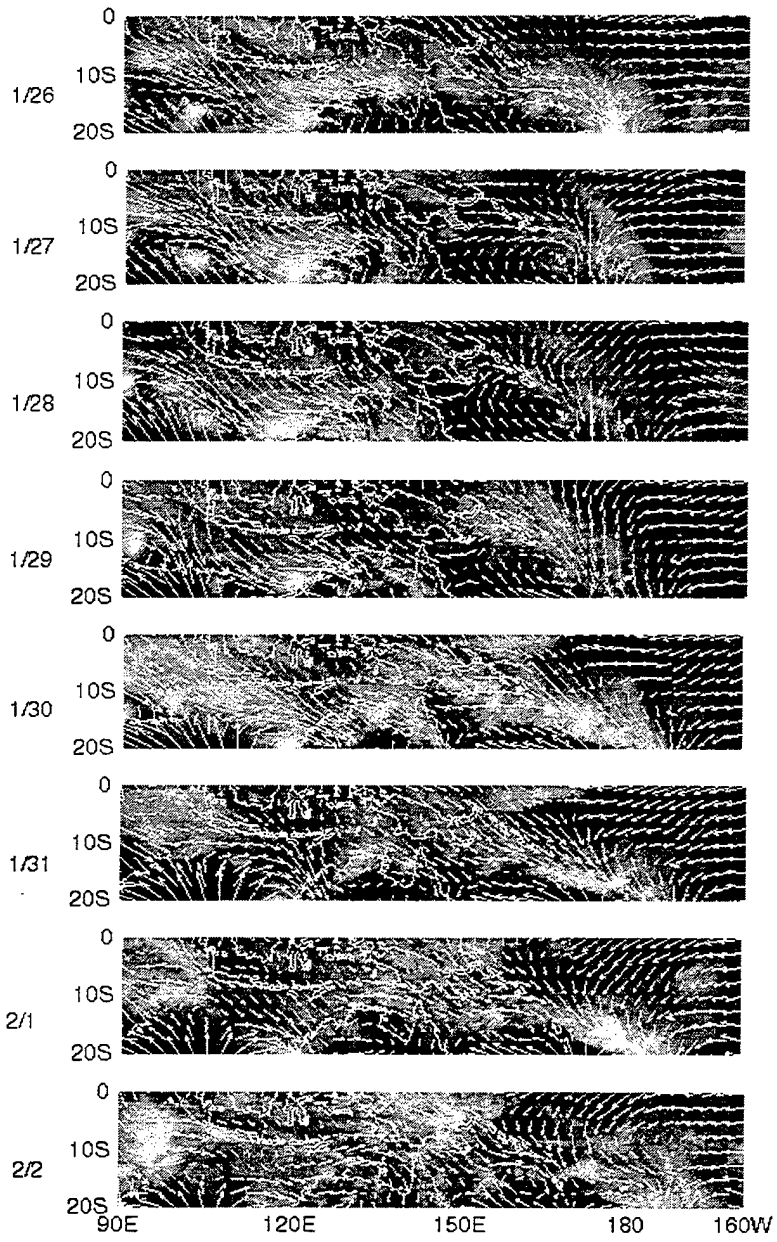

Figure 26 continued.

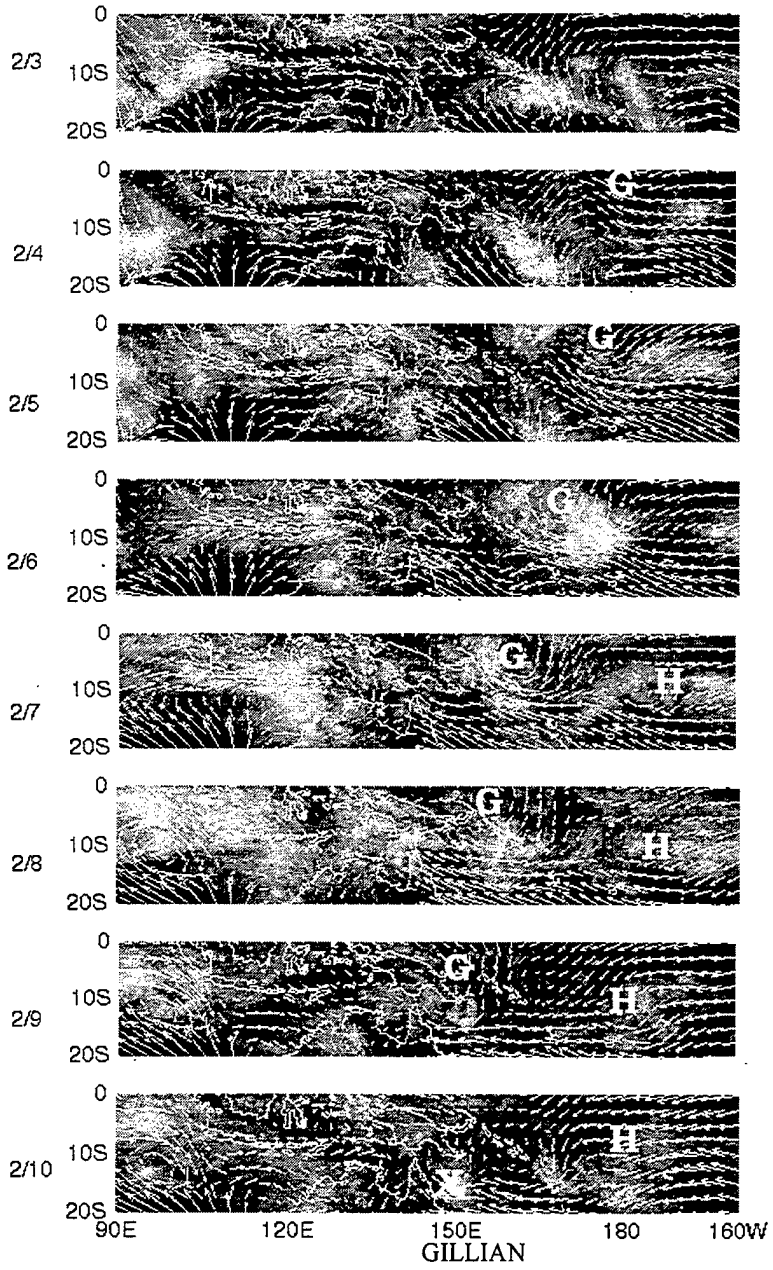

Figure 26 continued.

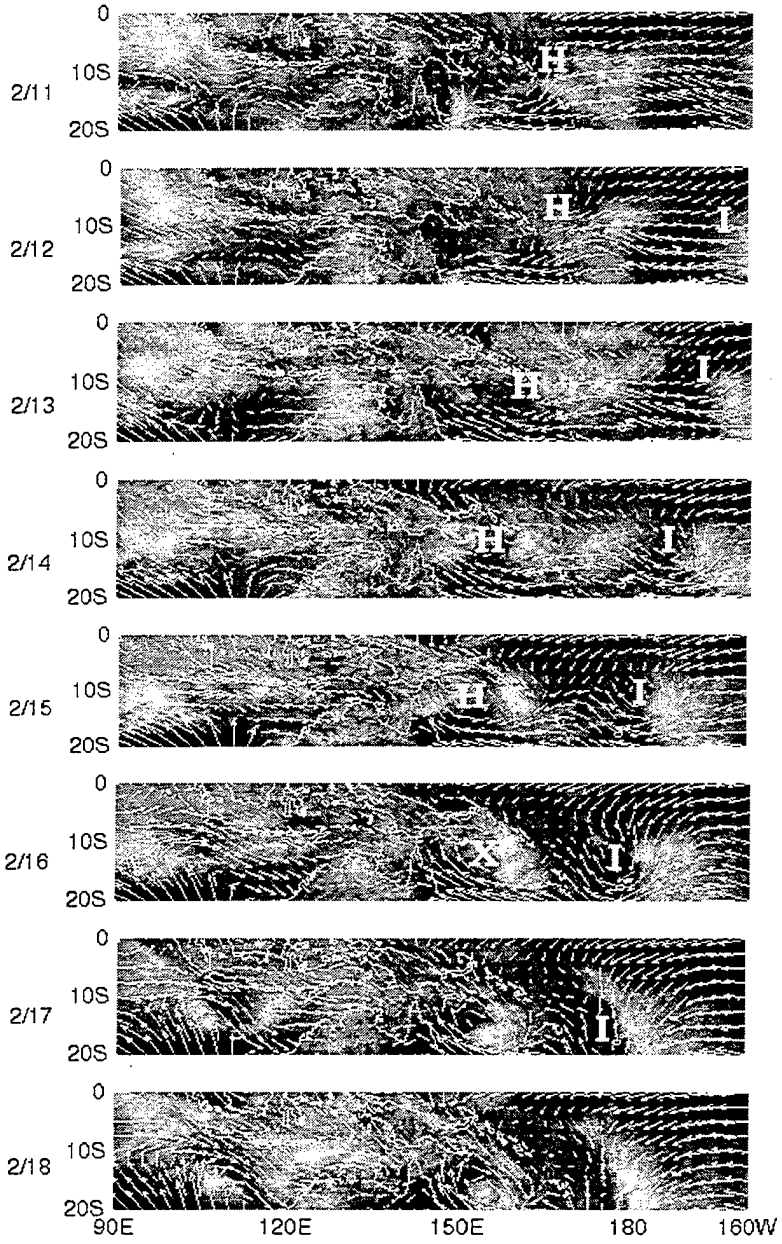

Figure 26 continued.

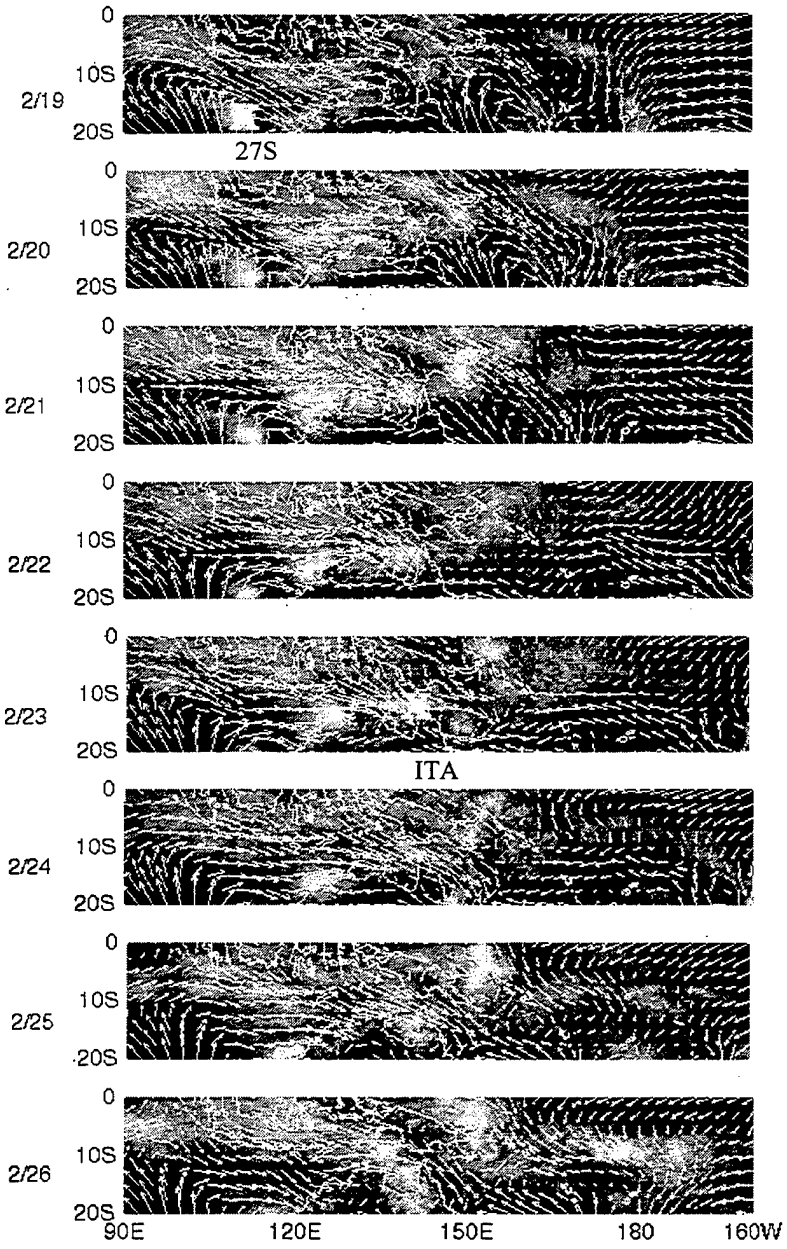

Figure 26 continued.

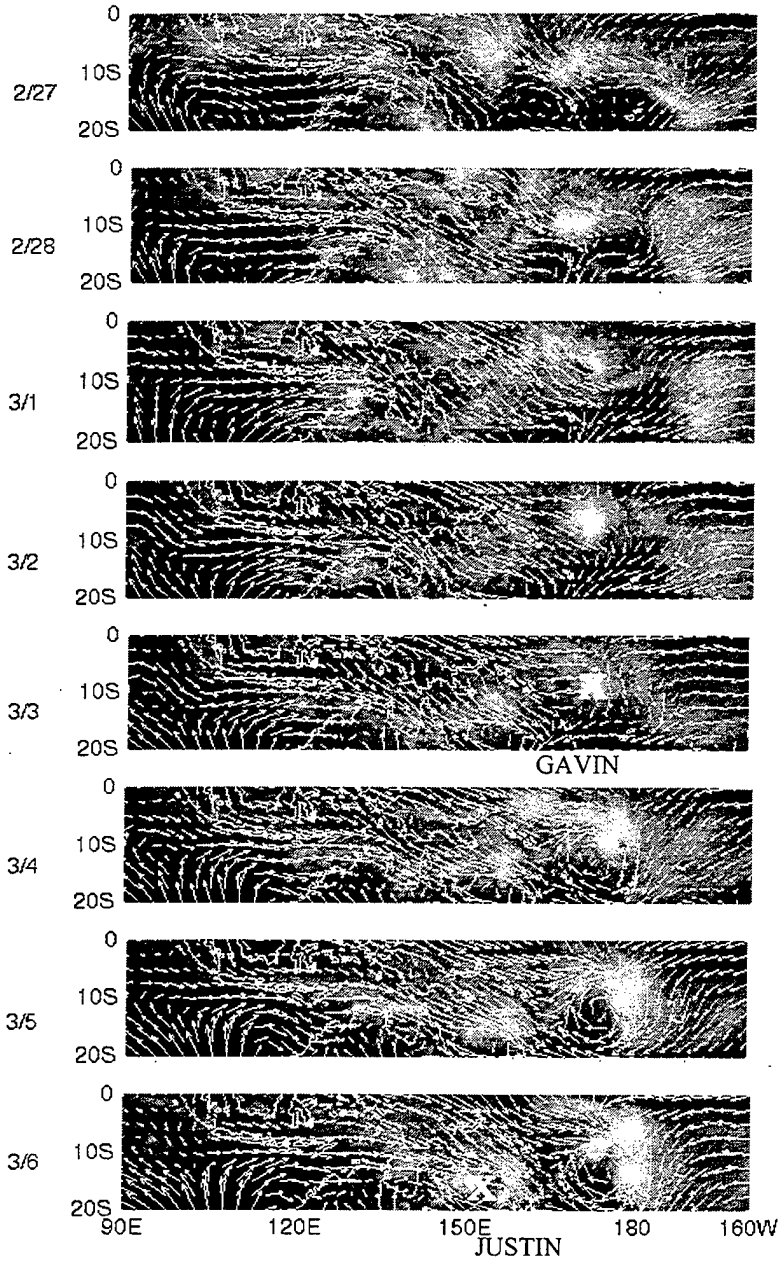

Figure 26 continued.

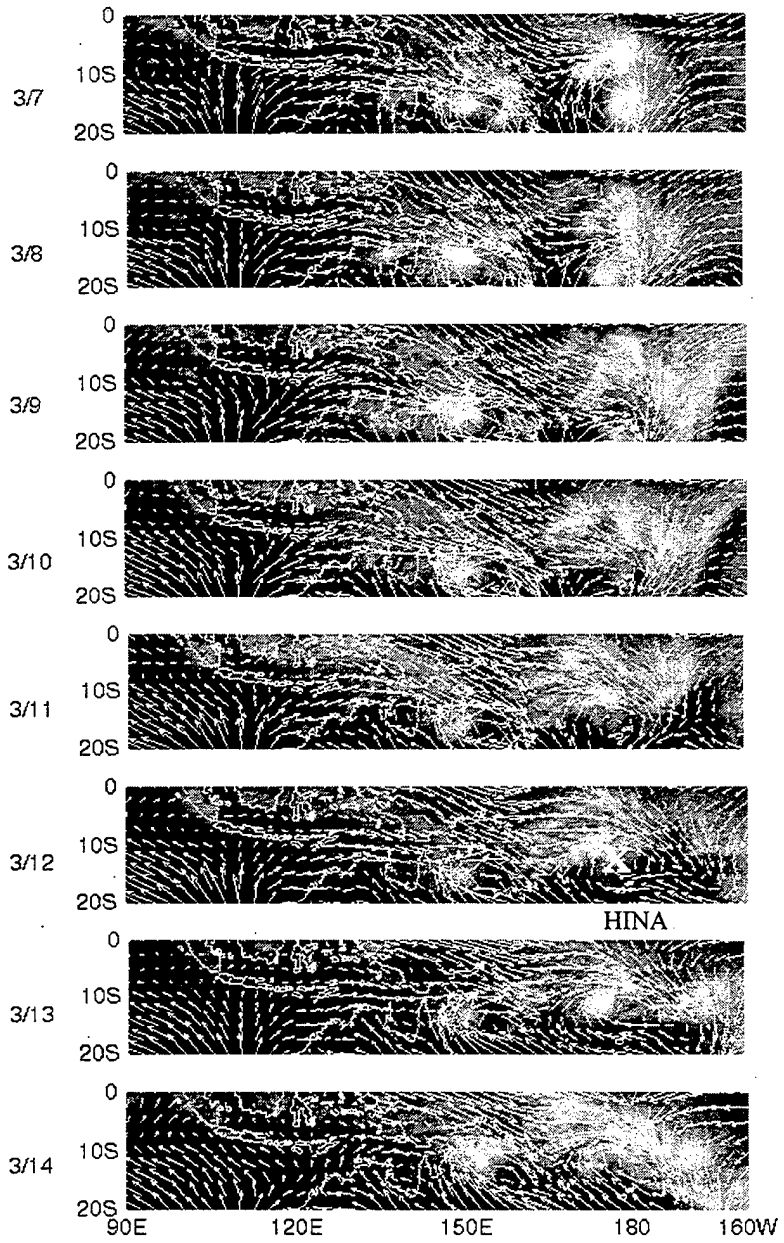

Figure 26 continued.

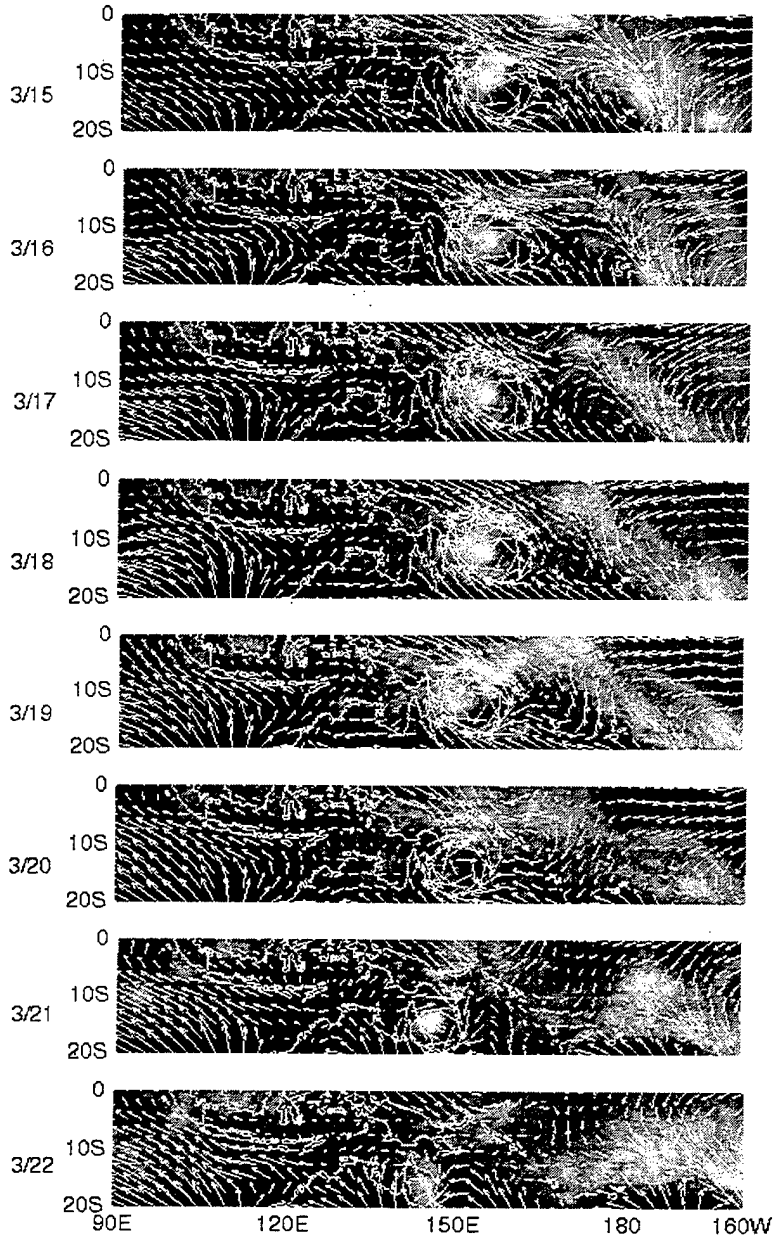

Figure 26 continued.

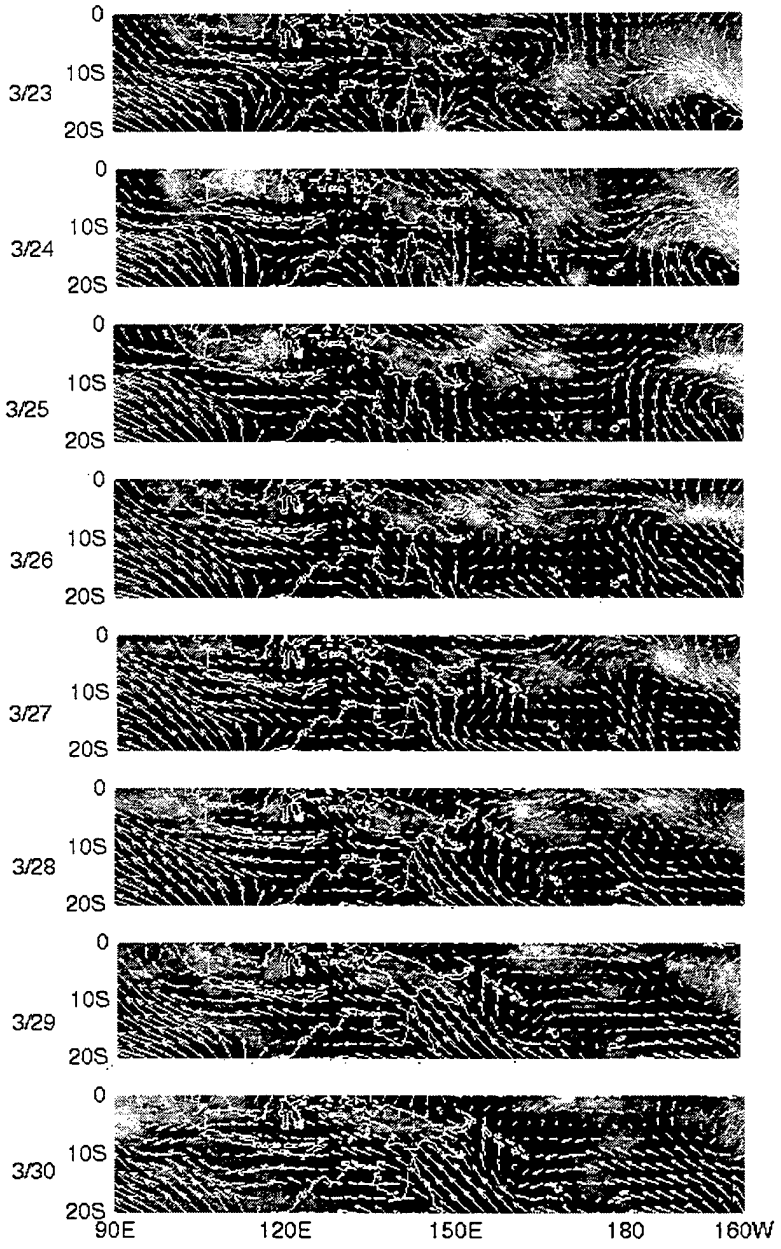

Figure 26 continued.

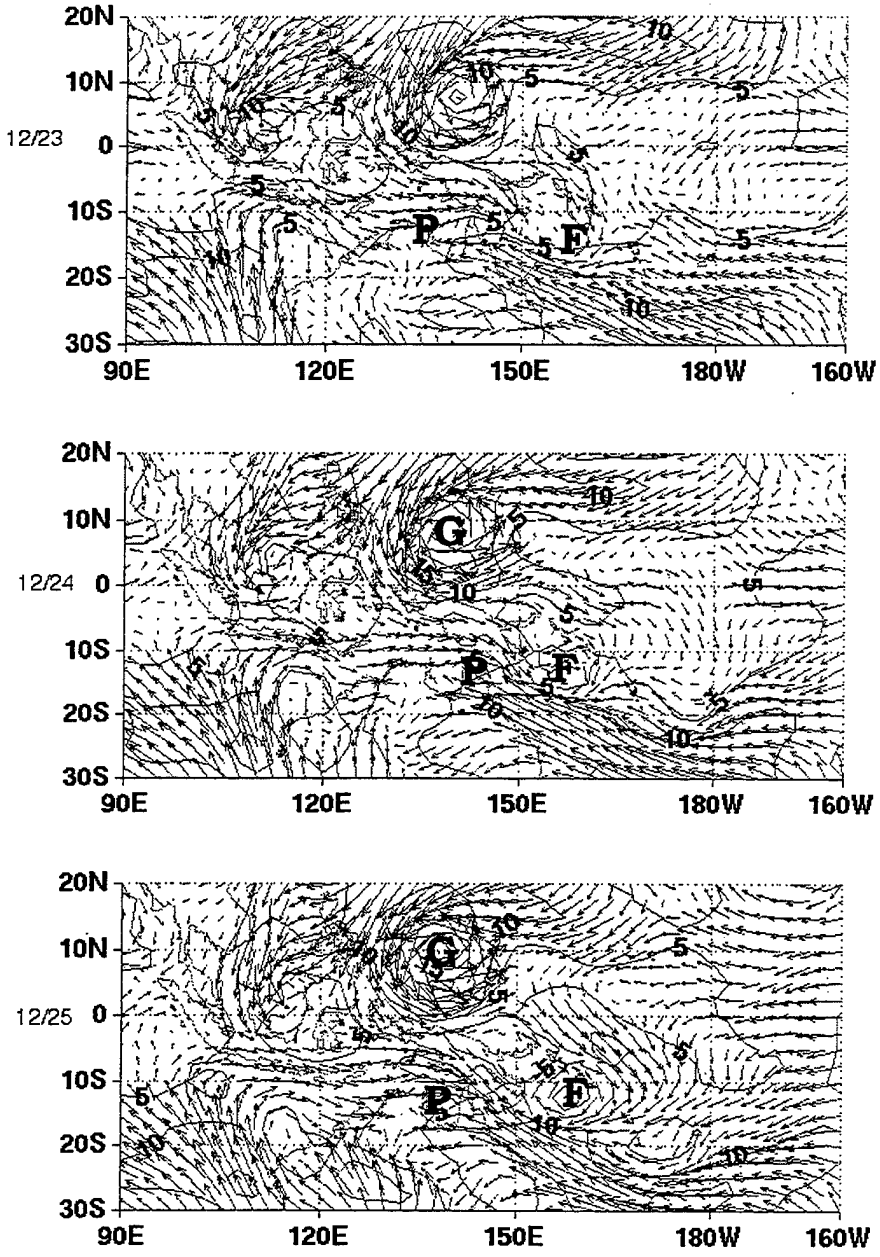

Figure 26.1. NCEP 1000 hPa winds from 23-25 December to show the sequence of the MJO "double vortex" signature. The pre-formation centers and continued development are labeled; G for Greg, P for Phil and F for Fergus.

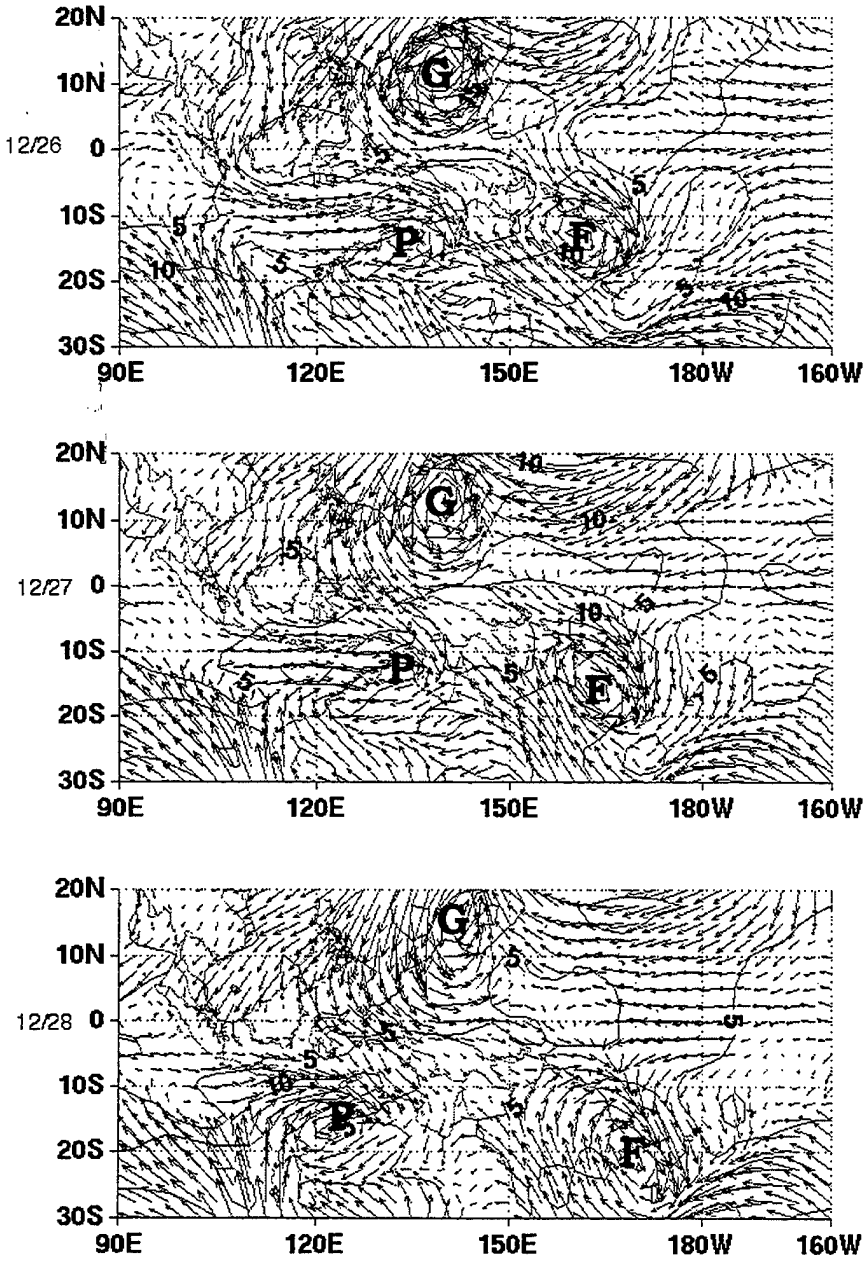

Figure 26.1 continued for 26-28 December.

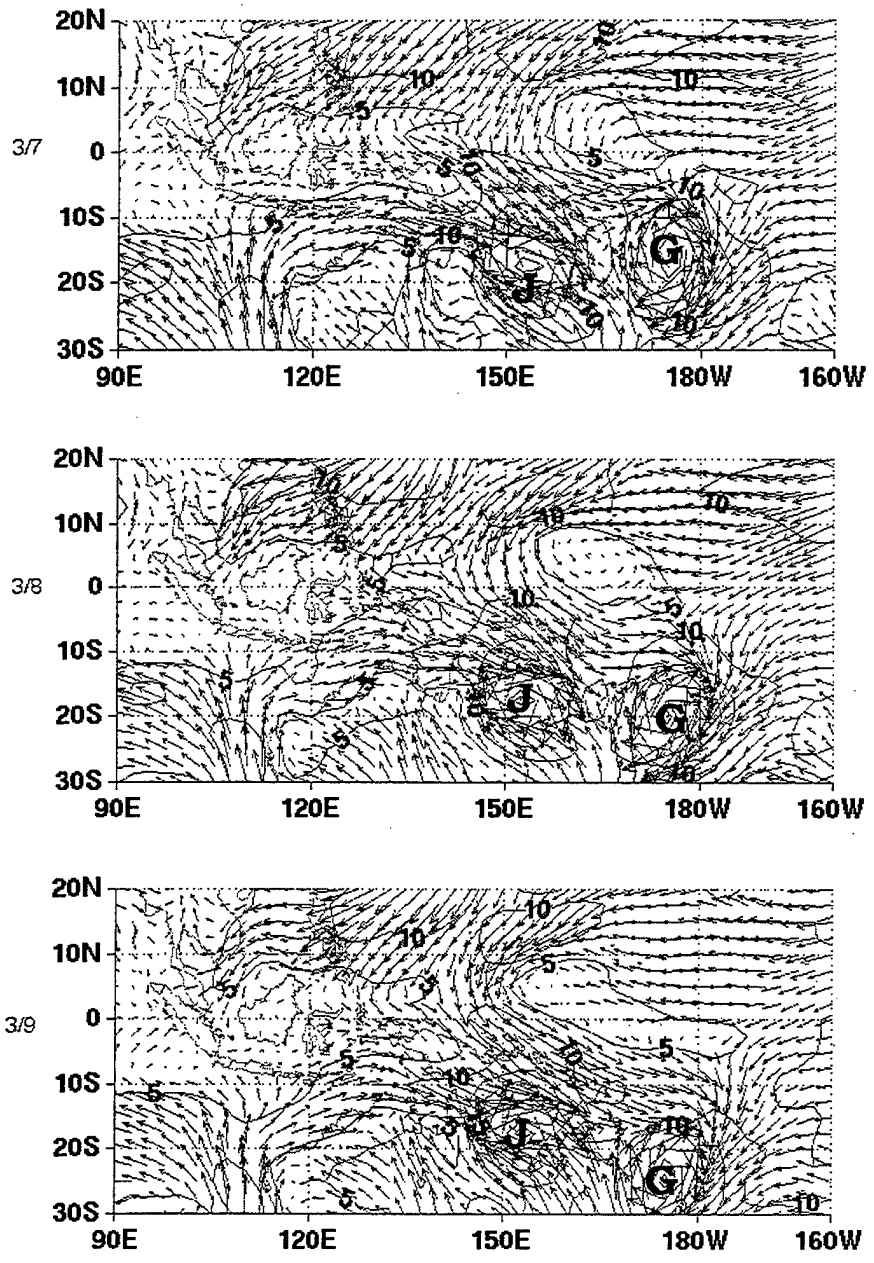

Figure 26.2. NCEP 1000 hPa winds from 7-10 March to show the sequence of the MJO "double vortex" signature. As in figure 26.1, labels are J for Justin, G for Gavin and H for Hina.

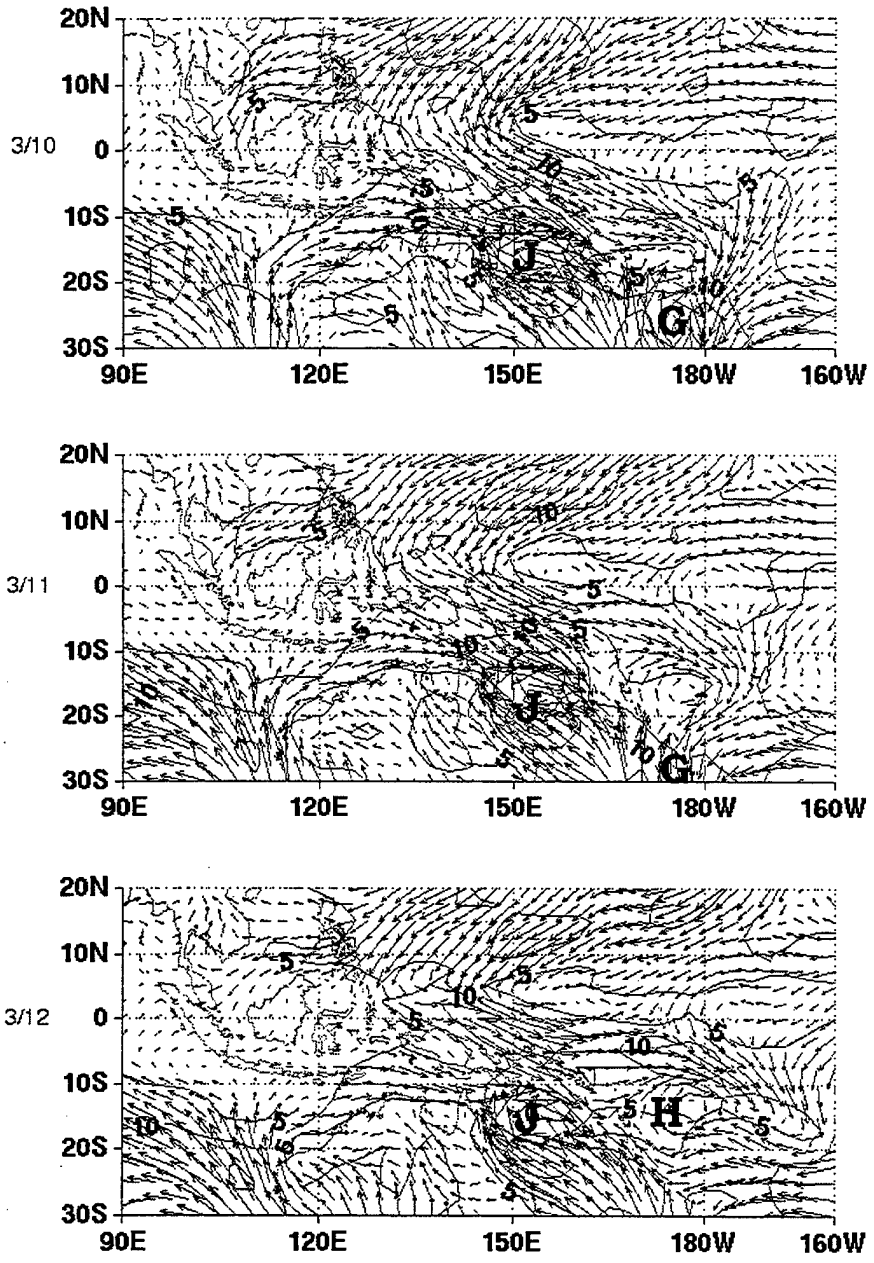

Figure 26.2 continued for 10-12 March.

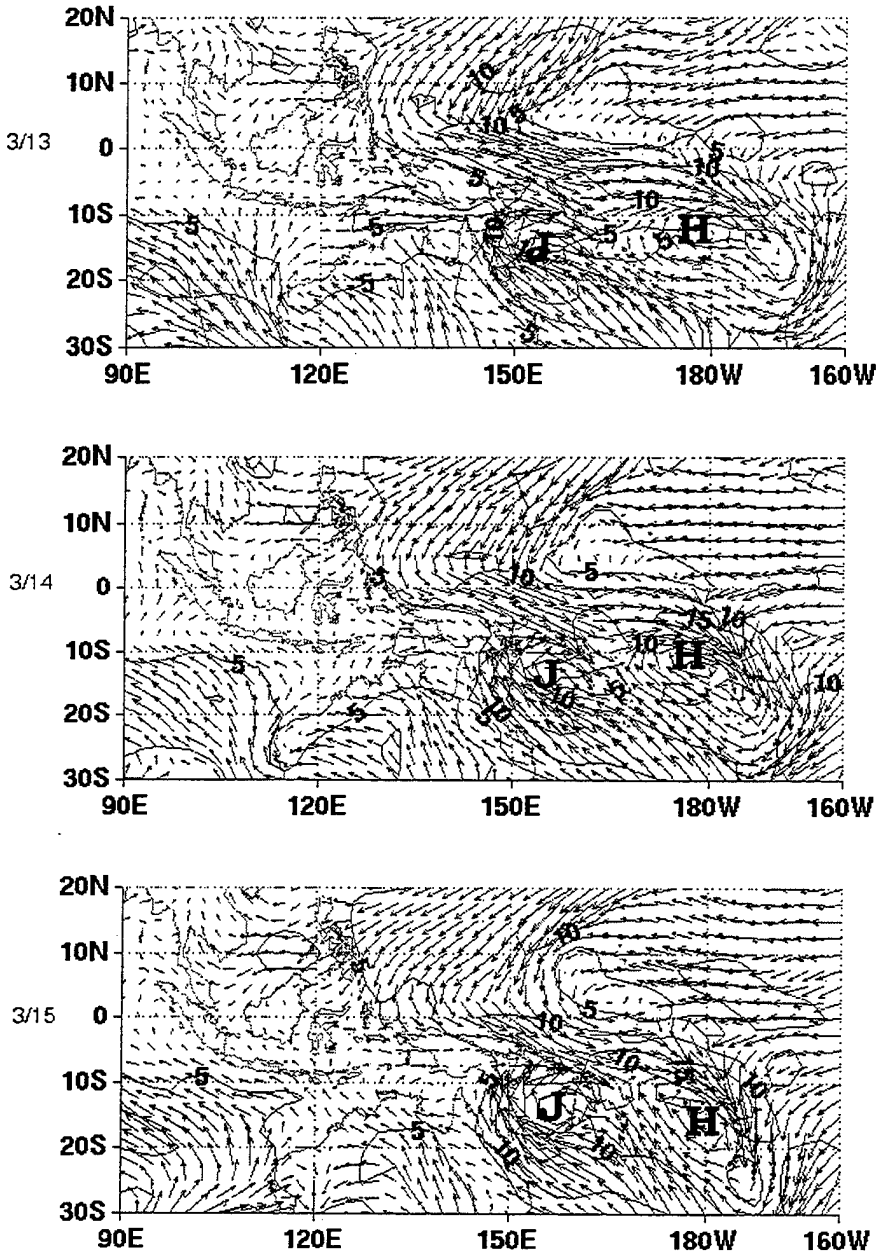

Figure 26.2 continued for 13-15 March.

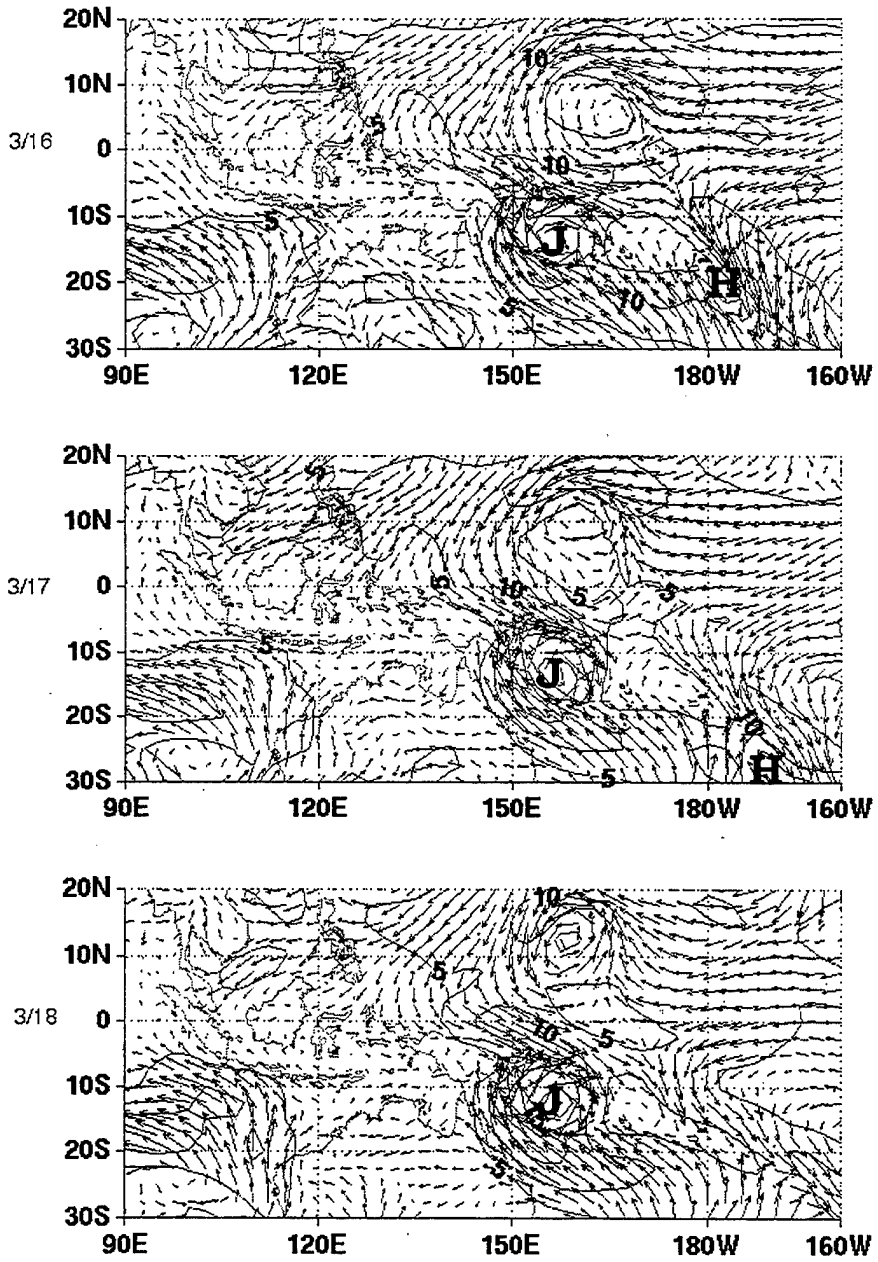

Figure 26.2 continued for 16-18 March.

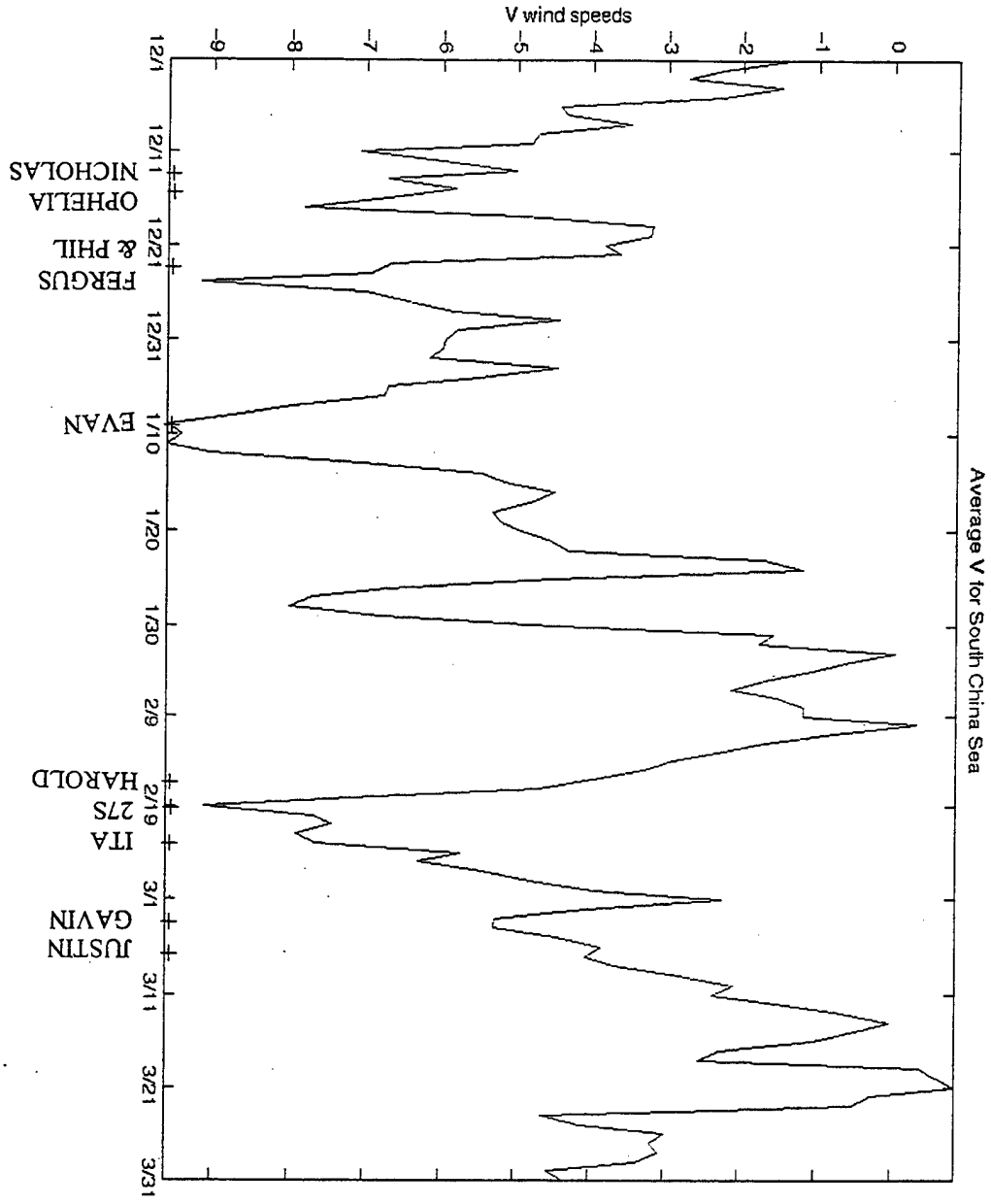

Figure 27. The meridional wind component or the base index averaged over the South China Sea. Southern Hemisphere tropical storms are plotted here.

			Association			
Storm	Date	Location	MJO	Surge	Wave	Other
Nicholas	12/13/96	12.0S 124.4E	X	X		
Ophelia	12/14/96	10.0S 108.0E	X	X		
Phil	12/23/96	11.9S 138.2E	X	X		
Fergus	12/23/96	13.1S 159.7E	X	X	X	
Rachel	1/2/97	11.3S 131.9E	X			
Drena	1/2/97	12.8S 168.8E	X		X	
Evan	1/9/97	16.5S 172.8W	X	X	X	
Pancho/Helinda	1/19/97	9.1S 96.2E				X
Gillian	2/10/97	14S 149.1E			X	
Harold	2/16/97	14.4S 157.2E		X	X	
27S	2/19/97	16.2S 113.7E	X	X		
Ita	2/23/97	15.9S 148.2E	X	X		
Gavin	3/3/97	9.1S 172.0E	X	X		
Justin	3/6/97	17.2S 156.1E	X	X		
Hina	3/12/97	12.7S 175.9E	X			

Table 3. A synopsis of the Southern Hemisphere tropical storms; the start of 30-knot winds and the factors associated with their development.

VII. SUMMARY AND CONCLUSIONS

This study used the GMS water vapor IR data, NCEP 1000 hPa wind reanalysis, and NSCAT surface wind data to examine the evolution and possible interactions among several large-scale transient motions in the tropical convection region of the northern winter (southern summer) monsoon during December 1996 - March 1997. This region includs the areas surrounding the maritime continent, northern Australia and the equatorial West Pacific,. During northern winter the seasonal-mean convection in this region is organized into the ITCZ just south of the equator and the SPCZ, with the former often influenced by low-level cross-equatorial flow from the north and the latter characterized by strong low-level cyclonic vorticity. Tropical cyclones often develop in these convergence zones. The large-scale transient motions include the Maddan-Julian Oscillation from the equatorial Indian Ocean, the northeasterly cold surges from the Northern Hemisphere, and the synoptic-scale equatorial easterly waves propagating from the central or eastern Pacific. Previous studies (Liebmann et al, 1994) have shown that development of the tropical cyclones tends to concentrate in the active phase region of the MJO. In this study we focused on the possible roles of the different transient large-scale motions in the development of the tropical storms during one season.

The cold surge from the northern midlatitudes covered a wide longitudinal band of the subtropical northwestern Pacific. When a strong event approached the equator it tended to split into two branches, one in the South China Sea and the other east of Philippines and Borneo. The meridional wind at 7.5N in the South China Sea was used as a surge index to identify these major events. A total of seven events were found, and composites of 1000 hPa wind fields from four days before to five days after the beginning of surges were constructed. The results indicate that systematic large-scale changes in the southern tropics occurred as the surges develop, such that the low-level vorticity tended to intensify to the northwest of Australia and in the vicinity of the SPCZ. This evolution makes these two areas more favorable for tropical cyclogenesis during the strong surges.

Two active phases of the MJO system moved across the region during the season. The first started in the eastern Indian Ocean in early December and moved to the eastern Pacific in late December. The second started in the eastern Indian Ocean in early February and moved to the eastern Pacific in early March. A total of 18 tropical storms formed between 18S-10N, with three in the northern tropics and 15 in the southern tropics. As was reported by Liebmann et al 1994, most of these storms developed in or near the MJO super cloud clusters. However, most of the development

also involved other motions systems, including the cold surge or the synoptic-scale easterly waves which propagated into the region from time to time on both sides of the equator.

Liebmann et al (1994) reported that more tropical cyclones developed in the active MJO areas not because of a higher percentage of development from tropical depressions, but rather because of the fact that more depressions existed in these convective areas. To examine the process leading to increased formation of tropical depressions, a pre-tropical storm formation center was defined when the maximum sustained wind of a tropical depression first reached 30 knots, this is still less than the definition for tropical storms. Based on this definition, it was determined that within the winter monsoon convection region, two of the three Northern Hemisphere pre-formations and 12 of the 14 Southern Hemisphere pre-formations occurred in the MJO. Of these, only one northern storm and two southern storms did not involve the cold surge or synoptic easterly waves. The most frequent occurrences involved the interaction of MJO and cold surges, followed by the interaction of MJO and easterly waves. In two cases all three systems were involved. Furthermore, both of the two southern storms that developed outside of the active phase of MJO involved easterly waves, and one of them formed under cold surge conditions. It thus appeared that the active phase of MJO

alone does not by itself give rise to most of the tropical storm formation. Rather, the cold surges from the Northern Hemisphere and the series of equatorial synoptic easterly waves propagating from the eastern or central Pacific provided additional mechanisms for development.

The equatorial westerly burst and associated cross-equatorial flow have been shown to cause double-vortex formation in which a pair of cyclonic vortices straddle the equator and led to the development of twin cyclones, particularly near the dateline (e.g., Keen 1992; Ferreira et al. 1996). In the 1996-1997 season two short periods of double vortex configurations were found in the 1000 hPa wind field. The first occurred around 27-28 December and consisted of the northern tropical cyclone Fern and the southern tropical cyclone Fergus. However, close examination revealed that the two storms formed in different processes, in particular Fergus formed two days after Fern as a result of MJO active convection, a cold surge and an easterly wave. It was several days after both cyclones developed that they move sufficiently close to result in a flow configuration of a northwest-southeast slanted double vortex. The other double vortex pattern occurred on 17 March after a complex evolution of the development of three tropical storms, Gavin, Justin and Hina, all of them in the southern tropics. Eventually Hina became the source of the southern equatorial vortex, and a weak northern circulation developed to its

north but never reached a stage close to a tropical storm. Therefore, in both double vortex cases no cyclones formed as a result of the MJO "double-vortex" mechanism.

In order to verify these relationships, further studies during this season need to be done. In addition, possible usage of other levels and satellite data to confirm these relationships might be useful.

LIST OF REFERENCES

Bureau of Meteorology Northern Territory Region, 1997: Darwin tropical diagnostic statement. Vol. 15, No. 12, Vol. 16, No.1-3.

Boyle, J. S., and T.-J. Chen, 1987: Synoptic aspects of the wintertime East Asian monsoon. *Monsoon Meteorlogy*, C.-P. Chang and T. N. Krishnamurti, Eds., Oxford University Press, 125-160.

Briegel, L. M., and W. M. Frank, 1997: Large-scale influences on tropical cyclogenesis in the western north Pacific. *Mon. Wea. Rev.*, **125**, 1397-1413.

Ferreira, R. N., W. H. Schubert, and J. J. Hack, 1996: Dynamical aspects of twin tropical cyclones associated with the Madden-Julian oscillation. *J. Atmos. Sci.*, **53**, 929-945.

Frank, W.M., 1982: Large-scale characteristics of tropical cyclones. *Mon. Wea. Rev.*, **110**, 572-586.

Gray, W. M., 1979: Hurricanes: Their formation, structure and likely role in the tropical circulation. *Supplement to Meterology Over the Tropical Oceans*, D. B. Shaw, Ed., Royal Meteorological Society, 155-218.

Johnson, R. H., and R. A. Houze, Jr., 1987: Precipitating cloud systems of the Asian monsoon. *Monsoon Meteorlogy*, C.-P. Chang and T. N. Krishnamurti, Eds., Oxford University Press, 298-353.

JTWC, cited 1998: Naval meteorology and oceanography operational support web. [Available on-line from http://www.npmocw.navy.mil/npmocw/prods/products/best_tracks/.]

Keen, R.A., 1982: The role of cross-equatorial tropical cyclone pairs in the southern oscillation. *Mon. Wea. Rev.*, **110**, 1405-1416.

Liebmann, B, H. H. Hendon and J. D. Glick, 1994: The relationship between tropical cyclones of the western Pacific and Indian Oceans and the Madden-Julian oscillation. *J. Meteor. Soc. Japan*, **72**, 401-412.

Madden, R. A., and P. R. Julian, 1971: Detection of a 40-50 day oscillation in the zonal wind in the tropical Pacific. *J. Atmos. Sci.*, **28**, 702-708.

Nakazawa, T., 1988: Tropical super clusters within intraseasonal variations over the western Pacific. *J. Meteor. Soc. Japan*, **66**, 823-839.

Rui, H., and B. Wang, 1990: Development characteristics and dynamic structure of tropical intraseasonal convection anomalies. *J. Atmos. Sci.*, **47**, 357-359.

Sui, C.-H., and Lau, K.-M, 1992: Multiscale phenomena in the tropical atmosphere over the western Pacific. *Mon. Wea. Rew.*, **120**, 407-430.

Wang, B., and H. Rui, 1990: Synoptic climatology of transient tropical intraseasonal convective anomalies. *Meteor. Atmos. Phys.*, **44**, 43-61.

Weickmann, K. M. and S. J. S. Khalsa, 1990: The shift of convection from the Indian Ocean to the western Pacific Ocean during a 30-60 day oscillation. *Mon. Wea. Rev.*, **118**, 964-978.

Zangvil, A., 1975: Temporal and spatial behavior of large-scale disturbances in tropical cloudiness deduced from satellite brightness data. *Mon. Wea. Rev.*, **103**, 904-920.

INITIAL DISTRIBUTION LIST

No. Copies

1. Defense Technical Information Center 2
   8725 John J. Kingman Rd., STE 90944
   Ft. Belvoir, Virginia 22060-6218

2. Dudley Knox Library.....2
   Naval Postgraduate School
   411 Dyer Rd.
   Monterey, California 93943-5101

3. Air Force Institute of Technology /CIG BLDG 125.....1
   2950 P Street
   Wright-Patterson AFB OH 45433-7765

4. Meteorology Department.....1
   Code MR/Wx
   Naval Postgraduate School
   589 Dyer Rd Rm 254
   Monterey CA 93943-5114

5. Prof. Chi-Pei Chang.....1
   Code MR/CP
   Naval Postgraduate School
   589 Dyer Rd Rm 254
   Monterey CA 93943-5114

6. Prof. Patrick Harr.....1
   Code MR/PH
   Naval Postgraduate School
   589 Dyer Rd Rm 254
   Monterey CA 93943-5114

7. Capt. Sylvia Taylor 2
   c/o D. Taylor
   6 Wiegand Lane
   Delmar, NY 12054